UNIVERSITY OF CALGARY

Measurement and Modeling of Emulsion Layer Growth in Continuous Oil-Water Separations

by

Nand Lal Khatri

A THESIS
SUBMITTED TO THE FACULTY OF GRADUATE STUDIES
IN PARTIAL FULFILMENT OF THE REQUIREMENTS FOR THE
DEGREE OF MASTER OF SCIENCE

DEPARTMENT OF CHEMICAL AND PETROLEUM ENGINEERING

CALGARY, ALBERTA
July, 2010

ABSTRACT

Water-in-crude oil emulsions present considerable challenges to the petroleum industry both during upstream production and downstream treatment of crude oil, especially in the case of oil sands separation processes, where these emulsions contribute to the formation of rag layers. A rag layer is the material that accumulates and persists at the oil/water interface and it consists of emulsified water and/or oil, clays, and solids. Sometimes, under poor processing conditions, rag layers grow large enough to cause a process upset.

This thesis is part of a study with an overall objective to understand the factors that trigger rag layer growth. In this thesis, the relationship between emulsion stability and rag layer growth was investigated using model emulsion systems. The model was developed based on the coalescence of the emulsified droplets. The methodology was first developed with relatively straightforward oil-in-water emulsions and then tested on the more challenging water-in-oil emulsions stabilized by asphaltenes which exhibit aging effects. To determine the coalescence rates of the model oil-in-water emulsions, batch experiments were performed with emulsions prepared from an aqueous phase consisting of reverse osmosis water with NEO-10 surfactant and an organic phase as 50_heptol (50 vol% toluene, and 50 vol% heptane) at the temperature of 45°C and with a mixer speed of 800 rpm. After mixing, the emulsion was allowed to coalesce and the heights of the emulsion, free oil and water layers were measured over time.

The time dependent coalescence rates were determined from the change in heights of the emulsion and free oil layer over time. Continuous experiments were also performed where the emulsion was continuously fed to the separator until a steady state condition was reached. Then, the feed was shut off and the decrease in emulsion layer height was measured over time and this part was called as the decay experiment. The decay experiments were also modeled to find the coalescence rates.

The coalescence rate was found to decrease exponentially with time. The decrease was not caused by a change in drop size distribution which remained invariant over time. The decrease in coalescence rate was found to correlate with the thinning of the continuous aqueous phase film between the oil droplets. It was speculated that the surfactant released from prior coalescence remained trapped in the film and enhanced the stability of the emulsion. Gentle mixing of the emulsion layer to liberate trapped surfactant caused a lasting increase in the coalescence rate.

It was found that the initial coalescence rate determined from a decay experiment could be used to predict the steady state emulsion layer height measured in continuous experiments. To check the predictive capability of the model, experiments were performed at different flow rates and model was able to predict emulsion layer growth using the known coalescence rate.

The effect of separator geometry was also studied by changing the separator diameter and volume. It was observed that coalescence is faster in the larger diameter separator than in the smaller diameter separator. The difference in coalescence rate was attributed to wall effects. A series of batch experiments were performed to assess the wall effect and it was found that as the surface area/volume (SA/V) ratio increased, the coalescence rate decreased; that is, the smaller the diameter, the lower the coalescence rate.

This study provides the first step to understand the rag layer growth and presents a methodology for relating rag layer growth to coalescence rates. Some experiments on asphaltene stabilized water-in-oil emulsions were also performed and were modeled with this methodology. These experiments were preliminary studies on water-in-oil emulsions which provide a base line for future studies on the role of precipitated asphaltenes and inorganic solids in rag layer growth in oil sands separation.

ACKNOWLEDGEMENTS

First and foremost, I am deeply indebted to my supervisor, Dr. H.W. Yarranton for his constant guidance, support and encouragement during my Master's degree program. It was my privilege and pleasure to be a member of his research group.

I also wish to thank Ms. Elaine Baydak, Jorge Andrade and Florian Schoeggl for their assistance and the great help during my Masters thesis.

I am thankful to the Department of Chemical and Petroleum Engineering, Faculty of Graduate Studies at the University of Calgary for their assistant, NSERC and Syncrude Canada Ltd. for their financial support throughout my Masters program.

I am grateful to Aakanksha Kalla, Karthik Lakshminarayanan, Aswin Hari, Diana Ortiz, Pawan Agrawal, Asphaltene and Emulsion Research group members at the University of Calgary and fellow graduate students for their encouragement and support.

Finally, from the deepest of my heart, I would like to thank my family for their constant support and encouragement. I am really grateful for their caring and understanding.

Dedication

To my Brother Ramesh Khatri and Sister Mamta Khatri

TABLE OF CONTENTS

LIST OF TABLES

LIST OF FIGURES

LIST OF SYMBOLS

A	Cross sectional area of the settler/separator
c	Decay constant
c_1, c_2	Constants
c_3, c_4	Constants
d_i	Diameter the droplets at the coalescing interface when the entire dispersion column is dense-packed
h	Emulsion layer height
h_o	Height of free oil layer
h_p	Height of dense-packed zone in batch settler
H_p	Steady state sedimentation zone height in continuous settler
h_s	Height of sedimentation zone in batch settler
H_s	Steady state sedimentation zone height in continuous settler
h_t	Total dispersion height in batch settler
h_{to}	Initial total dispersion height in batch settler
H_t	Total steady state dispersion height in continuous settler
h^o	Initial height of the emulsion layer during the batch experiment/Steady state emulsion layer height during the continuous experiment
$h_o^{\ o}$	Height of the free oil at the beginning of the batch experiment/Total oil liberated during the decay experiment
$k(t)$	Coalescence rate constant
k_{1B}, k_{2B}	Constants during batch dispersion
k_{1C}, k_{2C}	Constants during continuous dispersion
k_o	Initial coalescence rate constant
k_i, k_p	Constants
K_s, k_s'	Constants

k_s	Final coalescence rate constant
M_{fo}	Mass of the oil in free oil layer
M_o	Mass of oil in the emulsion layer
$\dot{m}_o$	Rate the oil is exiting the emulsion layer due to coalescence
$\dot{m}_{oi}$	Rate the emulsified oil is entering in the separator through the feed
Q_c	Continuous phase volumetric flow rate
Q_d	Dispersed phase volumetric flow rate
R	Ratio of volumetric flow of continuous phase to the dispersed phase
r_v^*	Dimensionless asymmetrical film radius
t	Elapsed time/droplet residence time
t_f	Measured separation time for the dispersion
t_*	Time when entire dispersion column becomes dense-packed
V	Volume of emulsion layer
$\dot{V}_{in}$	Flow rate of the feed to the separator
V_o	Volume of free oil layer
V_s	Relative sedimentation zone velocity in continuous settler during steady state
V_o^o	Volume of free oil at the beginning of the batch experiment
x	Position of sedimenting interface with respect to final undisturbed interface
x_o	Initial position of sedimenting interface with respect to final undisturbed interface
y	Position of coalescing interface with respect to final undisturbed interface
y_o	Initial position of coalescing interface with respect to final undisturbed interface
y_*	Position of coalescing interface with respect to the final undisturbed interface when the entire column becomes dense-packed
z	Locus of boundary between the sedimentation and dense-packed zones

Greek Letters

β	Constant, depends on circulation of phases and geometry of the settler
ρ_o	Density of the oil
τ	Lifetime of the film
τ_i	Coalescence time of droplets at the coalescing interface when the dispersion becomes dense-packed
ϕ_i	Fraction of dispersed phase at the coalescing interface
ϕ_F	Dispersed phase fraction in the feed dispersion
$\bar{\phi}$	Space time averaged dispersed phase hold-up
ϕ_o	Emulsified oil volume fraction
$\phi_o(t)$	Emulsified oil volume fraction during batch experiment at time t
ϕ_{oo}	Experimental value of initial oil volume fraction during batch experiment
ϕ_p	Dispersed phase fraction in the dense-packed zone
ϕ_s	Dispersed phase fraction in the sedimentation zone
ϕ_{so}	Initial dispersed phase fraction in the sedimentation zone
$\phi_o^{\ o}$	Emulsified oil volume fraction in the feed
$\phi_p^{\ *}$	Dispersed phase fraction in the dense-packed zone when sedimentation ceases
ψ	Dispersed phase throughput per unit area

Subscripts

B	Batch
c	Continuous phase
C	Continuous settler
d	Dispersed phase
f	Final
F	Feed
i	Coalescing interface
o	Oil
p	Dense-packed zone
s	Sedimentation zone
t	Total
to	Initial total
*	Inflection point

Superscripts

d	Coalescence
o	Feed oil
p	Dense-packed
s	Sedimentation

Abbreviation

AOT	Sodium bis (2-ethylhexyl) sulfosuccinate
Heptol	Mixture of heptane and toluene
NEO-10	Nonylphenol ethoxylate with 10 ethoxy groups in the molecule
RO	Reverse Osmosis

CHAPTER 1
INTRODUCTION

Crude oil is almost always produced with water from the reservoir whether from in situ or mined deposits. The water and oil must be separated before the oil is transported. The separation often requires heat and chemical treatment because, during production, both oil-in-water and water-in-oil emulsions are created and they must be broken to achieve a good separation. In practically all separation vessels, a thick viscous layer forms at the oil-water interface. This ill-defined thick material is known as a rag layer (Czarnecki *et al.*, 2007) and is comprised of emulsified water and/or oil, asphaltenes, clays and solids. In crude oil/water separations, water-in-oil emulsions appear to cause the more problematic rag layers. Rag layers are undesirable because they reduce separation efficiency and can upset the process.

The rag layer is an issue especially in oil sand separation processes where the presence of clays and other solids can make these layers grow faster compared with rag layers in conventional oil separation processes. Currently there are two widely used froth treatment processes for separation of oil from oil sands (Romanova *et al*., 2004): 1) the Syncrude Process where froth is diluted with naphtha and then centrifuged to remove the water and solids; 2) the Paraffinic Froth Treatment Process where froth is diluted with a paraffinic solvent and gravity settled to remove water, solids, and precipitated asphaltenes. In both treatment processes, rag layer formation can be observed due to the presence of the water-in-oil emulsions and also further stabilization of these emulsions by clays and fine solids (Chen *et al*., 1999; Jiang *et al.*, 2008). Figure 1.1 shows a typical rag layer during oil water separation processes.

With increasing oil sands production and the depletion of high quality oil sand deposits, it is becoming necessary to process lower quality oil sands. In poor processing conditions during oil-water separations, rag layers can grow so thick that they affect the separation. If the rag layer overflows into the oil stream, then impurities like water and solids are added in the oil stream. If the rag layer mixes with the free water stream, then oil recovery is reduced (Saadatmand *et al.*, 2008). To avoid rag layer accumulation, it is necessary to understand the mechanisms for rag layer formation and factors that trigger the rag layer growth in oils sands separation processes.

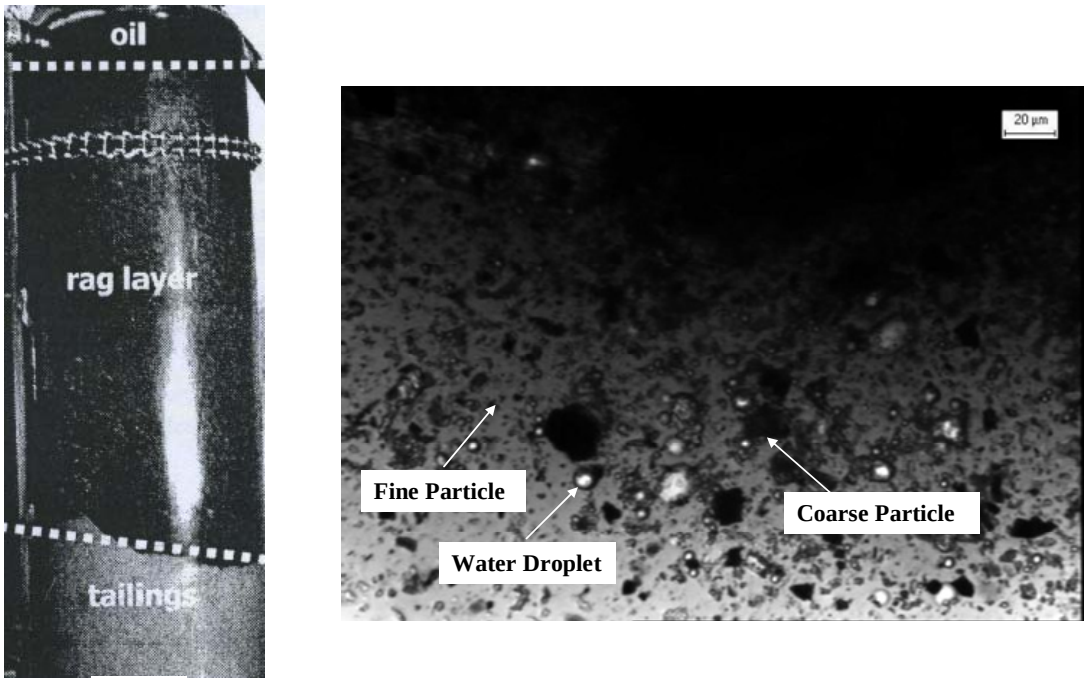

(a) (b)

Figure 1.1: (a) Photograph of a rag layer formed during the gravity separation of diluted bitumen froth in a continuous process (Moran, 2006); (b) Micrograph of the oil sand rag layer (Saadatmand, 2008).

The growth of rag layer depends on the settling/creaming and coalescence rates of the emulsified droplets. The slower the settling/creaming rate or the coalescence rate, the faster is the rag layer growth. The settling rate depends on the droplet size and the coalescence rate is function of droplet size and interfacial properties. These interfacial properties further depend on the adsorbed materials such as surfactant, asphaltenes, clay and solids (Chen *et al*., 1999; Sztukowski and Yarranton, 2005; Jiang *et al.*, 2008). Even the presence of these materials in the interfacial region can substantially reduce the coalescence. Also, sometimes large amount of clays and solids can form a mechanical barrier at the oil-water interface which subsequently prevents the droplets from passing through and coalescing with the bulk phase. When coalescence is reduced significantly, rag layers can grow so large that the process is upset (Saadatmand *et al.*, 2008).

Research on simpler liquid-liquid dispersions has progressed further and various models, based on the sedimentation and coalescence of emulsified droplets, have been proposed for these systems (Barnea and Mazrahi, 1975; Golob and Modic, 1977; Hartland and Jeelani, 1986ab, 1987, 1988; Henschke *et al*., 2002; Lobo *et al.*, 1993; Nadiv and Semiat, 1995). However, these models do not account for the presence of clays, asphaltenes and fine solids which are likely play an important role in rag layer growth in oil sands separation processes.

To date, the factors responsible for rag layer growth in oilfield water and oil separation have not been identified. Even the baseline relationship between coalescence and rag layer growth is not well defined for these systems. In this thesis, model emulsion systems were chosen in order to have better understanding of rag layer formation and growth. These model emulsions were modeled to simulate the rag layer growth in continuous systems. Liquid-liquid dispersion with model oils can be used to simulate the separation behavior of opaque crude oils (Jeelani *et al.*, 1999).

1.1 Thesis Objectives

This thesis is part of a research program with an overall aim to understand the mechanisms for the rag layer formation in oil sands separation processes and identify the factors that triggers the rag layer growth. This thesis focuses on the relationship between emulsion layer growth and emulsion stability (the rate of coalescence). Objectives of this research are to:

- measure coalescence rates in model emulsion systems
- measure emulsion layer growth in continuous separation of the same systems
- model emulsion layer growth using the measured coalescence rates
- experimentally validate the model assumptions

Model emulsions were used to simplify the problem and isolate the effect of coalescence on emulsion layer growth. These data are intended as baselines to be used in future work to identify the effects of other factors such as solids. The emulsions consisted of an aqueous phase consisting of water and a surfactant and an organic phase consisting of heptane and toluene. Most experiments were performed on oil-in-water emulsions and some preliminary experiments were performed on water-in-oil emulsions where asphaltenes had been added to the organic phase.

Emulsion layer growth was measured in a previously developed laboratory scale continuous separator (Andrade, 2009). Coalescence rates were determined from the rate at which oil/water exited a settled emulsion both in a beaker (batch experiment) and in the separator at the conclusion of a growth experiment (decay experiment).

1.2 Thesis Structure

This thesis is structured as follows:

In Chapter 2, the background concepts on surfactants, emulsion, emulsion stabilization and destabilization are reviewed. The rag layer is defined for oil sands separation and the related emulsion layer is defined for liquid-liquid dispersions. Models for emulsion layer growth in liquid-liquid dispersions are presented. Finally, previous research on rag layers formed during oil sands separation processes is presented.

In Chapter 3, the preparation of the model emulsions is explained. The continuous separator is described and the procedures for batch, decay, and continuous experiments are presented. Experiments to determine the emulsified oil volume fractions during the continuous experiments for the model emulsions are also presented.

In Chapter 4, the methodology to determine the coalescence rates is presented. Model equations are developed for batch, decay, and continuous experiments. The model assumptions and their validation are also discussed.

In Chapter 5, the experimental and modeling results are presented. Batch and decay coalescence rates are determined and used to predict the emulsion layer growth in continuous experiments. The predictive capability of the model is discussed including the role of wall effects observed in the experiments. Finally, some preliminary results for asphaltene stabilized water-in-oil emulsions are provided.

In Chapter 6, the thesis conclusions are presented along with recommendations for future work.

CHAPTER 2
LITERATURE REVIEW

In this chapter, emulsion basics are briefly reviewed including surfactants and emulsion stabilization and destabilization mechanisms. The literature on rag layers in oil sands, rag layers in liquid-liquid separations, and existing models to simulate these rag layers is also reviewed.

2.1 Surfactants

Emulsions are often stabilized by surfactants. A surfactant or surface-active agent is a substance that, even when present at low concentration, adsorbs onto surfaces or interfaces and alters the surface or interfacial free energies. An interface is the boundary between any two immiscible phases while a surface is an interface where one phase is a gas, usually air (Rosen, 2004).

2.1.1 Surfactant Structure

Surfactants typically consist of a structural group that has a very little attraction for the solvent medium, known as lyophobic group, together with a group that has strong attraction for the solvent medium, called the lyophilic group. This is known as an amphipathic structure. When the solvent is aqueous, the lyophobic group is called hydrophobic and the lyophilic group is the hydrophilic group.

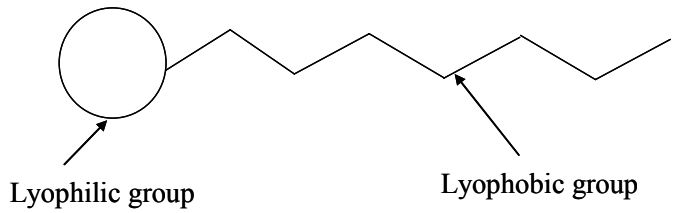

Figure 2.1: Structure of a surfactant in its simplest form (Adapted from Myers, 1992).

The hydrophobic group is usually a long-chain hydrocarbon and the hydrophilic group is a highly polar group. Depending on the nature of the hydrophilic group, surfactants are classified in the following categories:

1. Anionic: The surface active portion of the molecule bears a negative charge, for example, $RCOO^-Na^+$ (soap), $RC_6H_4SO_3^-Na^+$ (alkylbenzene sulfonate)
2. Cationic: The surface-active portion bears a positive charge, for example, $RNH3^+Cl^-$ (salt of a long-chain amine)
3. Zwitterionic: Both positive and negative charges may be present in the surface-active portion, for example, $RN^+H_2CH_2COO^-$ (long-chain amino acid)
4. Nonionic: The surface-active portion bears no apparent ionic charge, for example, $RC_6H_4(OC_2H_4)_xOH$ (polyoxyethylenated alkylphenol)

Griffin (1949) developed a method to quantitatively correlate surfactant structures with their effectiveness as emulsifiers and demulsifiers (Myers, 1992). He defined the hydrophile-lipophile balance (HLB) where the HLB number represents the geometric ratios of the hydrophilic and the hydrophobic moieties. HLB does not represent a fundamental property of the system but is based on experience (Farn, 2006). Surfactants with HLB in the range of 3-6 act as emulsifiers for water-in-oil emulsions, while surfactants with HLB in the range of 8-18 are suitable for oil-in-water emulsions (Becher, 2001). Cooper *et al.* (1980) related the HLB number of the surfactant with its ability to act as a demulsifier for heavy oil-water-clay emulsions. They found that surfactants with HLB values between either 4 and 6 or 13 and 15 were the effective de-watering agents. Surfactants with HLB above 20 were found to be very useful for clay removal. For water-in-toluene diluted bitumen emulsions, Gu *et al.* (2002) observed that water soluble natural surface active agents act as a demulsifier while water insoluble surface active agents stabilize emulsions.

2.1.2 Surfactant Behavior

When a surfactant is added in low concentration into a system of two immiscible liquids, it adsorbs on the interface and reduces interfacial free energy. At the interface, the hydrophobic tail of the surfactant molecule aligns itself to the less polar liquid while the hydrophilic head orientates itself towards the polar phase. The molecular interaction at the interface occurs between the hydrophilic head of the surfactant and the polar phase molecules and between the hydrophobic tail of the surfactant and the non-polar phase molecules. This arrangement reduces excess free energy of the system and hence the interfacial tension because the newly formed interactions are more attractive than the interactions between polar and non-polar molecules. Surfactant activity is at a maximum if the number of carbon atoms in hydrophobic tail is between 8 and 18 (Farn, 2006).

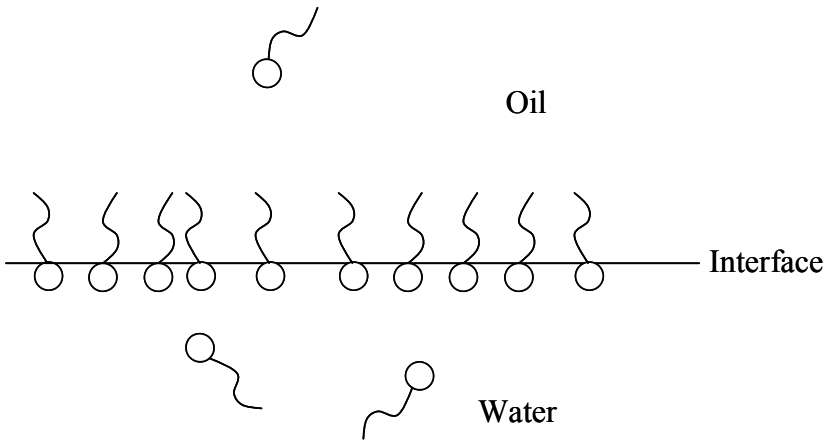

Figure 2.2: Adsorption of surfactant molecules at the oil-water interface (Adapted from Farn, 2006).

As surfactant concentration increases, surfactant monomers start to accumulate as aggregates in the bulk solution. The simplest aggregates are micelles, Figure 2.3, but may also include vesicles, liquid crystals and reverse micelles and the surfactant concentration where micelles begin to form is called the critical micelle concentration (CMC).

Above the CMC, the concentration of surfactant monomers is nearly constant and hence there are no significant changes in surfactant properties of the solution since the monomers are the cause of the surface activity. The typical CMC values at room temperature are 10^{-3} to 10^{-2} M for anionic surfactants, 10^{-3} to 10^{-1} M for amphoteric and cationic surfactants and 10^{-5} to 10^{-4} M for non-ionic surfactants. Surfactant structure, temperature, the presence of electrolyte, existence of organic compounds and the presence of a second liquid all affect the CMC (Farn, 2006).

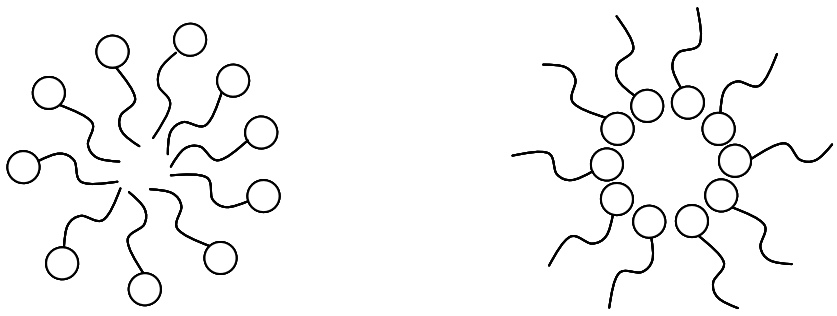

Figure 2.3: Surfactant structures at or above CMC, for both water and oil continuous phases, known as micelle and reverse micelle respectively (Adapted from Rosen, 2004).

2.2 Emulsions

An emulsion is a dispersion of one immiscible liquid in another. The phase present as finely divided droplets is called the dispersed or internal phase and the phase which forms the matrix in which these droplets are suspended is called the continuous or external phase (Becher, 2001). Some emulsions are thermodynamically stable; they have almost zero interfacial tension and are essentially swollen micelles. They are termed micro-emulsions. Most emulsions are macro-emulsions which consist of larger droplets with non-zero interfacial tension. Macro-emulsions are thermodynamically unstable but can be

kinetically stable over long periods of time. This review focuses on macro-emulsions only.

There are two main types of emulsions: water-in-oil emulsion where water is the dispersed phase (W/O) and oil-in-water emulsion where oil is the dispersed phase (O/W). Sometimes multiple emulsions like oil-in-water-in-oil (O/W/O) or water-in-oil-in-water (W/O/W) are also formed. Emulsions do not form spontaneously and require turbulence or shear to form. Once formed, emulsions tend to break back into the constituent bulk phases unless an agent such as a surfactant stabilizes the emulsion. For example, water-in-crude oil emulsions are stabilized by asphaltenes, clays and other solids (Kiran *et al.*, 2009, Sztukowski and Yarranton, 2005).

2.2.1 Emulsion Stabilization

Emulsions are thermodynamically unstable but the presence of an emulsifier (surfactants, asphaltenes, biwetted clays, solids) can make emulsions kinetically stable. The two main stability mechanisms are electrostatic and steric stabilization.

With electrostatic stabilization, the adsorbed emulsifier generates an electric charge on the surface of the droplets. The charge is neutralized by counter ions in the aqueous phase. If the counter ions are diffuse, the particles that closely approach have a net local charge and these equal charges create a repulsive force between the droplets (Fredrick *et al.*, 2009) and hence stabilize the emulsions. The charged surface and the surrounding layer of counter ions is known as the electric double layer (Heimenz and Rajagopalan, 1997). Electrostatic stabilization is significant for O/W emulsions where water is the continuous phase.

Another kind of stabilization is steric stabilization which usually results when high molecular weight materials such as polymers adsorb on the interface. The adsorbed polymers on different droplets begin to entangle, preventing close approach of droplets to

each other and hence stabilize emulsions. Solid particles can also stabilize emulsions by preventing close contact of the droplets.

In all cases, emulsion stability is sensitive to a number of factors including surfactant concentration, temperature, and droplet size distribution.

2.2.1.1 Stabilization of Crude Oil Emulsions

Water-in-oil emulsions are a contributing factor to rag layers in the oil industry and asphaltenes are commonly identified as the agent responsible for stabilizing these emulsions (Gu *et al.*, 2002; McLean and Kilpatrick, 1997; Sztukowski *et al.*, 2003; Yarranton *et al.*, 2000; Yarranton *et al.*, 2007). Asphaltenes are the fraction of the crude oil which is soluble in toluene, but insoluble in n-alkanes. Asphaltene molecules are large polyaromatic hydrocarbons with various heteroatom functional groups and have monomer molar masses in the order of 1000 g/mol (Yarranton *et al.*, 2000). Asphaltenes are known to self-associate into nano-aggregates with average molar masses in the order of 4000 to 10000 g/mol (Yarranton *et al*., 2000).

Asphaltenes form an irreversibly adsorbed insoluble monolayer at the oil-water interface (Freer and Radke, 2004; Sztukowski *et al*., 2003). Yarranton *et al*. (2007) showed that this irreversibly adsorbed film is compressed during coalescence. As it is compressed, it provides more resistance to coalescence and eventually stabilizes the emulsion.

Along with asphaltenes, solids naturally found in crude oils and bitumen is also a major factor for emulsion stabilization and rag layer formation (Sztukowski and Yarranton, 2005; Yan *et al*., 2001). Pickering (1907) was the first to discover that solids can stabilize emulsions when he found that colloidal particles wetted more by water than oil can act as an emulsifier for oil-in-water emulsions. Graham (1988) found that water-in-crude oil emulsions are stabilized by solids which are oil soluble. Yan *et al.* (2001) observed that stability of emulsions depend on the hydrophobicity of solid particles. They observed that

hydrophobic colloidal silica could only produce oil-in-water emulsions if it was suspended in aqueous phase prior to emulsion. Only particles with intermediate hydrophobicity could produce stable water-in-oil emulsions.

Tambe and Sharma (1993) observed that solid particles stabilize emulsions both by providing steric hindrance to the emulsion droplets and also by changing the rheological properties of the interface. They also showed that the presence of inorganic solids in the aqueous phase seems to decrease the stability of oil-in-water emulsions. Gu *et al*. (2002) found that when asphaltenes combine with fine solids then emulsion stability is increased significantly. Sztukowski and Yarranton (2005) found that for emulsions stabilized by asphaltenes and fine clays (50 to 500 nm), there was a maximum in emulsion stability as clay concentration increased. They also found that emulsions stabilized by coarse solids of 1-10 μm size were unstable at low solid concentrations, but were very stable at concentrations above 10 kg/m³.

2.2.2 Emulsion Destabilization

2.2.2.1 Emulsion Destabilization Mechanisms

Macro-emulsions are thermodynamically unstable; however, they can be metastable. Emulsions can be destabilized through various different breakdown processes shown in Figure 2.4. These processes may take place simultaneously or consecutively.

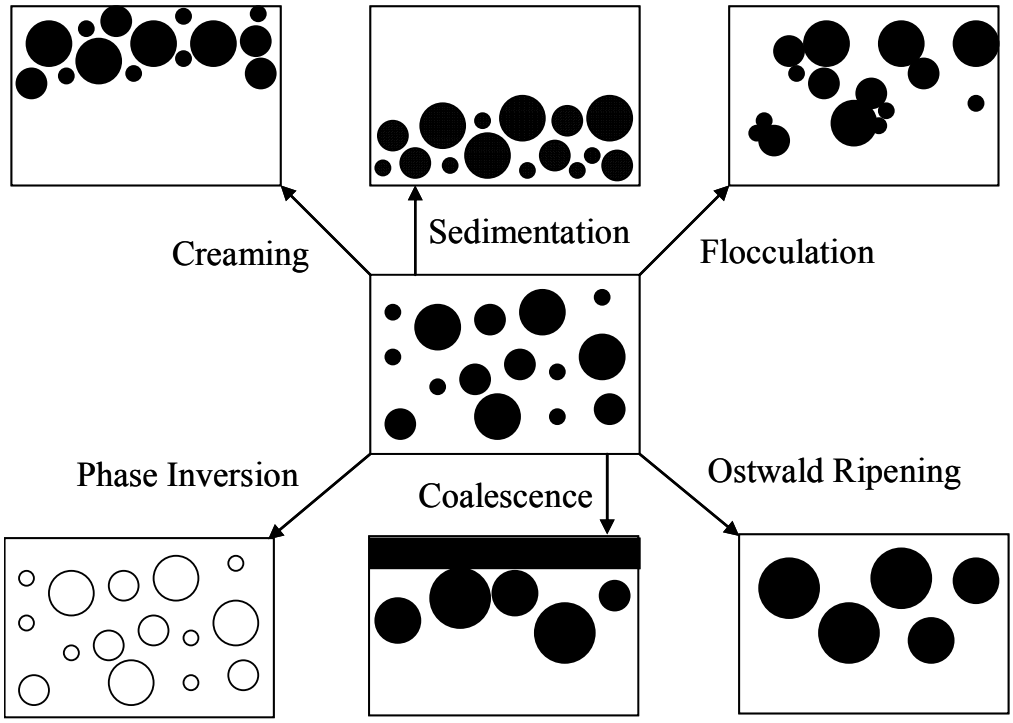

Figure 2.4: Schematic representation of various breakdown processes in emulsion (Adapted from Tadros, 2009).

Creaming and Sedimentation

Creaming and sedimentation occur independently from droplet-droplet interactions and the size distribution of the emulsion droplets does not change (Binks and Horozov, 2006). Creaming/sedimentation usually results from external forces such as gravitational and centrifugal forces acting on the density difference between the continuous and dispersed phases. In the case of a W/O emulsion, the denser water droplets sediment at the bottom but, in the case of an O/W emulsion, lighter oil droplets cream at the top (Tadros, 2009). Creaming/sedimentation can be slowed down by reducing the density difference between two phases, by thickening the continuous phase or by reducing the droplet size (Farn, 2006).

Flocculation

Flocculation is the aggregation of droplets without changing the original size of the droplet (Tadros, 2009). Flocculation can occur only if there is a large enough attraction between the droplets to overcome the thermal agitation or repulsive forces, so that droplets can remain as an aggregate (Binks and Horozov, 2006). The flocculation process is partially reversible (Singh, 1994). Flocculation can be strong or weak depending on the magnitude of attractive and repulsive forces between the droplets.

The plots in Figure 2.5 show the net interaction energy between droplets resulting from Van der Waals attractive forces and electrostatic and steric repulsive forces. In case (a), Van der Waals forces overcome the restoring electric double-layer force, and the interaction energy is negative. Hence, attractive forces are dominant compared to repulsive forces at all distances of separation and the emulsion droplets will tend to reside in the primary minimum; that is, where the energy of the system is minimized. This condition is sometimes referred to as coagulation and is a necessary step towards the coalescence of droplets. This case is the most favorable for emulsion destabilization.

In case (b), the interaction energy goes through a shallow minimum (i.e., secondary minimum) at large separation distances between droplets, a maximum at relatively small separation and a deep minimum (i.e., primary minimum) at very small separations. If the repulsive energy barrier between the primary and secondary energy minimum is large enough, droplets will tend to reside in the secondary minimum. This condition is referred to as flocculation. Such systems are considered metastable because the droplets are kinetically stable in a local rather than a global energy minimum.

In case (c), the interaction is positive for all separation distances between droplets, indicating that repulsive forces are stronger than attractive forces. In this case, repulsive forces prevent droplets from approaching each other and coagulating. The emulsion would be very stable in such a case.

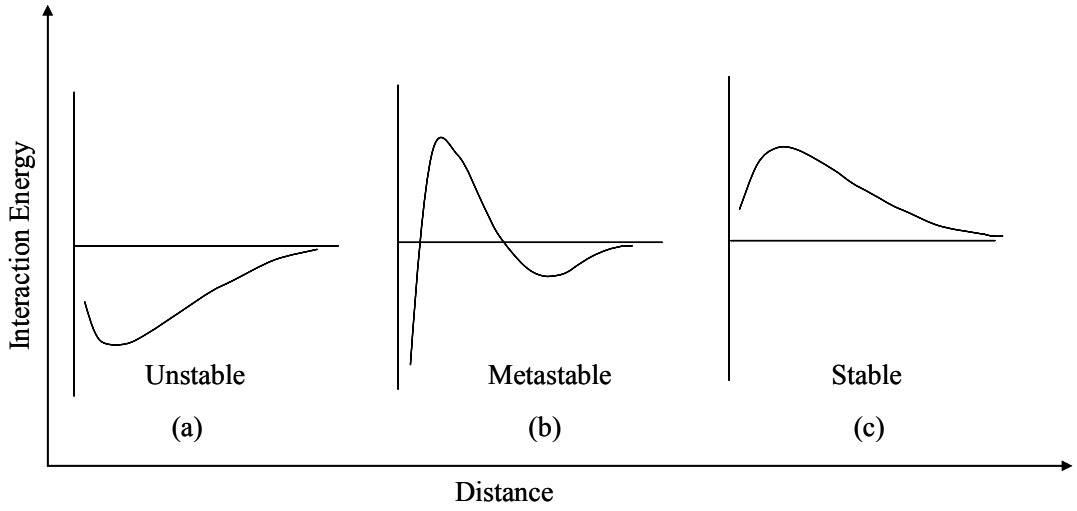

Figure 2.5: Potential energy curves for the interaction of two colloidal particles. Negative values correspond to attraction and positive values to repulsion: (a) repulsion is less than attraction; (b) repulsion and attraction are comparable in magnitude and range; (c) attraction is less than repulsion (Adapted from Heimenz and Rajagopalan, 1997).

Ostwald Ripening

The Ostwald ripening process is gradual growth of larger droplets at the expense of smaller ones by means of diffusion (Kabalnov and Shchukin, 1992; Tadros, 2009). The solubility of the dispersed phase in the continuous phase is greatest at a curved interface and the greater the curvature, the greater the solubility. Hence, the solubility is higher at the surface of smaller droplets and there is a concentration gradient from small to large droplets. This concentration gradient drives mass transfer from small to large droplets.

This destabilization technique is important for the cases where emulsions are stabilized against coalescence. Ostwald ripening results in lowering of the overall interfacial energy because larger droplets have a smaller surface area to volume ratio (Binks and Horozov, 2006).

Coalescence

Coalescence is the thinning and rupturing of liquid films between a pair of droplets and the subsequent fusion of the droplets. The limiting case for coalescence is complete separation of the emulsion into two distinct phases (Tadros, 2009). The coalescence process takes place in several steps (Barnea and Mizrahi, 1975; Frising *et al.*, 2006; Lobo *et al.*, 1993; Sztukowski and Yarranton, 2005), Figure 2.6:

1. Approach of droplets to within the near molecular dimensions.
2. Deformation and dimpling to form a planer interface between the droplets which results in the drainage of the continuous phase from the planar region, thinning the film.
3. Bridging between the droplets almost instantly causing irreversible fusion into a single droplet.

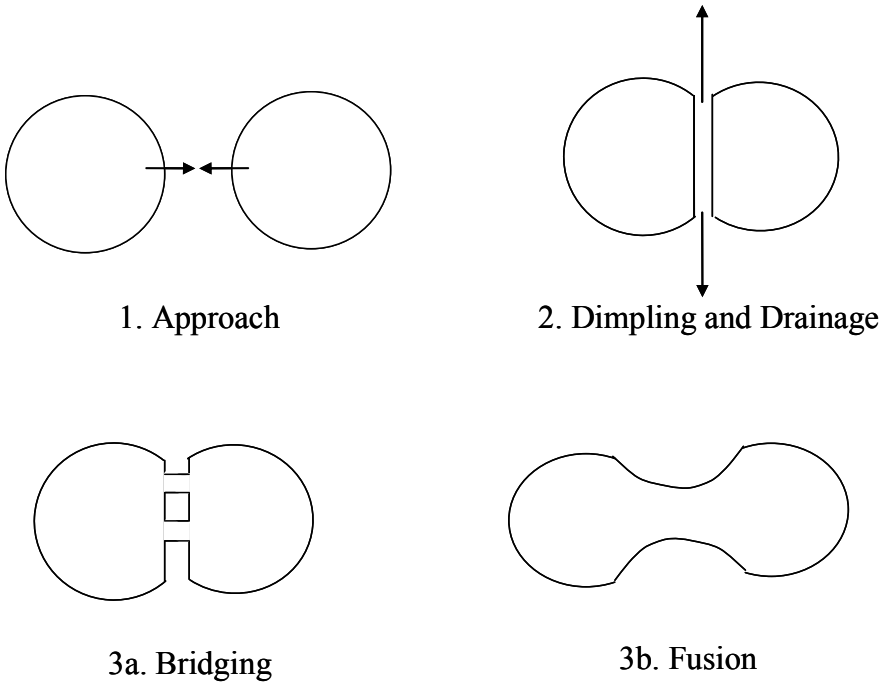

Figure 2.6: Schematic representation of coalescence process.

Coalescence is an irreversible process, resulting decrease in the number of droplets and eventually to the complete separation of phases (Singh, 1994). The rate of coalescence depends on the encounter rate between droplets and the properties of the droplets' surface (Binks and Horozov, 2006).

Phase Inversion

During this process there is an exchange between the dispersed and the continuous phases. With time or a change in conditions, one type of emulsion can change to the other; for example, a W/O emulsion may invert into an O/W emulsion. During this transition, multiple emulsions may also be observed. Factors like temperature, electrolyte concentration, and change in dispersed phase fraction can lead to phase inversion (Tadros, 2009).

2.2.2.2 External Factors for Emulsion Destabilization

Unaided demulsification is not usually effective in industrial separations. The demulsification rate can be increased using chemical, thermal, mechanical or electrical methods.

Chemical

Chemical treatment of an emulsion involves the addition of demulsifier to destabilize the emulsion. Demulsifiers are usually surface active agents which replace the existing emulsifiers present at the film sometimes to increase flocculation and sometimes to weaken the film and increase coalescence (Frising *et al.*, 2006; Singh, 1994). Addition of chemical demulsifier is the most common method for dealing with petroleum emulsions. If asphaltenes are adsorbed at an interface in a petroleum emulsion, a good demulsifier will need to effectively displace asphaltenes from the interface (Ortiz, 2009). Such demulsifiers usually partition effectively between the oil and aqueous phases and produce a low interfacial tension (Kim and Wasan, 1996). Selection of a suitable demulsifier and

dosage is very important as improper use can degrade their performance or even increase emulsion stability (Czarnecki *et al*., 2007).

Factors such as pH and temperature can influence demulsifier performance. Increased temperature reduces emulsion stability so that an emulsion can be broken with a lower dose of demulsifier. For petroleum emulsions, it has been observed that oil-in-water emulsions were produced at alkaline pH while water-in-oil emulsions were generated at acidic pH (Schramm, 1992). At extreme pH's, addition of acids or bases brings the pH to the neutral range where the maximum emulsion breaking is observed (Strassner, 1968) and hence reduces the amount of demulsifier required.

Thermal

Thermal methods have proven to be very beneficial for crude oil-water separation, although the effectiveness depends on crude oil properties (Strøm-Kristiansen *et al*., 1995). The addition of heat reduces the viscosity and density of the oil, increasing the sedimentation/creaming rate (Schramm, 1992; Singh, 1994). Heating weakens and ruptures the interfacial film between oil and water leading to increased coalescence.

Mechanical

Mechanical obstacles in the path of a flowing emulsion increase droplet collisions and therefore coalescence rates (Frising *et al.*, 2006). Many different configurations can be used such as grids, baffles, fibrous beds and membranes. Ultrasonication has also proven to be very effective for demulsification of relatively stable petroleum emulsions (Singh, 1995). However, this technique is only in the initial stages of development on a commercial level. High speed centrifugation could also be used as effective tool for oil-water separation in oil industry (Bourassin, 1985).

Electrical

The electric field is also useful in oil-water separation. An electric field can induce a charge on the droplets that weakens the interfacial film and improves agglomeration and coalescence (Frising *et al.*, 2006). Taylor (1988) showed that for water-in-crude oil emulsions in the presence of the high voltage electric field, droplets coalescence occurred in two different ways depending on the compressibility of the interfacial films. For incompressible films, the electrical field induced dipoles on the droplets causing the droplets to form chains. Chain formation resulted in faster gravity settling but the coalescence was limited due to incompressible interfacial films. For compressible films, the electric field facilitated droplet-droplet coalescence as the droplets aligned along field lines. Droplet-droplet coalescence was too rapid for chains formation to occur.

The separation due to electric field depends on many factors such as the strength and frequency of the electric field, droplet sizes, composition of crude oil, and the hydrodynamic conditions. This process is particularly valuable where space is of major consideration, because the use of an electric field accelerates the settling much faster than heating, therefore allowing working with small dimension vessels (Schramm, 1992).

2.3 Rag Layers

2.3.1 Rag Layer Definition

Figure 2.7 shows a simplified view of a rag layer during oil sands separation processes. The rag layer is typically a mixture of flocculated water/oil droplets, fine solids and emulsified oil and water sometimes including multiple emulsions. In any settling vessel, both flocs and emulsion droplets will sediment/cream to the water-oil interface and will accumulate there until they coalesce because their density is intermediate between the two bulk phases (Czarnecki *et al.*, 2007). Natural organic constituents, such as asphaltenes, can adsorb at the oil-water interface to help form relatively rigid skins that prevent the droplets from coalescing with the neighboring bulk phase as well as between

the droplets. Also both fine and coarse solids and clays can become trapped in this accumulated sticky mixture, further reducing coalescence. It is the interfaces between these different constituents that will determine the rag layer properties (Czarnecki *et al.*, 2007). There is very little known about these rag layers to date, largely because it is challenging to take undisturbed samples of rag layer out of industrial separation vessels for further study.

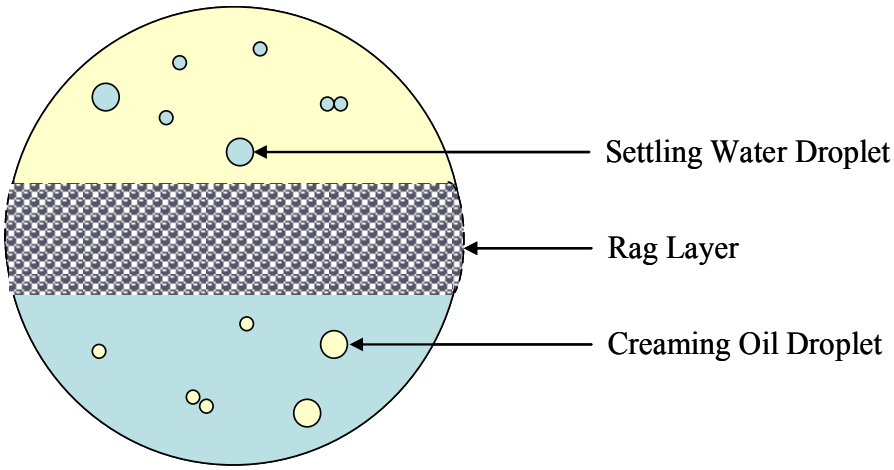

Figure 2.7: Simplified representation of a rag layer in oil sand separation processes.

2.3.2 Emulsion Layer in Model Emulsion Systems

Few studies have been done to describe oil sand rag layers in continuous processes. More work has been done on emulsion layers in liquid-liquid separations. Emulsion layers usually do not contain solids and are not as stable as rag layers. Nonetheless, the accumulation of emulsion at the oil-water interface in model emulsion systems is similar to rag layers in crude-oil water separations, in that a layer of emulsion with intermediate density resides between the pure light and dense phases. In this section, the basic concepts in emulsion layer formation and some mathematical models are presented.

Figure 2.8 shows the three zones that form in a settling dispersion (Barnea and Mizrahi, 1975; Dalingaros *et al.*, 1987; Hartland and Vohra, 1979; Hartland and Jeelani, 1985; Hartland and Jeelani, 1987; Jeelani and Hartland, 1986a; Jeelani *et al.*, 2005) and they are defined as follows:

I. Flocculating Zone: In this zone, droplets sedimenting (Figure 2.8a) or creaming (Figure 2.8b) form aggregates but individual droplets do not change diameter. This zone may or may not exist in all liquid-liquid separation processes.
II. Sedimenting or Creaming Zone: In this zone, droplets (or floccs) are closer together than in the flocculating zone but further apart than in the dense-packed zone. The dispersed phase fraction or holdup can vary from 0.5 to 0.75. Droplets move relative to each other and are deformed by interdrop collisions.
III. Dense-Packed Zone: In this zone, the dispersed phase fraction or holdup may vary from 0.75 to 1. The droplets do not move relative to each other except through interdrop coalescence and gravitational forces are transmitted from droplet to droplet. In this zone droplets at the interface coalesce with their own bulk phase through interfacial coalescence.

In liquid-liquid dispersions, the rate of droplet sedimentation is a function of droplet size, dispersed phase holdup and also circulation of pure phases in the case of continuous dispersion. The rate of interfacial coalescence is a function of droplet size at the coalescing interface and the height of the dense-packed zone, the latter affecting the gravitational forces pressing the draining film beneath the droplets at the coalescing interface (Hartland and Vohra, 1979; Hartland and Jeelani, 1987, 1988; Jeelani and Hartland, 1986).

The height of the sedimentation zone depends on the droplet size, holdup of the dispersed phase, binary coalescence in this zone and also holdup of dispersed phase in the feed in case of the continuous settler. The height of dense-packed zone depends on the droplet

size at the coalescing interface and also on the dispersed phase throughput for continuous system. At any point in time, the total dispersion height is the sum of the heights of both the sedimentation and dense-packed zones.

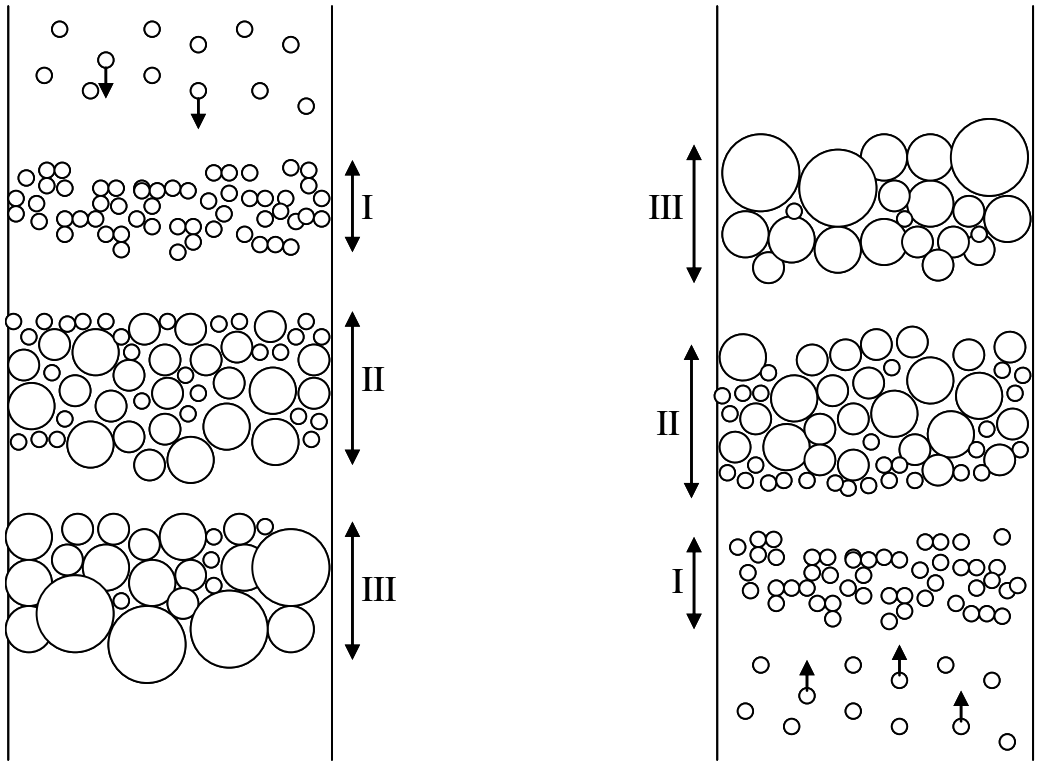

Figure 2.8: Arrangement of droplets in steady state close-packed dispersion. (a) Dense phase is dispersed phase; (b) Light phase is dispersed phase (Reproduced and modified from Hartland and Vohra, 1979).

Hartland and Jeelani (1987, 1988) showed that in a batch dispersion, sedimenting droplets grew in size due to interdrop coalescence before they enter the dense-packed zone, where they finally coalesced with their bulk phase at the coalescing interface. They also observed that in the batch settler, the height of the dense-packed zone initially increased when the sedimentation rate was faster than interfacial coalescence, but decreased once the sedimentation was complete and interfacial coalescence dominated. The heights of the sedimentation and dense-packed zones in a batch settler can be predicted from the profiles of sedimenting and coalescing interfaces (Hartland and Jeelani, 1987). Figure 2.9 shows the sedimentation and dense-packed zone heights in a batch dispersion at different times.

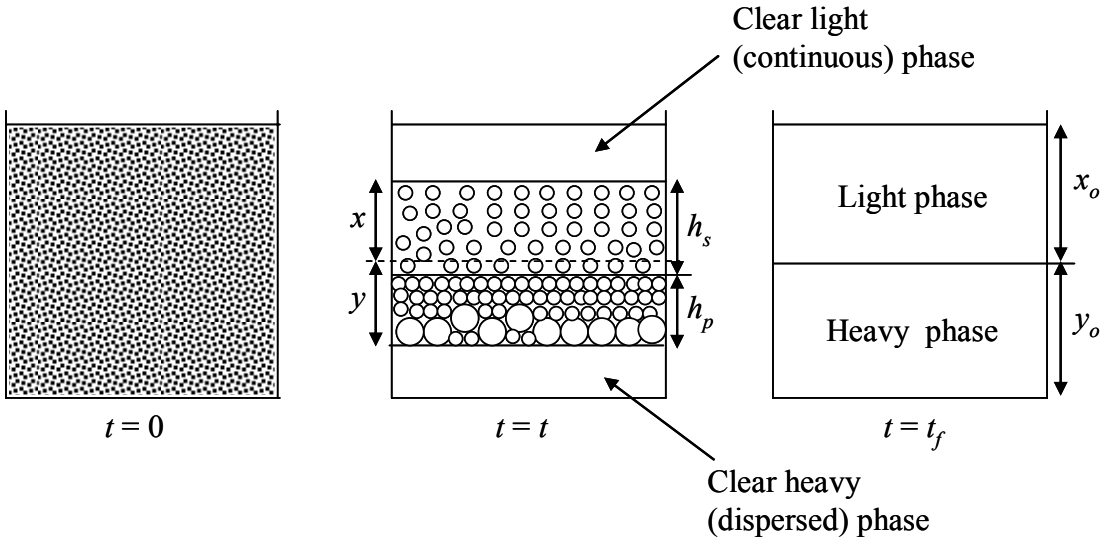

Figure 2.9: Representation of unsteady state batch dispersion showing development of sedimentation and dense-packed zones (Reproduced from Hartland and Jeelani, 1987).

Hartland and Jeelani (1987) observed that batch sedimentation and coalescence profiles were either sigmoidal or exponential in shape. When one or both were sigmoidal, then total height followed the sigmoidal profile but, if both sedimenting and coalescing

profiles were exponential (or one was exponential and the other was virtually non existent), then the overall curve followed the exponential shape. Figure 2.10 shows the sedimentation and coalescence profiles in a batch dispersion.

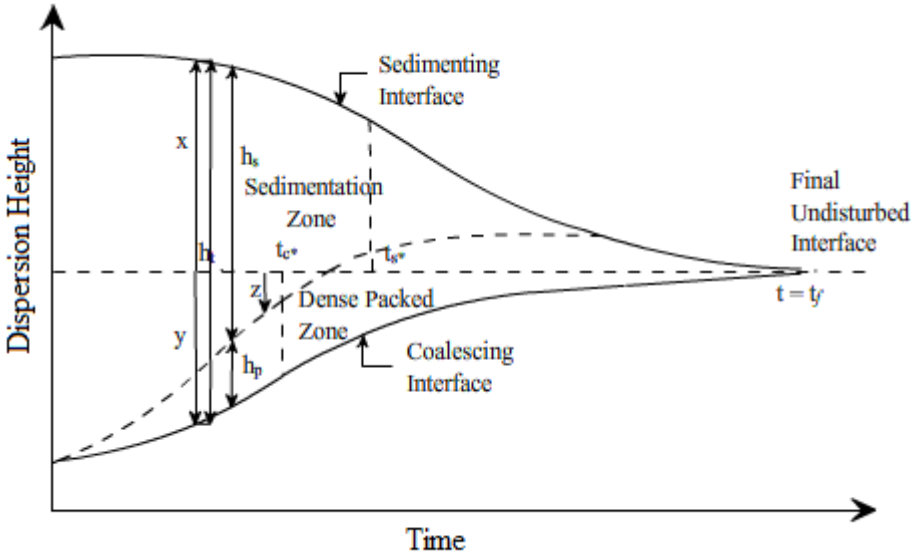

Figure 2.10: Schematic illustration of sedimenting and coalescing interfaces over time in an unsteady state batch separation; Also shown are the sedimentation and dense-packed zone heights, h_s and h_p, respectively (Reproduced from Hartland and Jeelani, 1987).

For the continuous settler, the height of the dispersion increases with time until the steady state is reached. At steady state the volume rate of droplet sedimentation and interfacial coalescence become equal to the volume throughput of the dispersed phase into the settler (Jeelani and Hartland, 1985; Hartland and Jeelani, 1987). At steady state the heights of these zones can be of similar magnitude or one of the zones can be of negligible height (Hartland and Jeelani, 1987). If the droplets in the feed dispersion are large, then their sedimentation rate would be faster than the dispersed phase throughput

and resulting in a sedimentation zone at steady state of negligible height (Godfrey *et al.*, 1979). On the other hand, if the droplets in the dispersion feed are very small, then they sediment at slower rate compare to the dispersed phase throughput, but coalesce quickly at the coalescing interface making a dense-packed zone height zero. The residence time of droplets in sedimentation zone is long enough that they grow in size, such that their volume rate of sedimentation becomes equal to dispersed phase throughput at steady state (Vieler *et al.*, 1979).

The third case, which lies between the two scenarios mentioned above, is where the droplets are moderately small in size so that both sedimentation and coalescence zones exist together. In this case droplets have the necessary residence time to grow through binary coalescence, move to dense-packed zone and finally coalesce with their homophase. Most of the previous work in the field of liquid-liquid dispersion falls under this category (Ryon *et al.*, 1960; Barnea and Mizrahi, 1975b; Jeelani and Hartland 1986ab; Hartland and Jeelani, 1987).

2.3.3 Liquid-Liquid Dispersion Models

Gravity settlers are the most common technology to separate dispersions (Frising *et al.*, 2006) and the two major mechanisms involved are droplet coalescence and droplet sedimentation. There are various models cited in literature for liquid-liquid dispersions; however, most are purely hydraulic in nature and they do not account for system chemical composition or intermolecular interactions (Frising *et al.*, 2006).

Kynch (1952) was first to describe the liquid-liquid dispersion separations in wastewater treatment primary settlers where he considered the sedimentation of flocculated particles. Most of the models presented are based on Kynch's theory and they mainly take two different approaches (Frising *et al.*, 2006) as follows:

- Sedimentation based models: Models which emphasize sedimentation of droplets as well as interfacial coalescence.

- Coalescence based models: Models which focus on binary coalescence.

2.3.3.1 Sedimentation Based Models

Extensive amount of work had been done by Hartland and colleagues in the field of liquid-liquid dispersion modeling using sedimentation based models. Various authors studied the unsteady state batch dispersions including Barnea and Mazrahi (1975), Golob and Modic (1977), Hartland and Jeelani (1986ab, 1987, 1988), Nadiv and Semiat (1995), Ryon *et al.* (1960). Barnea and Mazrahi (1975) modeled the dispersion based on hindered settling and interdrop coalescence. Hartland and Jeelani (1987, 1988) provided the most detailed modeling of liquid-liquid dispersions.

2.3.3.1.1 Batch Dispersion

Hartland and Jeelani (1988) developed the theoretical model for unsteady state dispersions. As shown in Figure 2.10, h_s, h_p and h_t are the heights of the sedimentation, dense-packed and total dispersion zones, x and y are the positions of sedimenting and coalescing interfaces with respect to final undisturbed interface at any time t. The profiles of the sedimenting and coalescing interfaces shown in Figure 2.10 can be written as a variation of x and y with respect to time and consequently the volume rates of release of free continuous and dispersed phases per unit settler area being $-\frac{dx}{dt}$ and $-\frac{dy}{dt}$, respectively.

Volume balances per unit settler area resulted in the following profiles:

$$h_t = x + y = h_s + h_p \qquad \text{Equation } \mathbf{2.1}$$

Assuming the continuous and dispersed phase volumes present in the dispersion are proportional to *x* and *y*, then the dispersed phase fraction or hold-up is $\phi = \frac{y}{h_t}$. The instantaneous position of sedimenting and coalescing interfaces at any time can be written as (Jeelani and Hartland 1985, 1986a; Hartland and Jeelani, 1987):

$$y = \phi_s h_s + \phi_p h_p \qquad \text{Equation } \mathbf{2.2}$$

$$x = (1 - \phi_s) h_s + (1 - \phi_p) h_p \qquad \text{Equation } \mathbf{2.3}$$

where ϕ_s and ϕ_p are dispersed phase hold-up or fraction in the sedimentation and dense-packed zones, respectively. The height for sedimentation and dense-packed zones then becomes,

$$h_s = \frac{(\phi_p h_t - y)}{(\phi_p - \phi_s)} \qquad \text{Equation } \mathbf{2.4}$$

$$h_p = \frac{(y - \phi_s h_t)}{(\phi_p - \phi_s)} \qquad \text{Equation } \mathbf{2.5}$$

The dense-packed zone height can provide the locus of the boundary between the sedimentation and dense-packed zones, given by,

$$z = y - h_p = \frac{[\phi_s x - (1 - \phi_p) y]}{(\phi_p - \phi_s)} \qquad \text{Equation } \mathbf{2.6}$$

The dispersed phase hold up was assumed constant in the sedimentation zone and equals the initial value of $\phi_{so} = \frac{y_o}{h_{to}}$. During sedimentation, hold-up in the dense-packed zone is also assumed to be constant and correspond to the value of hold-up ϕ_{p*} at time t_* when sedimentation ceases. Once the dense-packed zone occupies the entire dispersion zone, ϕ_p is no longer constant and changes from the value of ϕ_{p*} to almost unity when coalescence is complete. During that time, the relationship between x and y is given by,

$$x = \frac{(1-\phi_p)y}{\phi_p} \qquad \text{Equation } \mathbf{2.7}$$

Hartland and Jeelani (1988) also predicted the theoretical sedimentation and coalescence profiles using the initial height of the coalescing and sedimenting interfaces (y_o and x_o) and the measured separation time (t_f). Under these conditions, the interfacial coalescence was initially drop size controlled, during which the sedimentation rate was constant and interfacial coalescence was controlled by the dense-packed height once the sedimentation is complete.

Coalescence Profile

The volume rate of interfacial coalescence per unit cross sectional area of settler is $-\frac{dy}{dt}$.

For $0<t<t_*$ (where t_* is the time when sedimentation completed), assuming interfacial coalescence is drop size controlled, Hartland and Jeelani (1987) showed that:

$$-\frac{dy}{dt} = k_i t^{d} \qquad \text{Equation } \mathbf{2.8}$$

where k_i is a constant for a given liquid-liquid system. For d = 1, integration of the coalescence profile gives:

$$y = y_o - (k_i t^2 / 2) \qquad \text{Equation } \mathbf{2.9}$$

At later times, $t_*<t<t_f$, when the coalescence rate is dense-packed zone height controlled, the volume rate of interfacial coalescence rate is expressed as:

$$-\frac{dy}{dt} = k_p y^p \qquad \text{Equation } \mathbf{2.10}$$

where $k_p = (2\phi_i d_i / 3\tau_i y_*^{\ p})$ and $y = \phi_p h_p$ when the dispersion is completely dense-packed. ϕ_i is the fraction of dispersed phase at the coalescing interface, d_i is the diameter of the droplets at the coalescing interface when the entire dispersion column is dense-packed, τ_i is the coalescence time of droplets at the coalescing interface when the dispersion becomes dense-packed, and y_* is the position of coalescing interface with respect to the final undisturbed interface when the entire column is dense-packed.

Integration of Eq. 2.10 gives the following coalescence profile:

$$y = y_* \left(\frac{t_f - t}{t_f - t_*} \right)^2 \qquad \text{Equation } \mathbf{2.11}$$

By equating the slopes of Eq. 2.9 and 2.11 at $t = t_*$, the following constant is obtained:

$$k_i = \frac{2 y_*}{(t_f - t_*) t_*} \qquad \text{Equation } \mathbf{2.12}$$

where $$y_* = y_o - \frac{k_i}{2} t_*^{\,2}$$ Equation **2.13**

Sedimenting Profile

Assuming constant droplet size and holdup of dispersed phase in the sedimentation zone, sedimentation rate per unit cross sectional area of settler is given by Hartland and Jeelani (1988) as:

$$-\frac{dx}{dt} = k_s'$$ Equation **2.14**

where k_s' is a constant, depending on the droplet diameter, ϕ_s, and physical properties of the liquid-liquid system.

For $0<t<t_*$, Eq. 2.14 results in the following linear equation:

$$x = x_o - k_s' t$$ Equation **2.15**

For $t_*<t< t_f$, using Eq. 2.7 and assuming dispersed phase holdup, ϕ_p, varies linearly from ϕ_{p*} (average dispersed phase holdup in dense-packed zone when sedimentation completes) to unity for $t_*<t< t_f$, the following expression is obtained:

$$x = \frac{y_*(1-\phi_{p*})(t_f - t)^3}{(t_f - t_*)^2} \frac{1}{[\phi_{p*} t_f - t_* + (1-\phi_{p*})t]}$$ Equation **2.16**

By comparing slopes of both sedimenting profiles from Eq. 2.15 and 2.16 at $t = t_*$ and combining them with Eqs. 2.7, 2.12 and 2.13, the following expressions are derived:

$$t_* = \frac{\phi_{p*}(\phi_{p*} - \phi_{so})t_f}{\phi_{so}(1-\phi_{p*})^2} \qquad \text{Equation } \mathbf{2.17}$$

$$k_i = \frac{2y_o}{t_f t_*} \qquad \text{Equation } \mathbf{2.18}$$

$$k_s' = \frac{1}{\phi_{p*} t_* t_f}\left[\phi_{p*} x_o t_f - y_o(1-\phi_{p*})(t_f - t_*)\right] \qquad \text{Equation } \mathbf{2.19}$$

Hartland and Jeelani (1988) finally showed that, from the above set of equations, sedimenting and coalescing profiles can be predicted theoretically from measured values of t_f and known values of x_o, y_o, ϕ_{so} and ϕ_{p*} which may be estimated from operating conditions.

2.3.3.1.2 Continuous Dispersion

Steady State Sedimentation Zone Height

For unsteady state batch dispersion, the velocity of droplets in the sedimentation zone relative to the continuous phase is given by Hartland and Jeelani (1987, 1988) as:

$$v_s = -\frac{1}{(1-\phi_s)}\frac{dx}{dt} = \frac{k_s' t^{1/s}}{(1-\phi_s)} \qquad \text{Equation } \mathbf{2.20}$$

where k_s' is a function of the dispersed phase holdup for a given liquid-liquid dispersion. k_s' and $1/s$ both can be determined from the sedimenting profile.

In the steady state continuous settler of cross sectional area, A, the relative sedimentation zone velocity is expressed by Hartland and Jeelani (1987) as:

$$V_s = \left(\frac{Q_d \beta}{A \phi_s}\right) \frac{\left[1 + \phi_s (R-1)\right]}{(1-\phi_s)} \qquad \text{Equation } \mathbf{2.21}$$

where R is the ratio of volumetric flow rate of continuous phase Q_c to dispersed phase Q_d.

Using Eqs. 2.20, 2.21 and the residence time of droplet, $t = \frac{\phi_s H_s A}{Q_d}$, the steady state sedimentation zone height can be calculated as:

$$H_s = K_s \left(\frac{Q_d}{A \phi_s K_s}\right)^{1+s} \qquad \text{Equation } \mathbf{2.22}$$

where $K_s = \frac{k_s'}{\left[1 + \phi_s (R-1)\right]\beta}$, the value of β depends on the circulation and settler geometry.

Steady State Dense-Packed Zone Height

The steady state dense-packed zone height in continuous settler will be given by different expressions depending on the factors controlling the interfacial coalescence. Three different cases are discussed in this section.

1. *If the Interfacial Coalescence is Dense-Packed Zone Height Controlled*

The interfacial coalescence rate of droplets per unit area will be same as the rate of appearance of clear dispersed phase per unit area, which is written by Hartland and Jeelani (1988) as:

$$\psi = -\frac{dy}{dt} = -\frac{d(\phi h_t)}{dt} = -\frac{d(\phi_s h_s + \phi_p h_p)}{dt} \qquad \text{Equation } \mathbf{2.23}$$

Again, $\psi = Q_d / A$ is the dispersed phase throughput per unit area in case of continuous settler at steady state, where Q_d is the dispersed phase flow rate.

If the volumetric interfacial coalescence rate is dense-packed zone height controlled and is independent of the diameter of the droplet at the coalescing interface then the following equation can be written (Hartland and Vohra, 1978; Jeelani and Hartland, 1986a):

$$\psi = k_p h_p{}^p \qquad \text{Equation } \mathbf{2.24}$$

where, k_p and p are obtained from a least square fit of experimental data for $\psi = -\frac{dy}{dt}$

with h_p. From the values of k_p, p and $\psi = Q_d / A$, the steady state height in the continuous dispersion is calculated as:

$$H_p = \left(\frac{Q_d}{A k_p} \right)^{1/p} \qquad \text{Equation } \mathbf{2.25}$$

Barnea and Mizrahi (1975d) and Golob and Modic (1977) also obtained a similar form of Eq. 2.25 for the steady state dense-packed zone height in a continuous settler.

2. *If the Interfacial Coalescence is Droplet Size Controlled*

If the volumetric interfacial coalescence rate per unit area is controlled by droplet size and is independent of dense-packed zone height, then for the batch settler (Hartland and Jeelani, 1987):

$$\psi = k_d t^d \qquad \text{Equation } \mathbf{2.26}$$

where k_d and d are obtained from the coalescence profile.

From the values of k_d , d, $\psi = Q_d / A$ and droplet residence time, $t = \phi_C H_t A / Q_d$, the steady state dispersion height for continuous settler is written as:

$$H_t = \left(\frac{k_d}{\phi_C}\right)\left(\frac{Q_d}{Ak_d}\right)^{1+1/d} \qquad \text{Equation } \mathbf{2.27}$$

3. *If the Interfacial Coalescence is Total Dispersion Height Controlled*

In the third limiting case, when the interfacial coalescence rate is total dispersion height controlled, Hartland and Jeelani (1987) showed that,

$$\psi = \frac{\bar{\bar{\phi}}}{\left(\left(\frac{1}{k_{1B}h_t}\right)+\left(\frac{1}{k_{2B}}\right)\right)} \qquad \text{Equation } \mathbf{2.28}$$

where it is assumed that ψ is independent of the droplet diameter at the coalescing interface. k_{1B} and k_{2B} are constants which are determined from total dispersion height profile for batch settler and $\bar{\bar{\phi}}$ is the space time average dispersed phase holdup.

From the values of constants k_{1B}, k_{2B} and $\bar{\bar{\phi}}$ from the batch settler, the steady state dispersion height, H_t, in a continuous settler can be predicted by the following equation:

$$\frac{\phi_F}{\left(\frac{Q_d}{A}\right)} = \left(\frac{1}{k_{1C}H_t}\right)+\left(\frac{1}{k_{2C}}\right) \qquad \text{Equation } \mathbf{2.29}$$

where ϕ_F is the dispersed phase fraction in the feed dispersion, $k_{1C} = \frac{k_{1B}\bar{\bar{\phi}}}{\phi_F}$, $k_{2C} = \frac{k_{2B}\bar{\bar{\phi}}}{\phi_F}$.

Based on profiles of sedimentation and coalescence interfaces, Hartland and Jeelani (1987) concluded the following:

- The steady state heights for sedimentation and dense-packed zones can be predicted from the batch sedimentation and coalescence profiles.
- An exponential coalescence profile means that the dispersion is dense-packed or that the interfacial coalescence rate decreases as time increases. An exponential sedimentation profile suggests that the increase in the holdup is more important than an increase in drop size. An overall exponential decay in dispersion height indicates that sedimentation is controlled by holdup or the dispersion is completely dense-packed.
- Conversely, a sigmoidal coalescence profile suggests that the rate of interfacial coalescence increases and then decreases with the height of the dense-packed zone. A sigmoidal sedimentation profile suggests that the sedimentation rate increases with increase in drop size and then decreases as the holdup increases until the dispersion is completely dense-packed.

The appropriate mechanism is chosen based on the shape of batch sedimentation and coalescence profiles, holdup of the dispersed phase, and variations in the sedimentation and coalescence volume rates per unit area. Then the steady state dispersion height can be calculated for the continuous settler.

2.3.3.1.3 Model Developments

Nadiv and Semiat (1995) developed the methodology for the similar dispersion system used by Hartland and Jeelani. They confirmed that overall separation time was dependent on the initial dispersion height, diameter of the batch settler and on the type of dispersion

generated. Parameters such as mixing intensity and mixing time were considered less important.

Yu and Mao (2004) developed a simple method to obtain the key parameter, t_* (time at which sedimentation stops) for the Hartland and Jeelani batch model through the regression of experimental measurements of the coalescence profile. The sedimentation profile was predicted in the same way as developed by Jeelani and Hartland (1998). The advantage of this model is that it could be used without advance knowledge of the initial average drop diameter and interfacial coalescence time. Hence, is easy to use but the coalescence profile must be known in advance.

Jeelani and Hartland (1988) also studied the unsteady state behavior in the continuous settler by allowing dispersion to grow until it reached steady state. Two variations of zero and infinite mixing time were studied and the same steady state height was observed in both cases. However, the growth rate was faster for infinite mixing compared to the case of zero mixing. For zero mixing time, the droplet distribution changed slowly with time but, for infinite mixing time, the droplet size distribution corresponded to its steady state value leading to a faster rate of dispersion growth.

2.3.3.2 Coalescence Based Models

This model was developed by Ivanov and colleagues. Unlike Hartland, Lobo *et al.* (1993) assumed that the height of the dense-packed zone did not change significantly during the coalescence process, indicating that the dispersion did not separate into clear water and oil phases. Hence, interdrop coalescence increased the mean droplet size of the dispersed phase over time as well as the polydispersity of the droplet size. Figure 2.11 shows the coalescence process at different times.

In their model, they assumed the droplets size were less than 100 μm, much smaller than considered in Hartland's work. Due to small size of the droplets they were not

substantially deformed due to gravitational forces and maintained dispersion structure in the form of lattice. Lobo *et al.* (1993) also accounted for the presence of surfactants in their model and found that presence of surfactants did not influence the coalescence sequence. The presence of surfactant only changed the interfacial film lifetime indicating that surfactant only scales the time of the coalescence steps without changing the process itself. The biggest disadvantage with this method is that it is a stochastic mathematical model; even if tested with water/hexadecane system, remains rather theoretical.

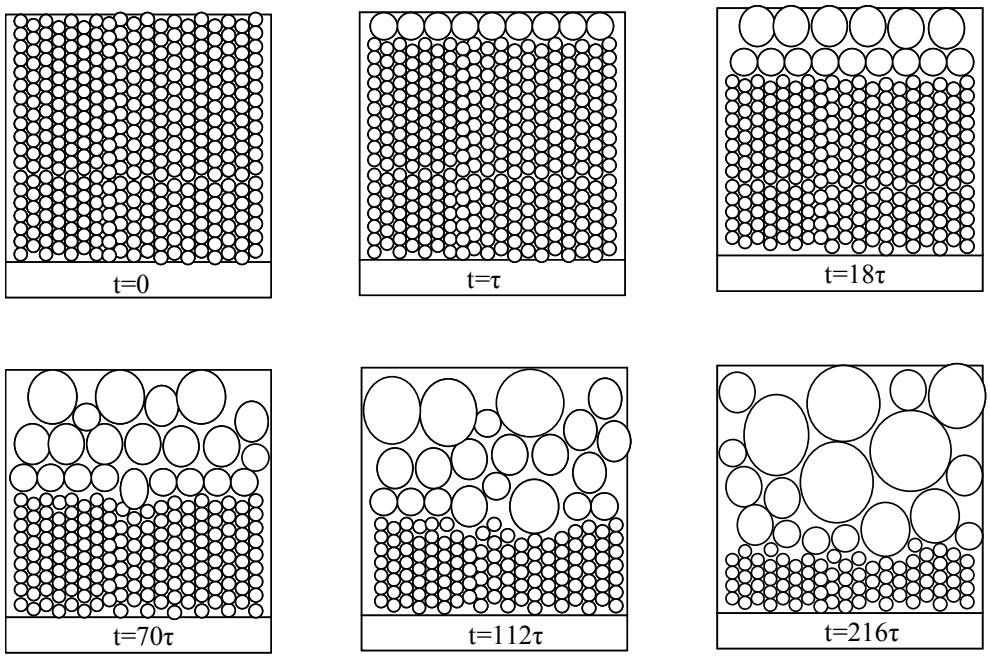

Figure 2.11: Schematic representation of coalescence sequence in dense-packed zone (Adapted from Lobo *et al.*, 1993).

By far the most comprehensive study of coalescence processes in liquid-liquid dispersions is performed by Henschke *et al.* (2002). This model detailed the coalescence process, taking into consideration droplet sedimentation, height of the dense-packed zone, droplet deformation in the dense-packed zone, and coalescence effects (droplet-

droplet and droplet-interface coalescence). Henschke *et al.* (2002) showed that it was possible to characterize coalescence processes with the help of a single parameter, r_v^* (dimensionless asymmetrical film radius) obtained from batch settling experiment. It was also found that this parameter was independent of the filling height of the dispersion, mixing intensity, and volume fraction of the dispersed phase. The model was also able to describe the increase in droplet diameter in the dense-packed zone without any additional parameter. The limitation of this model is that it is purely hydrodynamic (does not account for surfactant effects) and used significantly larger droplets (0.5-4 mm) compared to the droplet sizes present in crude-oil water emulsions.

All of the models proposed for emulsion layer growth were developed for pure liquid systems. These models are applicable for both oil-in-water dispersions and water-in-oil dispersions, except that the sedimentation front becomes the creaming front and lies below the coalescing front in the vertical column for oil-in-water dispersions. None of these models contained surfactants or other additives such as clays, and solids.

2.3.4 Rag Layers in Oil Sands Froth Treatment

As mentioned before, formation of rag layers in oil sands froth treatments is similar to emulsion layers in model emulsion dispersions. In case of oil sands separations, rag layers are more stable due to the presence of asphaltenes, clays and solids. These different components accumulate at the interface; increase the emulsion stability (Jiang *et al.*, 2008; Sztukowski and Yarranton, 2005) which in turn causes the rag layer to grow. To date, these rag layers are little investigated largely because it is challenging to take undisturbed samples of rag layer out of industrial separation vessels for further study. Nonetheless, some attempts have been made to characterize these rag layers.

Saadatmand *et al.* (2008) proposed that there are two possible mechanisms for rag layer formation and growth during oil sands froth treatment. One is that the rag layers can build up if the coalescence rate of dispersed phase droplets is slower than the accumulation

rate. Second is that the fine oil-wet solids can accumulate at the interface and create a mechanical barrier which may grow over time and provide an obstacle for droplets to pass through and mix with their own bulk phase. Saadatmand *et al*. (2008) showed that low quality oil sands produced much larger rag layers compared to average or high quality oil sands. This was due to the fact that the low quality oil sands contained more fine solids which formed the mechanical barrier at the interface and stabilized emulsion.

To break the rag layer and have better separation, asphaltenes, clays and biwetted solids should be removed from the oil/water interface. Basu *et al.* (1997) observed that increasing pH changes the wettability of sand to more water-wet, thus facilitating the separation of bitumen from oil sands.

Jiang *et al.* (2008) used sodium metasilicate and sodium hydroxide to separate clay solids from the rag layer. Sodium metasilicate enhanced the dispersion of clay solids and minimized bitumen clay coagulation. Sodium hydroxide and sodium metasilicate increase the pH and convert naphthenic acids naturally found in the oil to sodium naphtehnate (a soap), which can emulsify and separate oil from clay solids and form an oil-in-water emulsion. They also observed that after removal of free water containing clay solids, addition of HCl to the emulsion layer broke the oil-in-water emulsion and very good final separation was achieved.

Most of the studies with respect to oil sand rag layers have been done as batch bench-top laboratory experiments. These studies can provide insight into understanding rag layers in batch systems, but continuous systems are more complex and it is difficult to stop rag layer accumulation and subsequent flooding in the separator under poor operating conditions. Gu *et al.* (2007) characterized rag layers in continuous systems and proposed an approach for bitumen froth cleaning that can minimize the cost, hydrocarbon loss and produce a product that meet downstream process specifications. They designed a novel setup which allows for two step water washing of naphtha diluted bitumen froth (NDBF)

and built up a rag layer that could be analyzed for formation mechanisms and composition analysis. Studies for two different naphtha to bitumen mass ratios (N/B of 0.7 and 7), showed that even after the first washing water and solid contents of the organic phase were reduced by more than 91% and 87%, respectively. For the rag layer formation, it was found that chloroform soluble and asphaltene fraction of rag layer showed the highest emulsion stability. They also observed that the higher the separation efficiency, the faster the rag layer built up.

2.4 Summary

Emulsions often present challenges in petroleum industry, especially in case of oil sand separations, these emulsion can be stabilized further by presence of excess solids, asphaltenes, and natural surface active agents and this eventually leads to formation of rag layer at the interface. Rag layers need to be controlled for better oil recovery and the growth of rag layers depend on the coalescence rate of emulsified droplets and type and wettability of the solids. Usually chemical demulsifires are added to break these emulsions but there is no well defined chemical demulsifier or method to control them.

There are models presented in the past which can mimic the rag layer growth but these models are applicable for relatively simple liquid-liquid dispersions without the presence of surfactants, clays and solids as are present in oil sand rag layers. The accumulation of these materials can drastically alter rag layer growth. Hence, there is no complete model to simulate the rag layer growth in oil sand separations. Nonetheless, the sedimentation models presented above are suitable to examine the baseline relationship between coalescence rate and rag layer growth.

CHAPTER 3
EXPERIMENTAL METHODS

This chapter discusses the experiments performed to study emulsion layer growth and emulsion stability. Model emulsions were prepared from toluene, *n*-heptane and reverse osmosis water with dissolved surfactant. Batch experiments were performed on model oil-in-water emulsions to determine coalescence rates from the change in emulsion layer height over time. A laboratory scale separator was used to study emulsion layer growth in a continuously flowing emulsion as well as the decay of emulsion layers after cessation of flow. The effects of surfactant concentration, emulsion flow rate, and separator area were also studied. Some preliminary experiments on asphaltene stabilized water-in-oil emulsions were also performed. Methods and results are for oil-in-water emulsions unless specified for water-in-oil emulsions.

3.1 Materials

Toluene was ACS grade with 99.5%+ purity purchased from VWR. Commercial grade *n*-heptane with 96% purity was purchased from Conoco Phillips Co. Reverse osmosis (RO) water was supplied by the University of Calgary water plant. Nonylphenol ethoxylate (NEO-10) surfactant with 10 moles of ethylene oxide was provided by Champion Technologies, Ltd. Sodium bis (2-ethylhexyl) sulfosuccinate or AOT (98% purity) and Tween-80 surfactants were purchased from Aldrich Chemical Company, Inc. and Uniqema, Imperial Chemical Industries, PLC., respectively.

For oil-in-water emulsions, surfactant solutions were prepared with NEO-10 and for water-in-oil emulsions, surfactant solutions were prepared using AOT and Tween-80. All the surfactants used are water soluble. To make the solution, the surfactant was weighed

in a HDPE Nalgene bottle on an analytical balance and a given mass of RO water was added. The mixture in the bottle was placed in an ultrasonic bath for almost one hour or was left overnight to completely dissolve the surfactant.

3.2 Asphaltene Extraction

3.2.1 Precipitation of Asphaltenes and Associated Solids from Bitumen

Asphaltenes were extracted from the Coker feed Athabasca bitumen. 40 grams of bitumen was weighed in a 2000 mL beaker and then heptane was added at a ratio of 40 mL heptane per gram bitumen. The beaker was then covered with plastic wrap and aluminum foil to avoid any evaporation. The beaker was sonicated for 45-60 minutes and then left for 23 hours (total contact time of approximately 24 hours).

After 24 hours, the supernatant was decanted and filtered through Whatman 2 (8 μm) filter paper. When approximately 350-400 mL of solution remained, the filtration was stopped and additional heptane was added at a ratio of 4 mL per gram original bitumen. The beakers were again sonicated for 45 minutes and then left for approximately 16 hours. The entire solution in each beaker was then filtered through the same filter paper used in the first filtration. A very small amount of heptane was used to rinse out the beaker. The filter paper was left to dry until there was no change in mass (4 to 5 days). The filter cake consisted of asphaltenes and solids such as clays that separated with the asphaltenes.

3.2.2 Separation of Asphaltenes and Associated Solids

In order to remove the non-asphaltenic solids from the filter cake, the asphaltenes were dissolved in toluene at a 1:100 ratio (g/mL). The solution inside the flasks was sonicated for an hour and beakers were then allowed to sit undisturbed for another 2 hours. The solution was then transferred into 50 cm^3 Nalgene centrifuge tubes and centrifuged at 4000 rpm for 6 minutes. The same set of tubes was used repeatedly until the entire

solution was centrifuged. After each centrifuge run, the supernatant (asphaltenes + toluene) was carefully poured into a beaker. Once the entire solution was centrifuged, the beaker (with supernatant) and tubes (with solids) were dried in a fume hood for several days until there was no change in mass. The solids free asphaltenes were collected from the beaker and were used to prepare the water-in-oil emulsions.

3.3 Emulsion Preparation

The oil-in-water emulsions were prepared from an aqueous phase of RO water and a surfactant and an organic phase of 50% toluene and 50% *n*-heptane by volume. The aqueous phase was prepared by diluting the stock surfactant solution in RO water. Surfactant concentrations were typically in the range of 40-120 ppm (usually 80 ppm). The water volume fraction in the emulsions was 50% and the volume of the emulsion was 1600 mL unless otherwise stated. A 50% water volume fraction was selected to ensure that there was very little or almost no creaming/settling after the emulsion was created. That is, all of the emulsion was in the dense-packed zone. In the dense-packed zone, emulsified droplets coalesce by means of binary coalescence and also interfacial coalescence with the homo phase and result in free phase, without any settling/creaming before the coalescence.

A single beaker of volume 2000 mL with dimensions 125 mm diameter and 160 mm height was used for all experiments. The aqueous and the organic phase were both poured into the beaker prior to mixing. The beaker was fitted with a Teflon lid and Teflon baffles as shown in Figure 3.1. The two Teflon baffles (Figure 3.1b) were 11 mm wide and 170 mm high and were positioned along the glass beaker periphery to ensure uniform mixing. An IKA-RW20 digital variable speed overhead mixer with a 4-blade impeller (Figure 3.1c) having 50 mm diameter, 10 mm width, and 8 mm height was used to create the emulsion. The impeller was centered horizontally in the beaker and adjusted vertically by moving the mixer along a vertical stand. The impeller blades were positioned just below

the oil-water interface. A 20 L water bath was fitted with a water circulator with temperature controller to heat the solution inside the beaker to the experimental temperature. The beaker was kept inside the water bath to maintain the required temperature of 45^{o}C.

Once the solution inside the beaker reached the experimental temperature, the solution was mixed at 800 rpm for 15 minutes to create the oil-in-water emulsion. For batch experiments, the mixer was immediately turned off after 15 minutes. For continuous experiments, the mixer remained on throughout the emulsion layer growth experiment and was shut off once the steady state emulsion layer height was achieved to begin a decay experiment.

For the asphaltene stabilized water-in-oil emulsions, the following experimental conditions were chosen: a temperature of 60^{o}C; a mixer speed of 1000 rpm; an organic phase of pure toluene; an aqueous phase of 50 ppm of each AOT and Tween-80 in RO water; and an aqueous phase volume fraction of 50%. The same experimental procedure was used for these emulsion systems except that the aqueous phase was heated separately from the organic phase and was added to the top of the organic phase once the mixer was started.

3.4 Batch Experiments

The apparatus used for the batch experiments is shown in Figure 3.1. A schematic illustration of the batch experiments is provided in Figure 3.2. To start the batch experiment, both the aqueous and organic phases were placed in the beaker, as mentioned in the emulsion preparation section. The beaker (Figure 3.1d) was put inside the water bath for 20 to 25 minutes to heat the solution inside the beaker to the desired experimental temperature of 45^{o}C. During the heating time, the beaker top was covered

with the aluminum foil to prevent evaporation of the solvent. Once the beaker reached the desired temperature, the baffles, lid, and mixer were assembled as shown in Figure 3.1e.

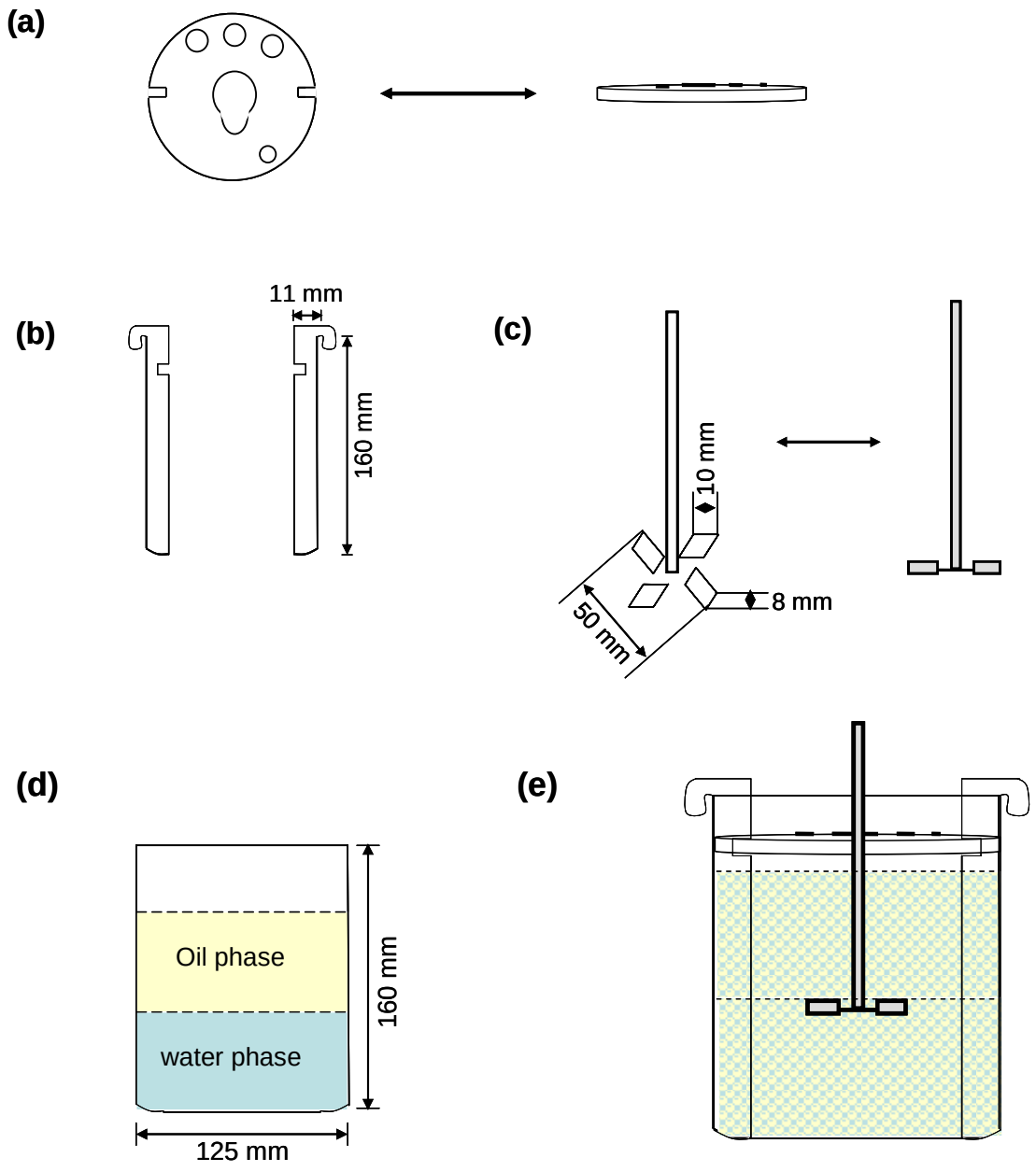

Figure 3.1: Emulsion preparation apparatus. (a) Teflon disc (Lid); (b) Teflon baffles; (c) Mixer; (d) Beaker; (e) Beaker setup, assembled with all parts from (a) to (d).

The solution was mixed for 15 minutes at 800 rpm to create the emulsion. After 15 minutes the mixer was shut off. At the same time, the timer was started, the mixer was pulled out of the solution and the lid and baffles were removed from the beaker. This dissembling process usually took a few seconds, and was performed carefully so that the emulsion inside the beaker was not disturbed. As soon the timer was started, the initial height of the emulsion layer was recorded. The emulsion started to coalesce and free oil and water separated from the emulsion layer. The heights of the free water, oil and emulsion layers were measured periodically until the emulsion layer completely coalesced or there was no further change in the emulsion layer height.

The experimental conditions were chosen so that at least 80% of the emulsified oil broke into free oil in 30-50 minutes. Emulsions with this lifetime were found to be suitable for use in the continuous system at practical feed flow rates. The experimental conditions were: a temperature of 45^{o}C; a mixer speed of 800 rpm; an organic phase of 50 vol% *n*-heptane and 50 vol% toluene; an aqueous phase of 40-120 ppm of NEO-10 in RO water; an aqueous phase volume fraction of 50%.

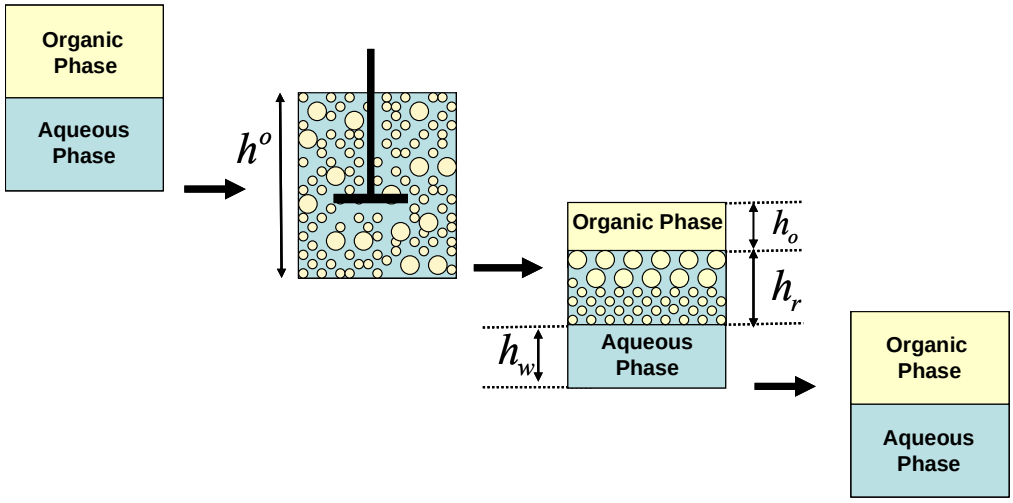

Figure 3.2: Schematic illustration of the batch experiment for model emulsions at different time steps.

The emulsified oil volume fraction in the emulsion layer at any time, t, is a significant experimental variable and was determined as follows:

$$\phi_o = \frac{V_o^{\,o} - V_o}{V} = \frac{h_o^{\,o} - h_o}{h} \qquad \text{Equation } \mathbf{3.1}$$

where, h^o is the initial height of the emulsion (just after the mixer is shut off), $V_o^{\,o}$ is the volume of the oil layer before creating the emulsion, V_o and V are respective volumes of the free oil and emulsion layers at any time, t, $h_o^{\,o}$ is the initial height of the oil layer before creating the emulsion, h_o and h are respective heights of the free oil and emulsion layers at any time, t.

3.5 Continuous Experiments

3.5.1 Apparatus

Figures 3.3 and 3.4 are a schematic and photograph, respectively, of the apparatus used to investigate emulsion layer growth in a continuously flowing system. The main components are: the beaker where the emulsion is prepared, the separator, the pump, and the tubing.

Emulsion Beaker: Figure 3.5 shows the beaker (equipped with baffles, mixer, lid, feed tubing and oil and water tubing) used to create the emulsion. The only difference from the beaker used in the batch experiments was the addition of tubing inlets and outlets for flow to and from the separator.

Separator: Two different graduated glass separators were used for this study. The smaller separator had a volume of 250 mL and a cross sectional area of 10.5 cm^2 and the larger separator had a volume of 500 mL with a cross sectional area of 14.4 cm^2. The separators were surrounded by a glass water jacket. A thermostatted water circulator was used to

feed the water to the jacket through the lower end and water was returned to the bath from the top end of the jacket. Tygon tubing was used across the water jacket for this purpose. Figure 3.6 shows the dimensions of the 250 mL separator and Figure 3.7 shows the components of the separators.

Pump: A Masterflex L/S peristaltic pump system was used to transfer the emulsion from the beaker to the separator. The pump consisted of an economy digital drive and a Masterflex pump head L/S (Easy-Load II). The pump was able to operate for any flow rate between 5 and 280 cm^3/min.

Tubing: Three different types of tubing were used. Masterflex tubing-Viton #24 was used to feed the emulsion from the beaker into the separator. One end of the tubing was kept at the oil-water interface inside the beaker (Figure 3.5(6)) and passed through the pump with the other end connected to the feed glass tube (Figure 3.7(5)) inside the separator. The length of this tubing used was approximately 130 cm. Masterflex tubing-Viton #36 was used to pass the water and the oil from the separator to the beaker. The tubing (Figure 3.5(2)) used to pass the water back into the beaker was approximately 26 cm in length and the tubing (Figure 3.5(1)) used to throw the oil back into the beaker was approximately 62 cm long. Tygon tubing, 8 mm diameter, was used for temperature control of the separator.

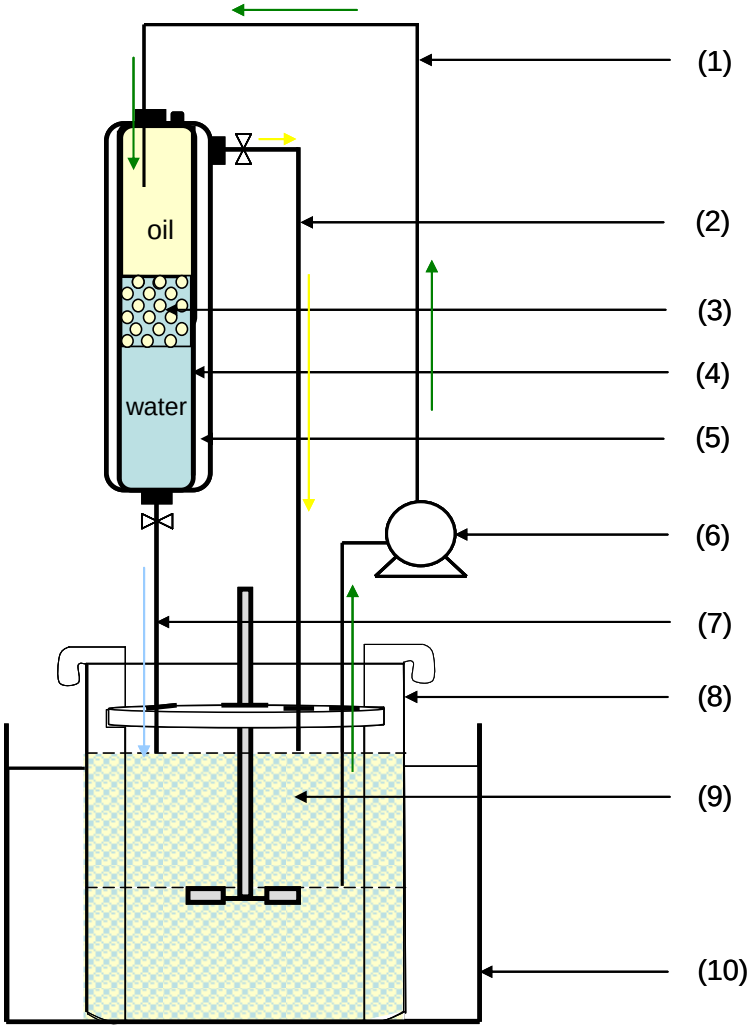

Figure 3.3: Schematic diagram of the continuous setup. (1) Feed tubing; (2) Oater exit tubing; (3) Emulsion layer; (4) Separator; (5) Water jacket; (6) Pump; (7) Water exit tubing; (8) Beaker; (9) Oil-in-water emulsion; (10) Water bath.

(a) **(b)**

Figure 3.4: Apparatus for continuous experiments: a) whole apparatus; b) separator with the emulsion layer in the middle, organic phase at the top and aqueous phase at the bottom.

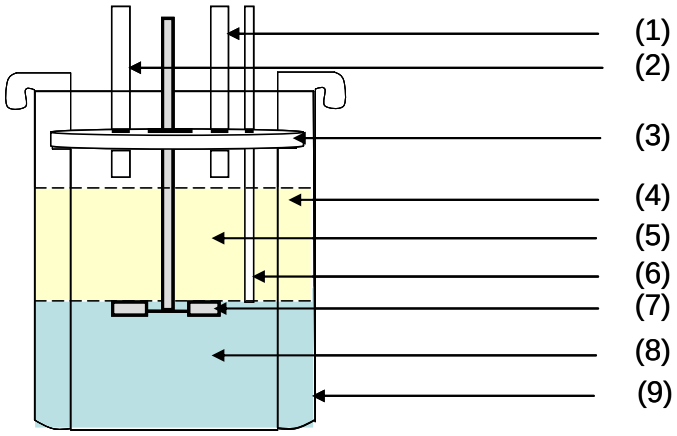

Figure 3.5: Schematic diagram of the beaker used to create the emulsion in the continuous experiment. (1) Oil exit tubing; (2) Water exit tubing; (3) Teflon lid; (4) Teflon baffle; (5) Oil phase; (6) Feed tubing; (7) Impeller; (8) Water phase; (9) Beaker.

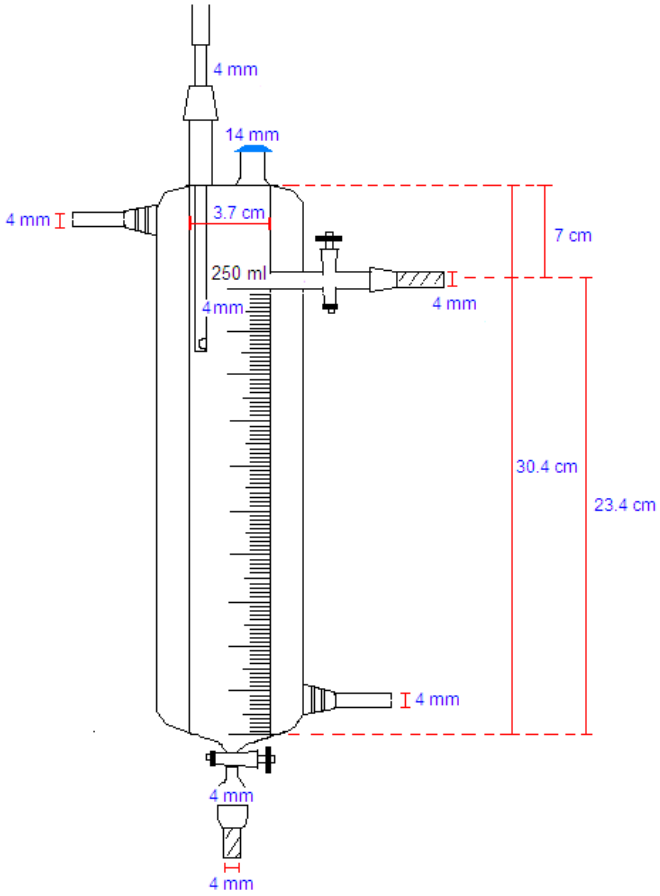

Figure 3.6: The 250 mL glass separator with all dimensions.

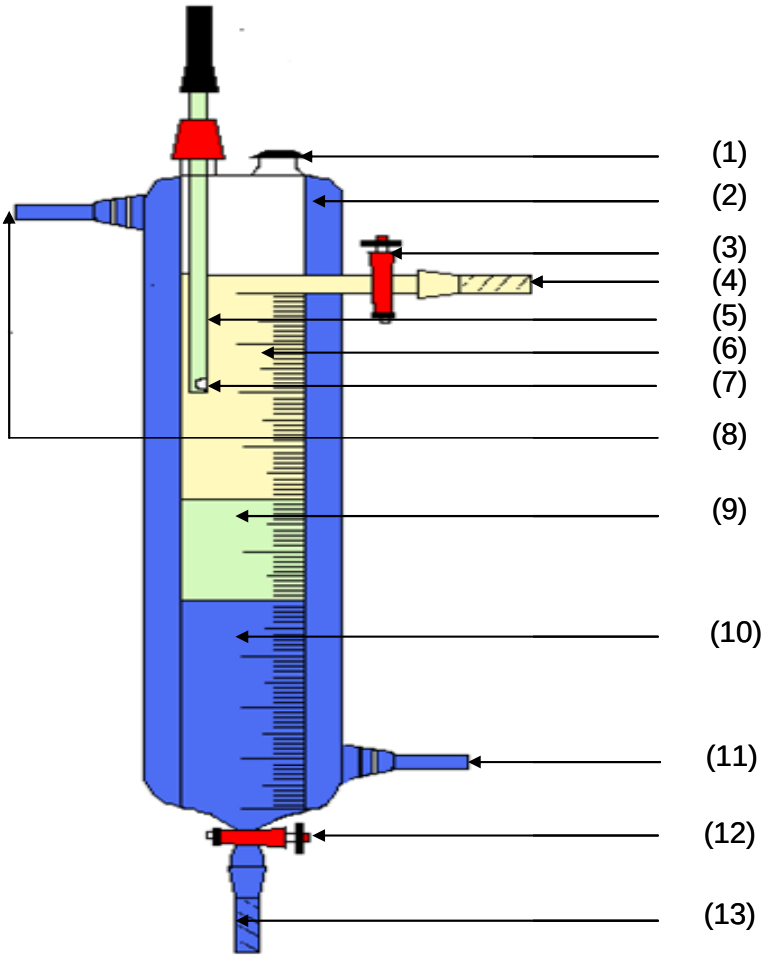

Figure 3.7: The glass separator used for continuous experiments. (1) Spare slot for feed; (2) Water jacket; (3) Oil exit valve; (4) Oil exit; (5) Feed glass tubing; (6) Oil phase; (7) Feed point; (8) Water exit from jacket; (9) Emulsion layer; (10) Water phase; (11) Water inlet for jacket; (12) Water exit valve; (13) Water exit.

3.5.2 Continuous Experiment Procedure

Emulsion Layer Growth Experiment

To start the continuous experiment, the apparatus was set up as shown in Figure 3.3 and the system was brought to the operating temperature. The emulsion was prepared in the

same way as was done during the batch experiments. The separator was filled separately with preheated aqueous and organic phases. For the 250 mL separator, 125 mL of the each phase was used to fill the separator and for the 500 mL separator, 250 mL of each phase. In either case, the oil-water interface resided at the middle of the separator.

The mixer was started at 800 rpm to create the emulsion inside the beaker. The pump was started after 10 minutes at some flow rate to feed the emulsion into the separator. Flow rates used were in the range of 40 to 50 cm^3/min for the small separator and 40 to 62 cm^3/min for the big separator. As soon the emulsion reached at the feed point (Figure 3.7(7)), the timer was started. The emulsion passed through the organic phase at the top, hit the oil-water interface and started to accumulate at the interface. The oil exit valve was always open throughout the continuous experiment to return the excess free oil back to the beaker. To keep the emulsion layer height in the middle of the separator, the water exit valve at the bottom of the separator was controlled during the entire continuous experiment. It was important to handle the water exit valve very carefully so that the emulsion layer structure did not change while volumes were adjusted because a disturbance could slow down or increase the coalescence rate. Ideally, the water outlet rate was held constant with only slight adjustments to hold the mid point of the emulsion layer at a constant position.

At the beginning of a continuous experiment, the emulsion layer started to grow in size, since the emulsion was entering the separator at a rate greater than the coalescence rate in the emulsion layer. After some time, the emulsion layer height grew to the point where the coalescence rate became equal to the feed rate of the emulsion and a steady state emulsion layer height was achieved. The height of the emulsion layer was measured periodically throughout the experiment.

Decay Experiment

At this point, the pump was turned off, the oil exit valve at the top and the water exit valve at the bottom were closed, the mixer was turned off and the timer was reset. Since the feed was no longer entering the separator but coalescence continued, the emulsion layer height started to decrease.

The decay experiment is similar to the batch experiment and the decrease in the height of the emulsion layer and the increase in the free oil layer height were measured over time. The heights were measured until the emulsion layer volume diminished to zero or there was no more change in the emulsion layer height (no further coalescence). The change in the emulsion layer height during both the continuous and decay parts of the experiment is shown in Figure 3.8.

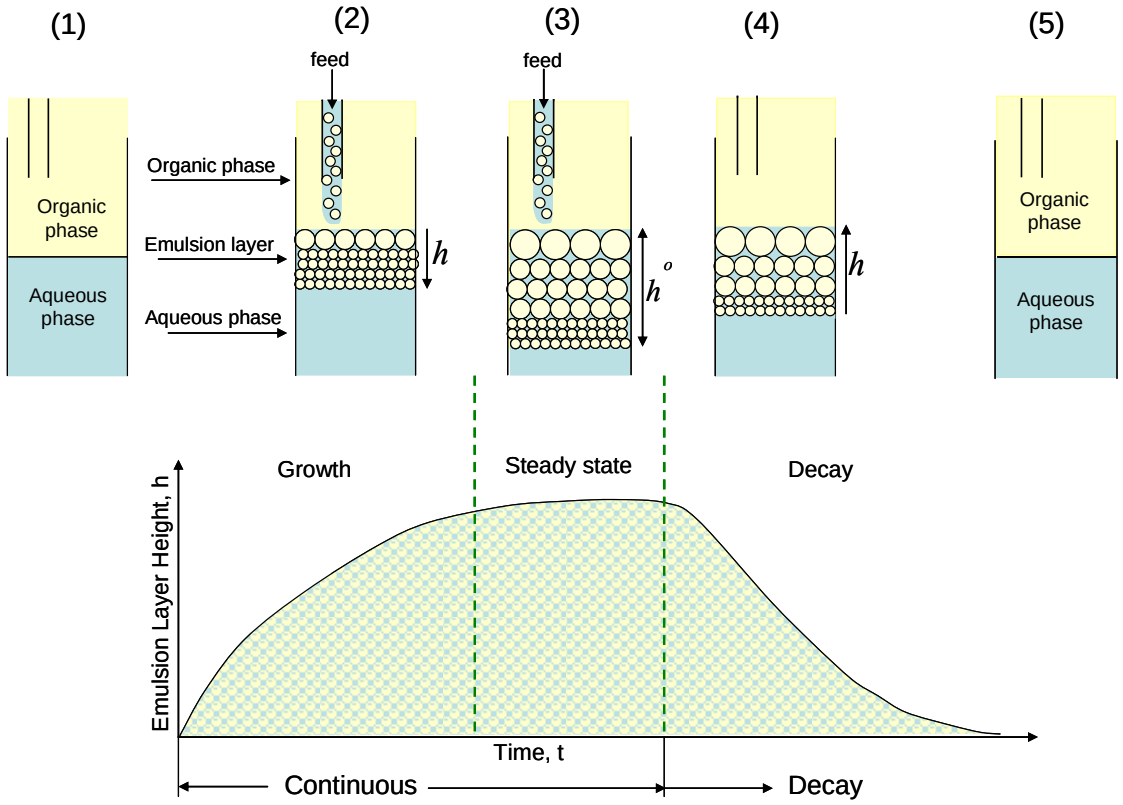

Figure 3.8: Schematic representation of the emulsion layer height over time during the continuous and the decay experiment.

3.5.3 Emulsified Oil Volume Fraction during Continuous Experiment

The volume fraction of oil in the emulsion layer during the decay experiment was determined using Eq. 3.1 and was found to be invariant with time. This method could not be used for the growth experiment because emulsion was continuously fed to the emulsion layer.

To find the emulsified oil fraction in the emulsion layer at different times, a series of continuous experiments were performed at the same experimental conditions. The

continuous experiment with given experimental conditions was started in the same way as discussed before, but the experiment was carried out only for 3 minutes, rather than until the time corresponding to the steady state. After 3 minutes, the decay experiment was performed on the developed emulsion layer inside the separator. From the decay experiment oil fraction was found out for the continuous experiment at t = 3 minutes. The entire experimental set up was cleaned and a new emulsion was prepared at the same experimental conditions. The same procedure was repeated for three more times for 7, 10 and 15 minutes. For the latter case, steady state was achieved before going on to the decay experiment.

The plot in Figure 3.9 shows the experimental emulsion layer heights for different continuous runs and oil fractions at different times. The measurements show some scatter but it appears the oil volume fraction in the emulsion layer is invariant over time. For both the growth and decay experiments the oil volume fraction is invariant at a value of approximately 64%. In other words, the continuous aqueous phase occupies approximately 36% of the volume indicated a reasonably well packed structure for which no compaction upon coalescence is expected.

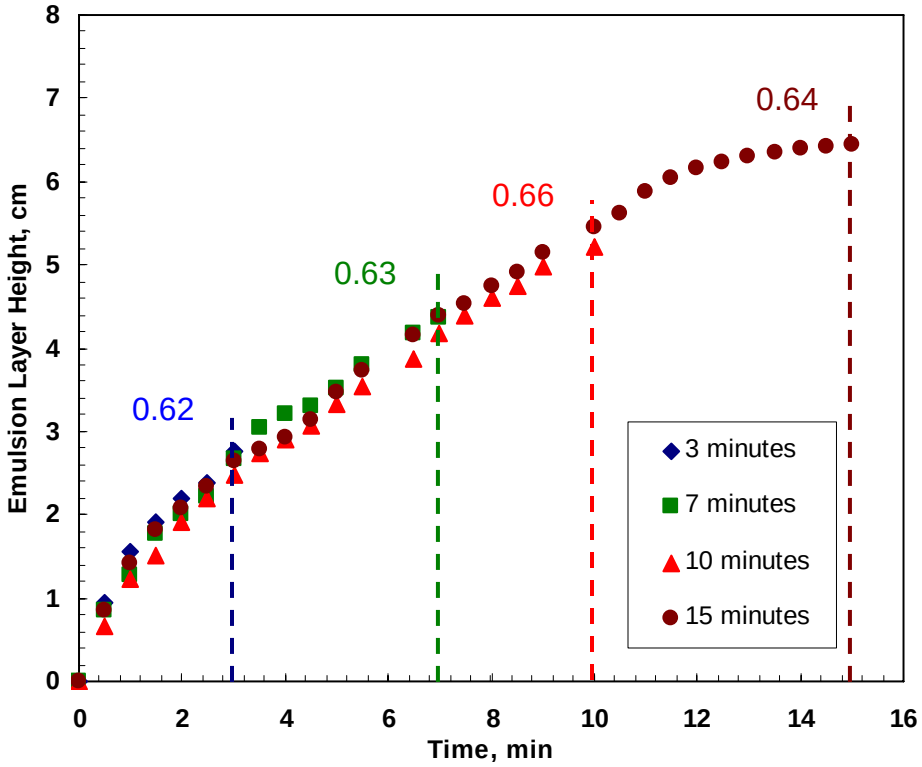

Figure 3.9: Emulsified oil fraction in the emulsion layer at different times during the continuous experiment performed at the feed flow rate of 45 cm^3/min. in the 250 mL separator with 80 ppm concentration of NEO-10.

3.5.4 Emulsified Oil Volume Fraction in the Feed during Continuous Experiment

In a continuous experiment, coalescence can occur before the feed enters the separator during the time the feed moved from point (a) to point (b) (Figure 3.10). If there was no coalescence during that time then the value of $\phi_o^{\,o}$ would have been 0.5 because the emulsion entering the feed tubing at point (a) had 50% of dispersed oil by volume. Two variations on the continuous experiments were designed in order to determine the value of ϕ_o°.

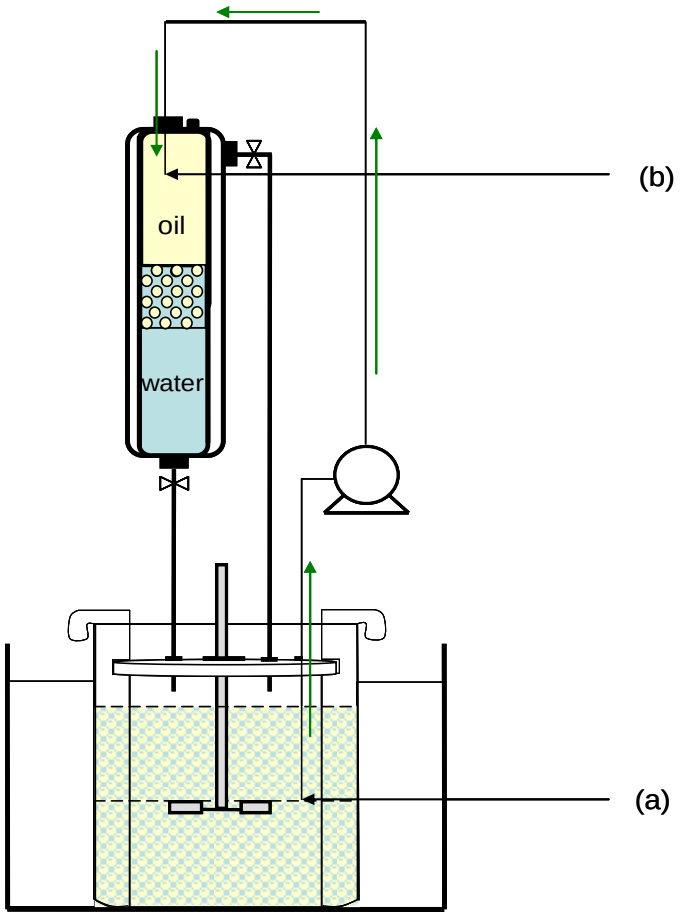

Figure 3.10: Flow of emulsion from the beaker to the separator through tubing during the continuous experiment.

First Experiment: After 90 seconds, the feed was continued but the water and oil exit valves of the separator were closed and the emulsion and oil layer heights were measured at 10 second intervals. The heights were recorded for another 40-50 seconds. From the change in the oil layer height, the volume of oil coalesced was determined at 10 second intervals. For each interval, the coalesced oil was the result of two different mechanisms: (i) the oil coalesced in the emulsion layer and separated out as free oil and (ii) the free oil

in the feed (oil which coalesced during the time the feed flowed from point (a) to the point (b)).

Second Experiment: After 90 seconds, the continuous experiment was continued until the emulsion layer reached almost the same height as was found for the first experiment at the end of almost two minutes. Then the feed was stopped and both water and oil valves were closed. The emulsion layer started to coalesce and the emulsion and oil layer heights were measured at 10 second intervals. This time, the change in the oil layer height was a result of the oil coalesced in the emulsion layer which separated as free oil.

The volume of oil exiting the emulsion layer was compared between the two experiments at approximately the same height of emulsion layer during the time interval. The difference in oil volume gives the contribution of free oil from the feed. This free oil volume is subtracted from the amount of oil entering the feed tube to determine the amount of emulsified oil entering the separator.

3.6 Emulsion Droplet Size and Size Distribution

To measure a drop size distribution for an emulsion, a sample of the emulsion was taken using a plastic pipette and placed onto a hanging-drop-glass slide. The cavity of the slide was prefilled with the continuous phase (aqueous phase in this case). A slip cover was placed over the cavity to prevent solvent evaporation. The amount of emulsion added to the cavity was small enough that the droplets were able to disperse into approximately a single layer over most of the cavity.

The emulsion sample was observed through a Carl Zeiss Axiovert S100 inverted microscope equipped with video camera and AxioVision Release 4.6.3 analysis software. Several images were collected for each sample. In this work, approximately 700 oil

droplets for batch experiments and 1500 oil droplets for decay experiments were analyzed to determine the droplet size distributions, Figure 5.2 and 5.7.

3.7 Apparatus Cleaning

Cleanliness of each part of the setup was very important. Sometimes, especially in case of continuous experiments, even very minute impurities when associated with the emulsion layer, slowed down the coalescence and in turn caused the emulsion layer to grow faster. These impurities were mainly originated from the glass separator or from the tubings used. During the experiment, traces of surfactant could remain on the glass surface and if glass surfaces were not cleaned properly then it could alter the coalescence. Also, tubings used in the continuous experiments had limited lifetime and started to wear out after using for about 20 times. The tubing was required to be cleaned at regular intervals or replaced with new ones.

The following few steps were taken to ensure the complete cleaning of the setup.

1. After every experiment, the beaker and the glass separator were rinsed twice with the acetone, dried completely, then rinsed with toluene and dried again.
2. The separator was flushed thoroughly with RO water, scrubbed with a long bottle brush to remove any material stuck on the glass surface and then rinsed again with RO water.
3. Tubing was dried after every use. After a few uses, tubing was sonicated in RO water and then dried completely.
4. Teflon baffles and the lid were rinsed with acetone, and then with toluene and dried completely.
5. The glass beaker, separator, Teflon baffles and lid were rinsed with acetone and dried completely again just before using for the next experiment.

CHAPTER 4
MODELING EMULSION LAYER GROWTH

This chapter discusses the methodology used to model the experimental data for the batch, decay and continuous experiments. The methodology is based on the assumption that the emulsion layer volume changes with coalescence and compaction of the dispersed phase but not through free settling. The emulsion layer was assumed to be in the form of a dense-packed zone, where the dispersed phase separated from the emulsion layer only through coalescence. Model development, assumptions, and verifications are described below.

4.1 Model Development

Models were required for three types of experiments: batch, decay, and continuous. Batch and decay experiments were used to determine the emulsion coalescence rate from the change in the volumes of the emulsion and the free oil layers over time. The coalescence rate was then used to predict the height of the emulsion layer over time for the continuous experiments. The models developed for each case are described below for oil-in-water emulsions. The same methodology was used to model the asphaltene stabilized water-in-oil emulsions except that the material balance was performed for water instead of oil.

4.1.1 Batch Experiment

During the batch experiments, the oil-in-water emulsion was created inside a beaker and allowed to coalesce into free organic and aqueous phases. The changes in the heights of the emulsion and oil layers were measured over time. The heights were modeled to find the emulsions stability or coalescence rates. The model is developed by performing a

material balance on the dispersed phase (oil in this example) in the emulsion layer, Figure 4.1

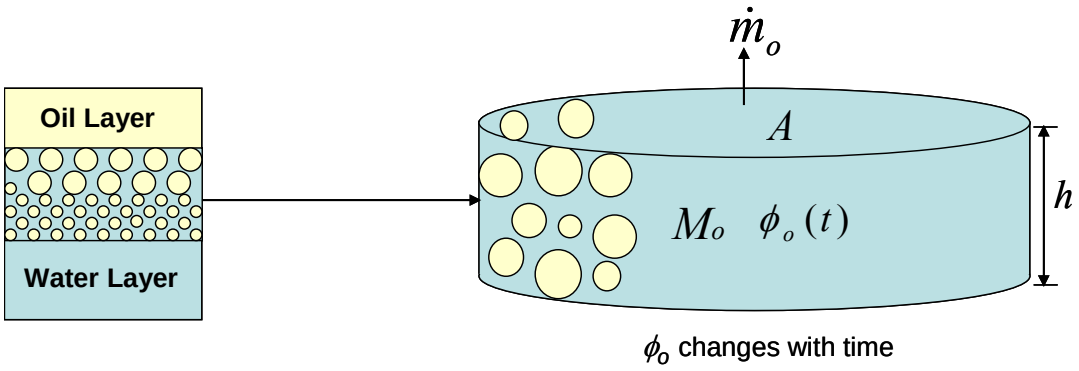

Figure 4.1: Material balance on the oil in the emulsion layer during a batch experiment.

The material balance for the oil across the emulsion layer is given by:

$$\frac{dM_o}{dt} = -\dot{m}_o \qquad \text{Equation } \mathbf{4.1}$$

where M_o is mass of the oil in the emulsion layer at any time, t, and $\dot{m}_o$ is the rate at which oil is exiting the emulsion layer as free oil due to coalescence. The mass of the oil inside the emulsion layer at time, t, is given by:

$$M_o = Ah\rho_o\phi_o(t) \qquad \text{Equation } \mathbf{4.2}$$

where A is the cross sectional area of the emulsion layer (or beaker), h is the rag layer height, and $\phi_o(t)$ is the volume fraction of the oil inside the rag layer at that time.

It was assumed that the rate the free oil is coming out of the emulsion layer due to coalescence is proportional to number of droplet to droplet contacts within the emulsion. If the size distribution of the droplets is invariant, the number of contacts is proportional to the volume of the oil in the emulsion layer at that time and therefore $\dot{m}_o$ can expressed as,

$$\dot{m}_o = k(t) A h \rho_o \phi_o(t) \qquad \text{Equation } \mathbf{4.3}$$

where k(t) is the proportionality constant or bulk coalescence rate constant. The coalescence rate constant was observed to decrease over time and the following exponential function for $k(t)$ was found to fit the experimental data at all the examined experimental conditions:

$$k(t) = k_o + (k_s - k_o)\{1 - \exp(-ct)\} \qquad \text{Equation } \mathbf{4.4}$$

where k_o and k_s are the coalescence rate constants at the beginning and end of the experiment, respectively, and c is a decay constant.

Eq. 4.2 and 4.3 are substituted into Eq. 4.1 to obtain:

$$\frac{d(Ah\rho_o\phi_o(t))}{dt} = -k(t) A h \rho_o \phi_o(t) \qquad \text{Equation } \mathbf{4.5}$$

Since A and ρ_o are constant, Eq. 4.5 simplifies to:

$$\frac{d(h\phi_o(t))}{dt} = -k(t) h \phi_o(t) \qquad \text{Equation } \mathbf{4.6}$$

It was found that the oil fraction in the emulsion layer, $\phi_o(t)$, changed over time during the batch experiments. Hence, on solving Eq. 4.6, the change in emulsion layer height over time is given by:

$$\frac{dh}{dt} = -k(t)h - \frac{h}{\phi_o(t)}\frac{d\phi_o(t)}{dt} \qquad \text{Equation } \mathbf{4.7}$$

Eq. 4.7 was made dimensionless by dividing by the height of the emulsion layer at the beginning of the batch experiment, h^o, as follows:

$$\frac{d\left(\frac{h}{h^o}\right)}{dt} = -k(t)\frac{h}{h^o} - \frac{1}{\phi_o(t)}\frac{h}{h^o}\frac{d\phi_o(t)}{dt} \qquad \text{Equation } \mathbf{4.8}$$

Eq. 4.8 was used to model the emulsion layer height in the batch experiments. Note, the oil volume fraction at any give time and its derivative were determined experimentally.

The height of the free oil layer was modeled by performing the material balance for the oil in the free oil layer, Figure 4.2. The instantaneous oil balance across the free oil layer is given by:

$$\frac{dM_{fo}}{dt} = \dot{m}_o \qquad \text{Equation } \mathbf{4.9}$$

where M_{fo} is the mass of oil in the free oil layer and $\dot{m}_o$ is again the rate at which the oil from the emulsion layer exits as free oil due to coalescence. The mass of the free oil at any time is expressed as:

$$M_{fo} = Ah_o\rho_o \qquad \text{Equation } \mathbf{4.10}$$

where, h_o is the height of the oil layer and A is the cross sectional area of the oil layer which is same as the cross section area of the emulsion layer or of the beaker.

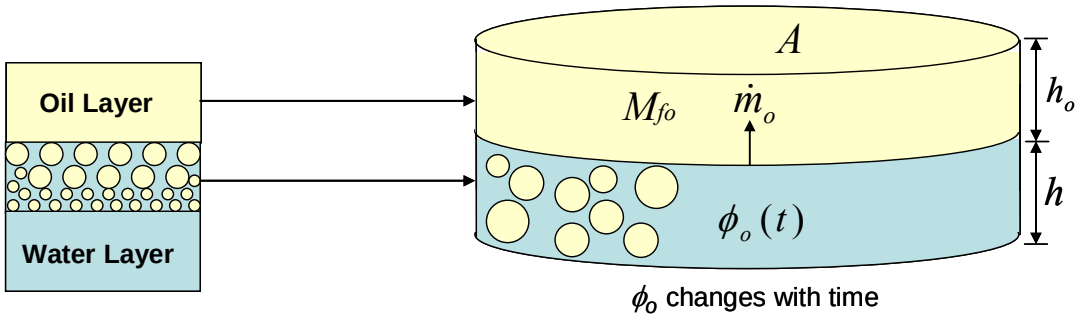

Figure 4.2: Material balance on the oil in the free oil layer during a batch experiment.

Eq. 4.3 and 4.10 are substituted into Eq. 4.9 to obtain:

$$\frac{dh_o}{dt} = k(t)h\phi_o(t) \qquad \text{Equation } \mathbf{4.11}$$

Eq. 4.11 is made dimensionless by dividing by the total height all of the oil would occupy if unemulsified, $h_o^{\,o}$, as follows:

$$\frac{d\left(\frac{h_o}{h_o^{\,o}}\right)}{dt} = k(t)\phi_o(t)\frac{h}{h_o^{\,o}} \qquad \text{Equation } \mathbf{4.12}$$

Eq. 4.12 was used to model the free oil layer height in the batch experiments. The bulk coalescence rate for the emulsion is determined by fitting the calculated oil and emulsion layer heights to the experimental data.

4.1.2 Decay Experiment

The decay experiment was identical to the batch experiment except that it was performed at the end of a continuous experiment on the emulsion layer formed during the continuous separation, Figure 4.3. The emulsion and the oil layer heights were modeled in the same manner as the batch experiments to determine the coalescence rates. Unlike the batch experiment, the oil fraction in the emulsion layer did not change over time and a simpler model is derived.

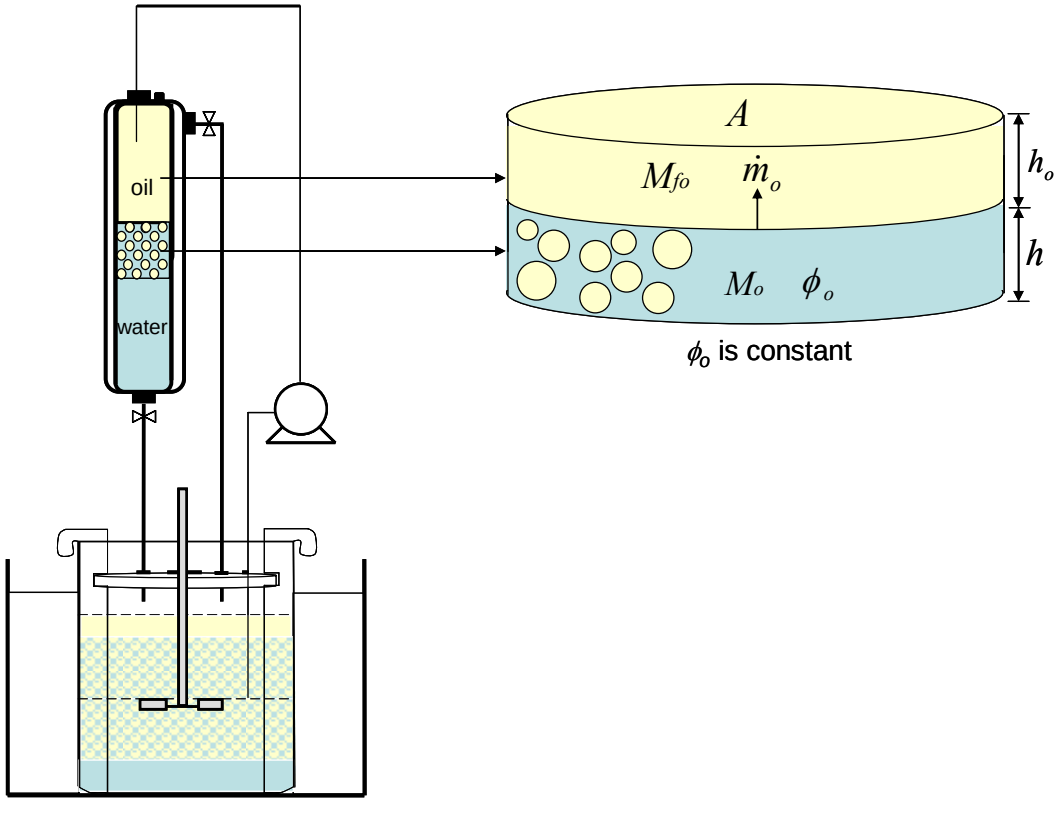

Figure 4.3: The emulsion layer inside the separator during a decay experiment (left side), and the enlarged representation of the oil and the emulsion layer (right side).

The emulsion layer height over time during a decay experiment is given by Eq. 4.7. Since the oil fraction in the emulsion layer, ϕ_o, did not change over time, Eq. 7 simplifies to:

$$\frac{dh}{dt} = -k(t)h \qquad \text{Equation } \mathbf{4.13}$$

Eq. 4.13 was made dimensionless by dividing by the steady state emulsion layer height during the continuous experiment (the initial height of the emulsion layer at the beginning of the decay experiment), h^o, to obtain:

$$\frac{d\left(\frac{h}{h^o}\right)}{dt} = -k(t)\frac{h}{h^o} \qquad \text{Equation } \mathbf{4.14}$$

The experimental oil layer height during the decay experiment is given by Eq. 4.12 but with a constant oil fraction in the emulsion layer as follows:

$$\frac{d\left(\frac{h_o}{h_o{}^o}\right)}{dt} = k(t)\phi_o \frac{h}{h_o{}^o} \qquad \text{Equation } \mathbf{4.15}$$

where $h_o{}^o$ is the height of the total free oil liberated at the end of the decay experiment which corresponds to the total height of the oil in the emulsion layer at the beginning of the decay experiment.

Eqs. 4.14 and 4.15 were fitted to the dimensionless emulsion and oil layer heights to obtain the coalescence rates. Eq. 4.4 was used as the functional form for the coalescence rate constant.

4.1.3 Continuous Experiment

In a continuous experiment the emulsion was continuously fed to the separator, and the emulsion layer growth was observed over time. The emulsion layer was modeled with a material balance on the dispersed phase inside the separator. Figure 4.4 shows the emulsion layer in the continuous experiment. As with the decay experiment, the oil fraction in the emulsion layer, ϕ_o, was invariant.

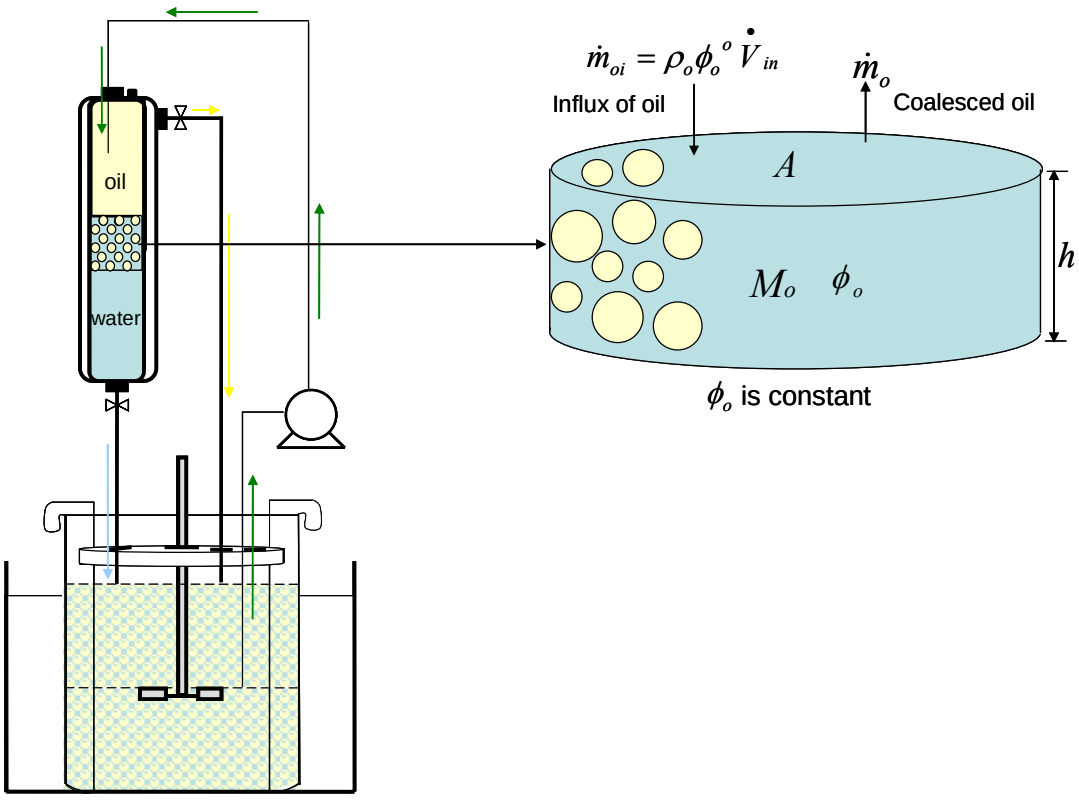

Figure 4.4: The emulsion layer in a continuous experiment (Left side). Enlarged view of the emulsion layer showing material flow (Right side).

In the continuous experiment, emulsified oil is fed to the emulsion layer and the material balance is given by:

$$\frac{dM_o}{dt} = \dot{m}_{oi} - \dot{m}_o \qquad \text{Equation } \mathbf{4.16}$$

where $\dot{m}_{oi}$ is the rate the emulsified oil is entering inside the separator through the feed. The mass of the oil in the emulsion layer is given by Eq. 4.2 but with a constant ϕ_o. The mass flow rate of oil out of the emulsion is given by Eq. 4.3, also with constant ϕ_o. The coalescence rate constant $k(t)$ is given by Eq. 4.4.

The influx of the emulsified oil in the feed is expressed as:

$$\dot{m}_{oi} = \rho_o \phi_o^{\,o} \dot{V}_{in} \qquad \text{Equation } \mathbf{4.17}$$

where ρ_o is the density of the oil, $\phi_o^{\,o}$ is the emulsified oil fraction in the feed, and $\dot{V}_{in}$ is the flow rate of the feed to the separator. Eqs. 4.2, 4.3 and 4.17 are substituted into Eq. 4.16 to obtain:

$$\frac{d(Ah\rho_o\phi_o)}{dt} = \rho_o \phi_o^{\,o} \dot{V}_{in} - k(t)Ah\rho_o\phi_o \qquad \text{Equation } \mathbf{4.18}$$

Eq. 4.18 simplifies to the following:

$$\frac{dh}{dt} = \frac{\phi_o^{\,o}}{\phi_o}\frac{\dot{V}_{in}}{A} - k(t)h \qquad \text{Equation } \mathbf{4.19}$$

Both the emulsified oil fraction in the feed, $\phi_o^{\,o}$, and the volume fraction of oil in the emulsion layer, ϕ_o, were determined experimentally. Eq. 4.19 was used to predict the emulsion layer growth in a continuous system using a known coalescence rate.

4.2 Verification of Model Assumption

The major assumption in the methodology was that the free oil coming out of the emulsion layer due to coalescence was proportional to the volume of the oil in the emulsion layer. This assumption led us to an exponential profile of height over time. In order to prove the assumption, a series of batch experiments was performed at the same experimental set of conditions, but with different total initial heights of the emulsion. These batch experiments were performed as described in Chapter 3 but in a beaker of volume 3500 mL and cross sectional area of 184 cm^2. The three different initial total volumes used were 1600 mL (initial total height = 8.7 cm), 2300 mL (initial total height = 12.3 cm) and 3000 mL (initial total height = 16 cm). All three experiments were performed at a temperature of 45^{o}C, a mixer speed of 800 rpm, an organic phase 50 vol% *n*-heptane and 50 vol% toluene, a NEO-10 surfactant concentration of 80 ppm in RO-water, and an aqueous phase volume fraction of 0.5.

Figure 4.5 shows the dimensionless free oil and emulsion layer heights versus time. All three data sets are nearly identical. On a dimensionless plot, data from three different initial heights only collapse onto a single dimensionless curve if the data follow an exponential profile. While the profile is modified slightly due to the time dependent coalescence rate, the common exponential profile provides strong evidence that the bulk coalescence rate is proportional to the volume of oil within the emulsion layer. Note the relatively small deviations between the data sets could be caused by differences in the initial droplet size distribution. Since the height of the emulsion was different in each

case, the mixing conditions were not identical and different droplet sizes may have been generated. Different droplet sizes will lead to different coalescence rates.

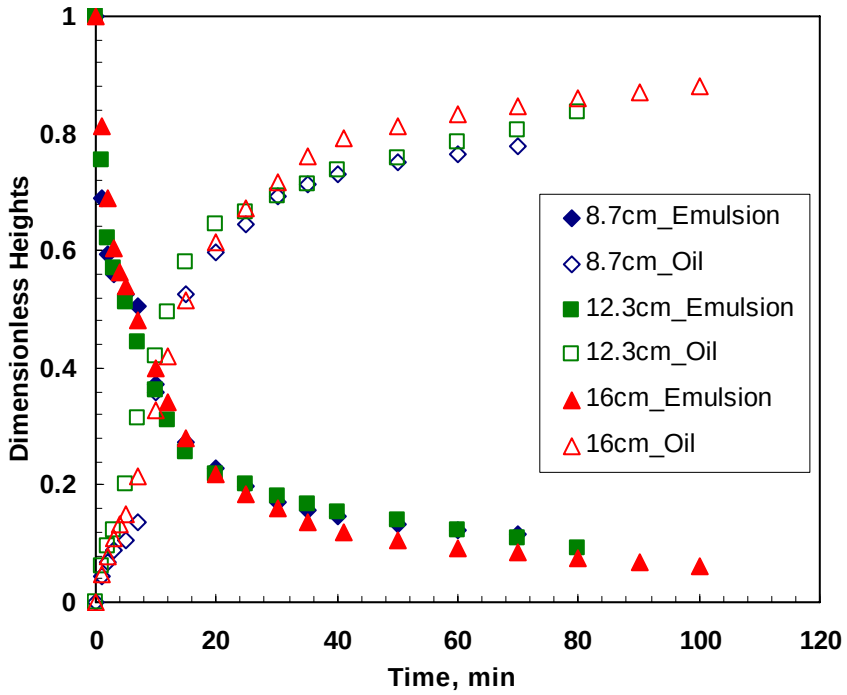

Figure 4.5: Batch experiments performed at the 80 ppm concentration of NEO-10 surfactant with different initial heights of the emulsion.

CHAPTER 5
RESULTS AND DISCUSSION

Data and modeling of emulsion layer growth for oil-in-water and water-in-oil model emulsions are presented. The bulk of the data was collected for the oil-in-water emulsions and this data is used to present the interpretation of the batch, decay, and continuous experiments. The use of coalescence rates from decay experiments to predict emulsion layer growth in continuous experiments is presented. The effects of surfactant concentration, feed flow rate, separator area, and wall effects are discussed. Finally, the emulsion layer growth model developed from the oil-in-water emulsion data is applied to the model water-in-oil emulsions.

5.1 Emulsion Layers from Oil-in-Water Emulsions

5.1.1 Coalescence Rates from Batch Experiments

During a batch experiment, the emulsion was created inside a beaker and was left undisturbed to coalesce into free organic and aqueous phases. Figure 5.1 shows the change in the oil and emulsion layer heights over time during a batch experiment. Note the rapid decrease in the emulsion layer height and increase in the oil layer height over the first few minutes of the experiment. This rapid decrease is beyond what would be predicted with a constant coalescence rate and, in fact, the coalescence rate was found to decrease exponentially with time.

One possible explanation for the decreasing coalescence rate is that droplets are polydisperse, Figure 5.2. Large droplets are known to coalesce more rapidly than small droplets (Dickinson *et al*., 1988). Hence, the large droplets are expected to coalesce first giving a high initial coalescence rate. If the abundance of the large droplets decreases,

smaller droplets will predominate and the coalescence rate is expected to decrease. However, the final drop size distribution is similar to the initial drop size distribution and even includes some larger droplets, Figure 5.2. Therefore, polydispersity is not the explanation.

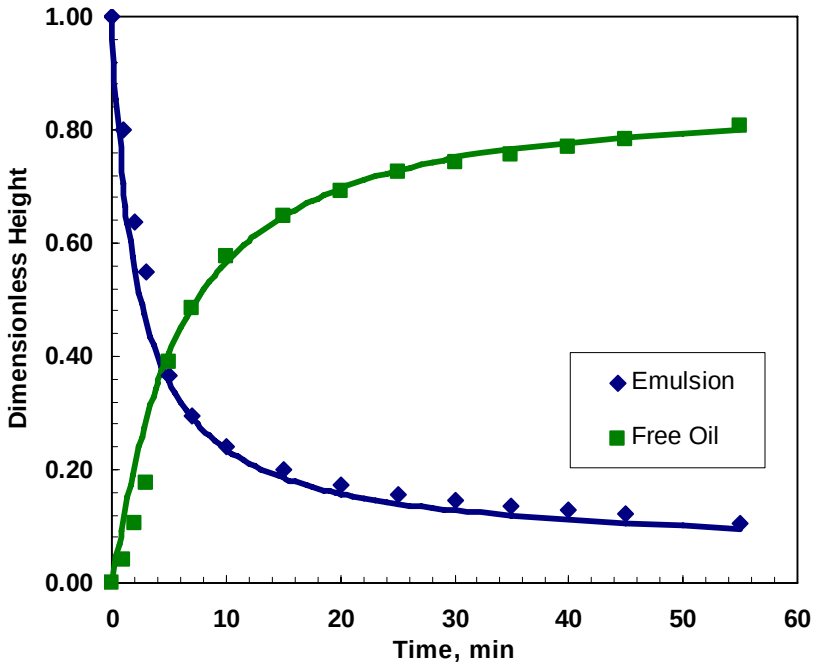

Figure 5.1: The emulsion and oil layer heights over time for a batch experiment performed at 45°C and 80 ppm concentration of NEO-10. The oil volume fraction in the initial emulsion was 50%. The symbols correspond to the experimental data and solid lines indicate the modeled profiles.

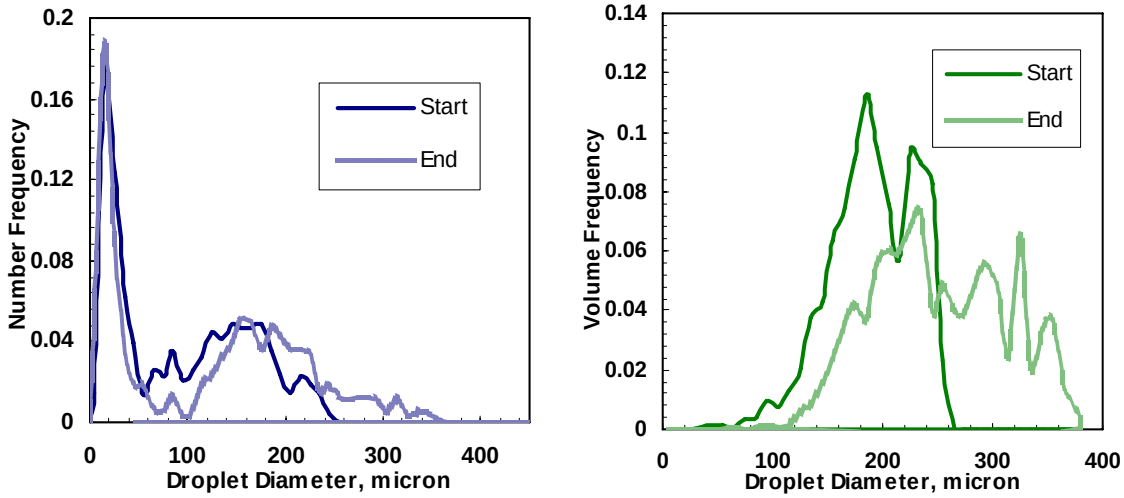

Figure 5.2: Droplet size distribution at the start and end of a batch experiment performed at 45^{o}C and 80 ppm concentration of NEO-10. The oil volume fraction in the initial emulsion was 50%.

Another possible explanation is that the structure of the emulsion layer changes over time. Figure 5.3 shows that, for batch experiments, the volume fraction of the dispersed oil phase increases over time; that is, the emulsion layer compacts. Since the droplet size distribution is unchanged, there must be thinner water films between the oil droplets. Normally, as the film thins coalescence rates are expected to increase. However, for these emulsion layers, coalescence rates appear to be inversely correlated to the volume fraction of the dispersed phase. It is possible that surface active material liberated from the initial coalescence of droplets becomes concentrated in the film between the droplets and enhances emulsion stability.

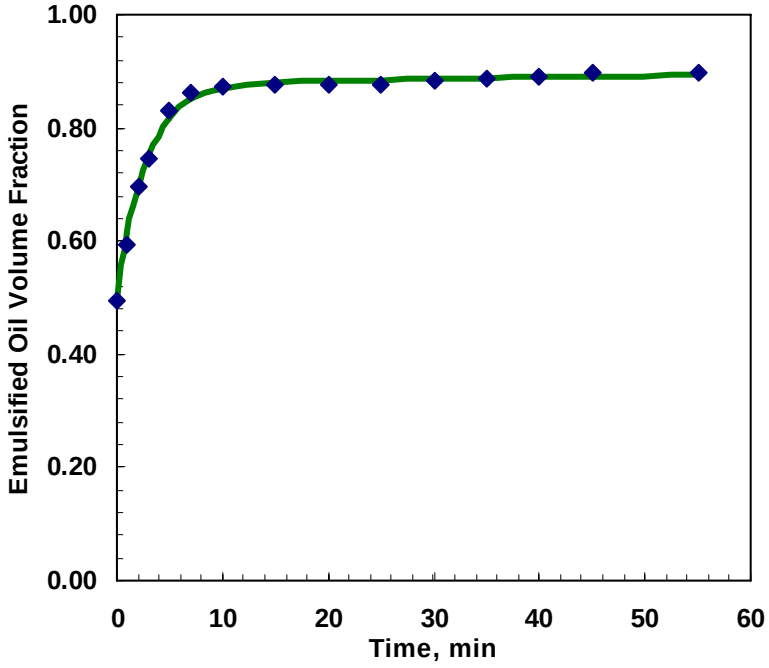

Figure 5.3: Emulsified oil volume fraction in the emulsion layer during a batch experiment performed at 45°C and 80 ppm concentration of NEO-10. The oil volume fraction in the initial emulsion was 50%. The symbols correspond to the experimental data and solid line is a curve fit.

If this interpretation is correct, gentle mixing of the emulsion layer should liberate the trapped surfactant and increase the coalescence rate. To test the hypothesis, the experiment of Figure 5.1 was repeated first with no change in procedure and second with a brief gentle stirring of the emulsion layer 20 minutes after the mixer was stopped. After the disturbance, the emulsion layer was allowed to coalesce as before. Figure 5.4 shows that the gentle mixing caused a sustained increase in the coalescence rate as predicted. The free oil and emulsion layer heights were again modeled to find the coalescence rate, Table 5.1. The final coalescence rate of the disturbed emulsion is 2.5 times greater than

the undisturbed emulsion. Hence, it appears surfactant molecules accumulate in thinning films in the emulsion layer causing the coalescence rate to decrease over time.

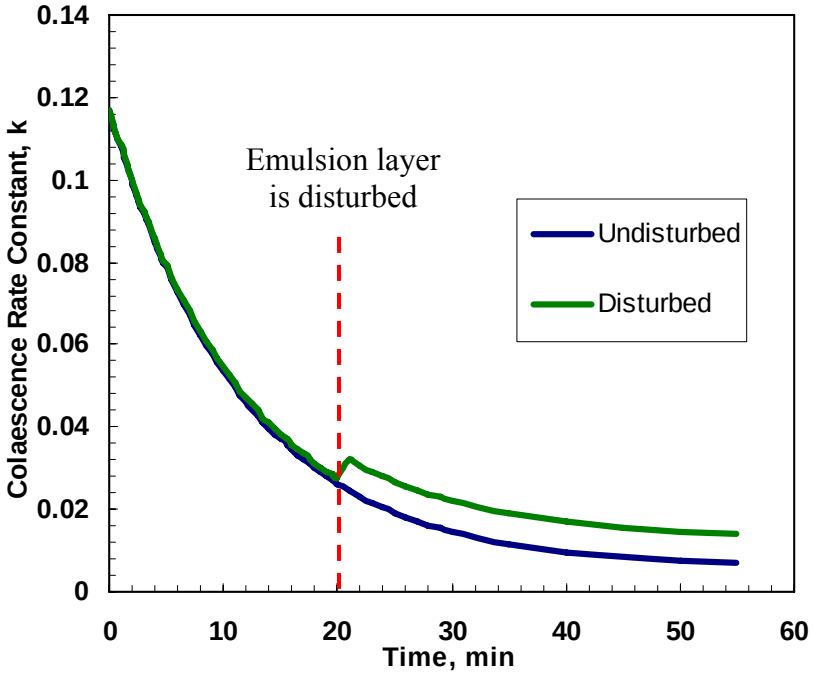

Figure 5.4: The variation of coalescence rate constant over time for the two different batch experiments performed at 80 ppm concentration of NEO-10. In one case the emulsion is disturbed after 20 minutes to check the local accumulation of surfactant at oil-water interface.

Table 5.1: Model parameters for the two different batch experiments performed at 80 ppm concentration of NEO-10. In one case the emulsion is disturbed after 20 minutes.

Parameter	Undisturbed	Disturbed
k_o, min^{-1}	0.117	0.119
k_s, min^{-1}	**0.006**	**0.014**
c, min^{-1}	0.085	0.083

Figure 5.3 also showed that over the first 10 minutes the oil volume fraction increased from an initial condition of 50% to a stable value of approximately 85%. In other words, the emulsion compacted to a continuous phase volume fraction of 15%. This volume fraction is consistent with the polydispersity of the droplets, perhaps with some deformation under film drainage. The volume fraction and its derivative at any given time were required for modeling. The data was fitted with an equation of the form:

$$\phi_o(t) = \phi_{oo} + c_1\left(1 - \exp\left(-c_2 t\right)\right) + c_3\left(1 - \exp\left(-c_4 t\right)\right) \qquad \text{Equation } \mathbf{5.1}$$

where $\phi_o(t)$ is fitted oil volume fraction at time t, ϕ_{oo} is experimental value of oil volume fraction at t = 0, and c_1, c_2, c_3 and c_4 are constants, which were determined to fit the experimental oil volume fractions with above mentioned Eq. 5.1.

The derivative of Eq. 5.1 is given by:

$$\frac{d\phi_o(t)}{dt} = c_1 c_2 \exp\left(-c_2 t\right) + c_3 c_4 \exp\left(-c_4 t\right) \qquad \text{Equation } \mathbf{5.2}$$

The fit to the data is shown in Figure 5.3. Note Eq. 5.1 is empirical and only used for data fitting.

The dimensionless heights for the emulsion and oil layers were modeled with the methodology developed in Chapter 4 using Eqs. 4.9 and 4.13. The fitted oil volume fraction and its derivative were inputs to the model. The model was fitted to the dimensionless height data by adjusting the coalescence rates, Eq. 4.4. The fitted model is shown in Figure 5.1. Table 5.2 provides the model parameters used to fit the oil and emulsion layer heights.

The effect of surfactant concentration was also examined, Figure 5.5. The emulsion and oil layer heights were fitted as described above and the coalescence rate parameters are given in Table 5.2. As expected, the coalescence rate decreased as the surfactant concentration increased because the emulsion became more stable. In all cases, the model fit the data with an average absolute relative deviation (AARD) of 0.051.

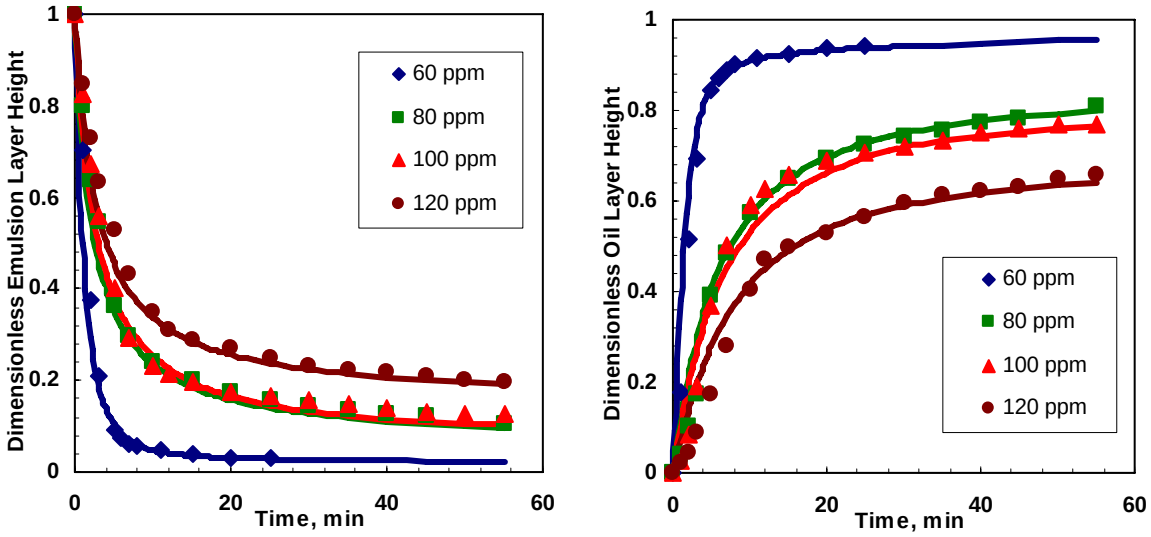

(a) **(b)**

Figure 5.5: The dimensionless emulsion layer (a), and the oil layer (b), heights over time for batch experiments performed at 45°C with different concentrations of NEO-10. The oil volume fraction in the initial emulsion was 50%. The symbols correspond to the experimental data and solid lines indicate the modeled profiles.

Table 5.2: Coalescence rate parameters used to model the batch experiments performed at 45°C with concentrations of NEO-10 ranging from 60 to 120 ppm.

Parameter	Concentration (ppm)			
	60	**80**	**100**	**120**
k_o, min^{-1}	0.500	0.117	0.105	0.072
k_s, min^{-1}	0.007	0.006	0.002	0.003
c, min^{-1}	0.200	0.085	0.070	0.080

5.1.2 Coalescence Rates from Decay Experiments

In a decay experiment, the emulsion layer formed inside the separator at the end of a continuous experiment was left undisturbed to coalesce into free oil and water with no feed or outlet flow. Figure 5.6 shows the change in the oil and emulsion layer heights over time during a decay experiment. The results are qualitatively similar to the batch experiments.

Unlike the batch experiments, the volume fraction of oil was invariant (64±4% for the emulsion in Figure 5.6) throughout the decay experiment. The emulsion layer is more compact than that the initial emulsion layer from a batch experiment but less compact than the final batch emulsion layer. The emulsion layer in the decay experiment is the average accumulation over the time of a continuous experiment and it is not surprising that it is initially more compact than in a batch experiment. The initial droplet size distribution is shifted to smaller droplet sizes relative to the batch experiment, Figure 5.7, indicating that larger droplets have been eliminated as the emulsion layer grew. The final droplet size distribution is smaller and narrower indicating that the largest droplets have disappeared. The lower polydispersity may account for the lower packing (volume of dispersed phase) in the decay experiment.

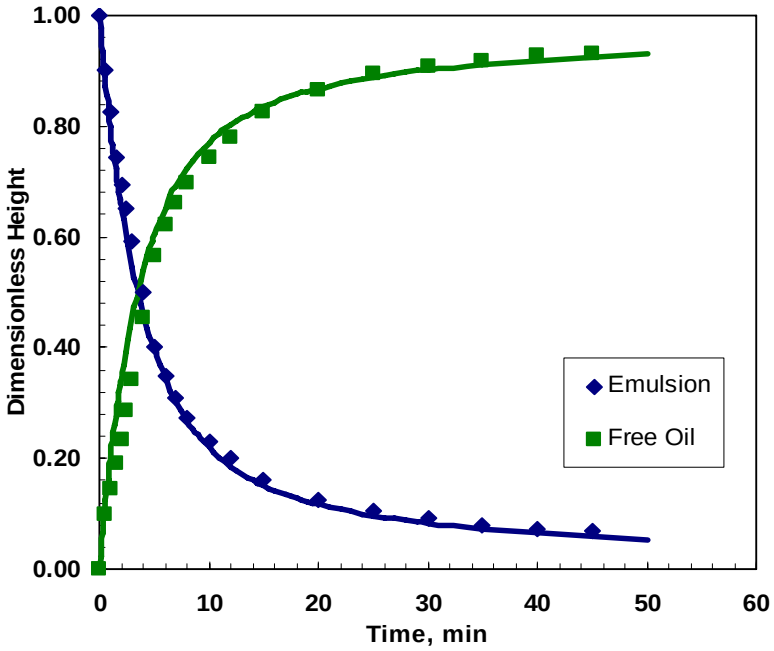

Figure 5.6: The emulsion and oil layer heights over time for a decay experiment performed at 45°C and 80 ppm concentration of NEO-10 in the 250 mL separator. The symbols are experimental values and solid lines are the modeled profiles. The continuous run prior to this decay experiment was performed at the feed flow rate of 45 cm^3/min.

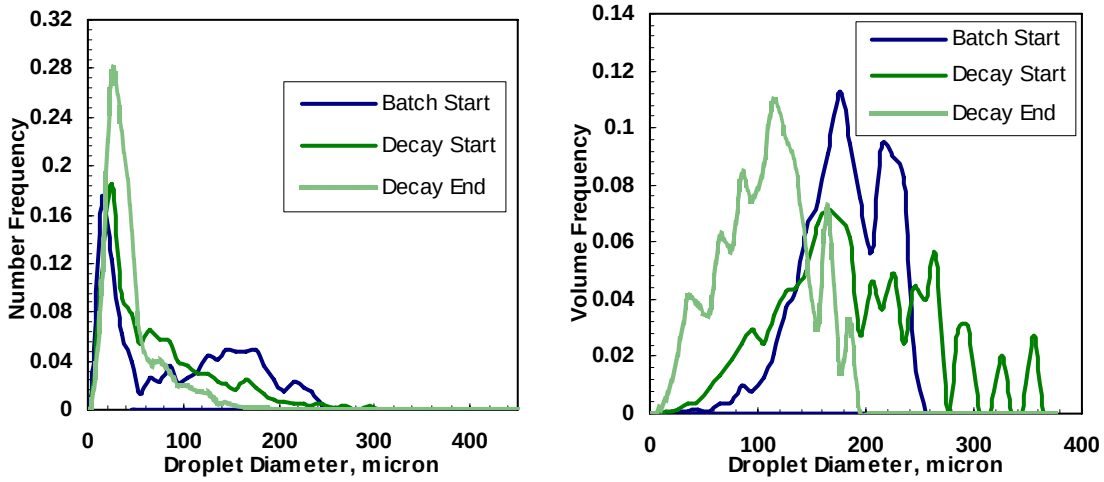

Figure 5.7: Droplet size distribution at the start and end of a decay experiment performed at 45°C and 80 ppm concentration of NEO-10. The oil volume fraction in the initial emulsion was 50%. The flow rate for the continuous run prior to this decay experiment was 45 cm^3/min.

The dimensionless heights for the emulsion and oil layers were modeled with the methodology using Eqs. 4.15 and 4.16. A constant oil volume fraction of 0.64 was used and the model was fitted to the dimensionless height data by adjusting the coalescence rate, Eq. 4.4. The fitted model is shown in Figure 5.6. Table 5.3 provides the model parameters used to fit the oil and emulsion layer heights.

Figure 5.8 shows the effect of surfactant concentration. As observed with the batch experiments, the coalescence rate decreased as the surfactant concentration increased, Table 5.3. In all cases, the model fit the data with an AARD of 0.044.

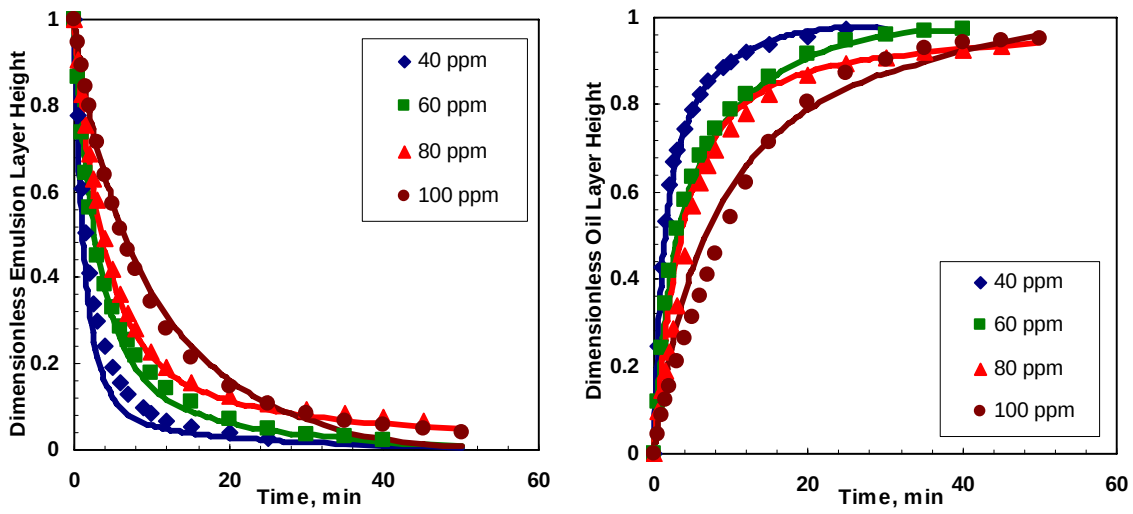

(a) **(b)**

Figure 5.8: The dimensionless emulsion layer (a), and oil layer (b), heights over time for decay experiments performed at 45°C and different concentrations of NEO-10. The oil volume fraction in the initial emulsion was 50%. The symbols correspond to the experimental data and solid lines indicate the modeled profiles.

Table 5.3: Coalescence rate parameters used to model the decay experiments performed in the 250 ml separator at 45°C with concentrations of NEO-10 from 60 to 120 ppm. The prior continuous experiment was performed at the feed flow rate of 45 cm³/min.

Parameter	Concentration (ppm)			
	40	**60**	**80**	**100**
ϕ_o	0.65	0.64	0.64	0.60
k_o, min^{-1}	0.75	0.30	0.23	0.14
k_s, min^{-1}	0.03	0.05	0.02	0.08
c, min^{-1}	0.30	0.14	0.11	0.32

The coalescence rate parameters for batch and decay experiments, performed at the same conditions, are compared in Table 5.4. The initial and steady state rate constants are higher for the decay experiments than for the batch experiments except at 60 ppm. Given that the droplet size distributions are similar in both batch and decay experiments, the difference in coalescence rate appears to be related to the dispersed oil phase volume fraction; that is, the proximity of the droplets to each other. Recall that the oil volume fraction in the decay experiment was initially higher than the batch experiment. A high dispersed phase volume fraction provides closer contact between the droplets and is expected to provide a higher coalescence rate. To test this hypothesis, a batch experiment was performed at 80 ppm NEO-10 with an initial oil volume fraction of 0.64, the oil fraction found during the equivalent decay experiment. Table 5.5 shows that at this oil volume fraction, the coalescence rate for the batch experiment is the same as for the decay experiment. Hence, the difference in the initial coalescence rates in Table 5.4 is caused by the dispersed phase volume fraction. If batch experiments are to be used to predict continuous and decay experiment coalescence rates, the same initial dispersed oil phase volume fraction must be used.

The final coalescence rate of the batch experiments is consistently lower than that of the decay experiments even though the average droplet size is larger and the droplet size distribution is wider. The final dispersed oil phase volume fraction is higher in the batch experiments which as mentioned above is expected to give higher not lower coalescence rates. Again, it appears that surface active material may accumulate in the thin films that occur at high dispersed phase volume fraction. The accumulation of surface active material would reduce coalescence rates. It appears that initially high dispersed phase volume fractions increase coalescence rates as expected but, over time, as surface active material accumulates, coalescence rates decrease.

Note that, contrary to the observations at higher concentrations, the initial batch coalescence rate is higher than that of the decay experiment at 60 ppm. The droplets are

very large at this low surfactant concentration and the coalescence rate is initially very high and likely insensitive to the dispersed phase volume fraction. Therefore, the initial coalescence rate in the batch experiment is undiminished. The coalescence rate also decreases rapidly as the emulsion layer compacts into an extremely dense-packed layer with a dispersed oil phase volume fraction of more than 95%. For the decay experiment, some of the initial rapid coalescence had already occurred during the continuous experiment and the starting coalescence rate is therefore lower than the batch experiment.

Table 5.4: Model parameters for the batch and decay experiments performed at 45°C with concentrations of NEO-10 ranging from 60 to 100 ppm. All other experimental conditions were same.

Parameter	**60 ppm**		**80 ppm**		**100 ppm**	
	Batch	*Decay*	*Batch*	*Decay*	*Batch*	*Decay*
ϕ_o	--	0.64	--	0.64	--	0.60
k_o, min^{-1}	0.50	0.30	0.117	0.23	0.105	0.14
k_s, min^{-1}	0.007	0.05	0.006	0.02	0.002	0.08
c, min^{-1}	0.20	0.13	0.085	0.11	0.070	0.32

Table 5.5: Coalescence rate parameters used to model the batch experiments performed at 45°C with NEO-10 concentration of 80 ppm and initial oil volume fraction of 0.64.

Parameter	Batch ϕ_o = 0.50	Batch ϕ_o = 0.65	Decay ϕ_o = 0.65
k_o, min^{-1}	0.117	0.23	0.23
k_s, min^{-1}	0.006	0.015	0.02
c, min^{-1}	0.085	0.16	0.11

5.1.3 Emulsion Layer Growth in Continuous Experiments

In a continuous experiment, the emulsion was continuously fed to the separator where the emulsion layer grew over time until it reached a steady state and there was no further increase in the emulsion layer height. Figure 5.9 shows the growth of an emulsion layer during a continuous experiment at 45°C and 80 ppm NEO-10. In this case, a steady state condition was reached at approximately 15 minutes.

The emulsion layer height was predicted using Eq. 4.19. The oil volume fraction in the feed was determined experimentally. The oil volume fraction in the emulsion layer was also determined experimentally and, as with the decay experiments, was found to be invariant. The steady state coalescence rate constant was set to the initial coalescence rate constant from either a batch or a decay experiment. Recall that the beginning of a decay experiment is the end (or steady state) of a continuous experiment. The initial rate constant could not be predicted and was fitted to the continuous data.

In Figure 5.9, the green solid line corresponds to the prediction from the decay coalescence rate constant and the red solid line corresponds to the prediction from the batch coalescence rate constant. It can be seen that the initial batch coalescence rate constant (k_o = 0.117 min^{-1}) over-predicted the steady state emulsion layer height. On the

other hand, initial decay coalescence rate constant (k_o = 0.23 min^{-1}) correctly predicted the steady state emulsion layer height.

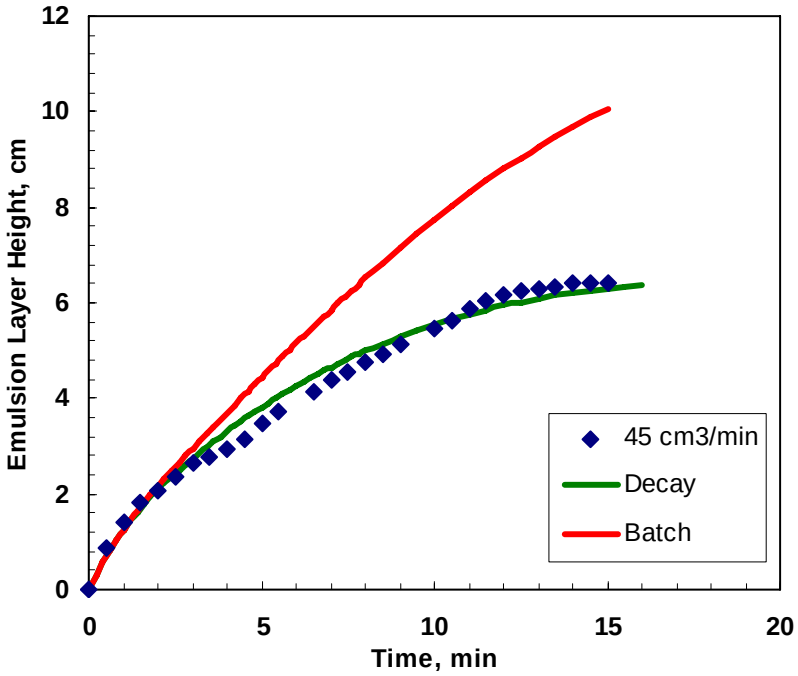

Figure 5.9: The emulsion layer growth during the continuous experiment performed at 45°C and 80 ppm concentration of NEO-10 in the 250 mL separator at the feed flow rate of 45 cm^3/min. The symbols are experimental data points and solid lines correspond to the modeled profiles.

Figure 5.10 shows the effect of surfactant concentration on emulsion layer growth. As expected, as the surfactant concentration increased, the coalesce rate decreased and the emulsion layer grew faster. Table 5.6 provides the parameters used to fit the continuous experimental data at NEO-10 concentrations of 40 to 100 ppm. In all cases, the initial coalescence rate constants from the decay experiments provided a good fit of the continuous steady state condition. The model fit the data with an AARD of 0.042.

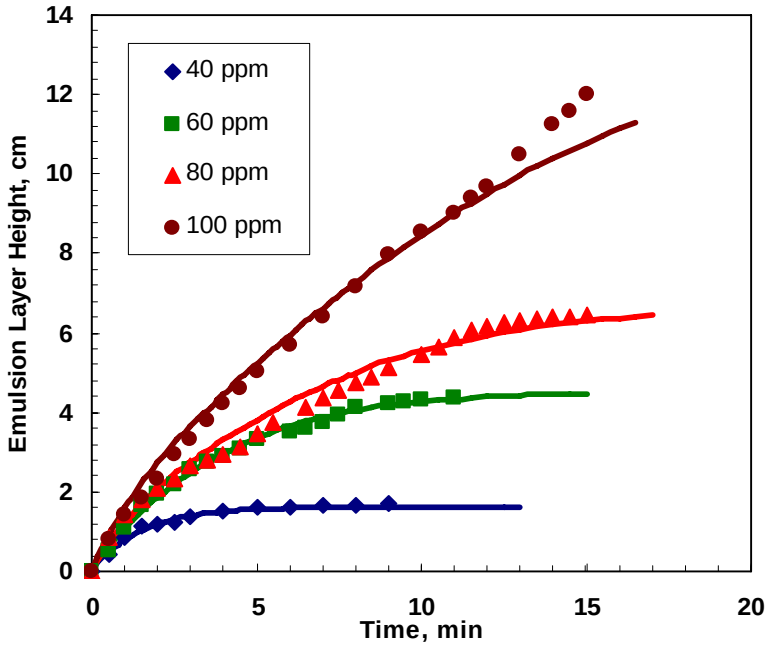

Figure 5.10: The emulsion layer height over time for continuous experiments performed at 45°C and different concentrations of NEO-10 in the 250 mL separator with feed flow rate of 45 cm^3/min. The symbols correspond to the experimental data and solid lines indicate the modeled profiles.

Table 5.6: Model parameters for the continuous and decay experiments performed at various concentrations of NEO-10 in the 250 mL separator with the feed flow rate of 45 cm^3/min for the continuous experiments. All other experimental conditions were identical.

Parameter	Concentration (ppm)							
	40		60		80		100	
	Decay	*Cont.*	*Decay*	*Cont.*	*Decay*	*Cont.*	*Decay*	*Cont.*
ϕ_o^o	--	0.165	--	0.20	--	0.23	--	0.27
ϕ_o	0.65	0.65	0.64	0.64	0.64	0.64	0.60	0.60
k_o, min^{-1}	**0.69**	1.00	**0.30**	0.65	**0.23**	0.60	**0.14**	0.50
k_s, min^{-1}	0.05	**0.69**	0.05	**0.30**	0.02	**0.23**	0.08	**0.14**
c, min^{-1}	0.27	1.20	0.14	0.80	0.11	0.40	0.32	0.28

5.1.3.1 Effect of Flow Rate

The feed flow rate is an input parameter to the model and is independent of the coalescence rates. Hence, varying the flow rate provides a good test of the model's predictive capabilities. Continuous experiments were performed at feed flow rates ranging from 40 cm^3/min to 55 cm^3/min in the 250 mL separator (cross sectional area of 10.5 cm^2), Figure 5.11. As the flow rate increased, the emulsion layer reached larger steady state heights because more height was required to achieve a sufficient coalescence rate to balance the higher feed rate. Note, at feed rates greater than 50 cm^3/min, the emulsion layer overflowed the separator before reaching steady state.

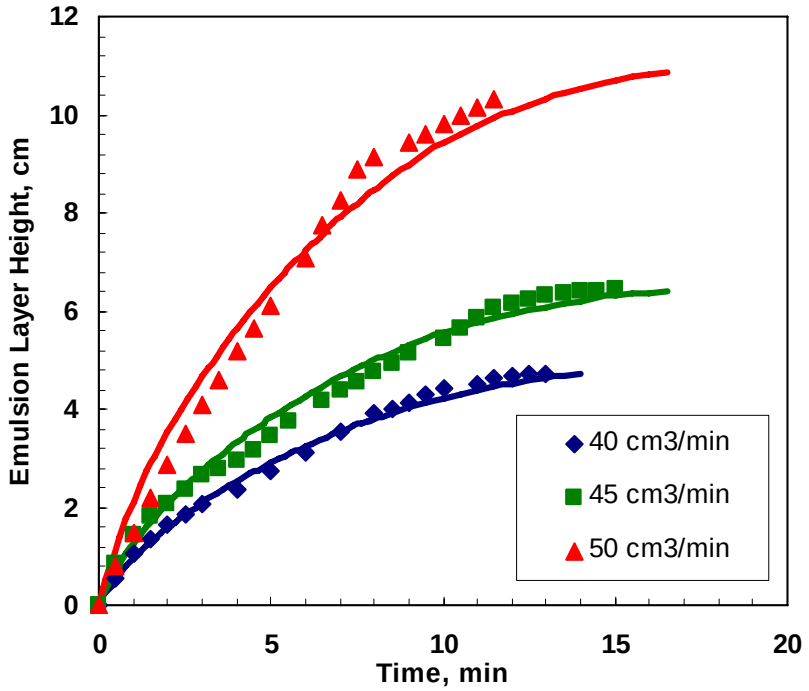

Figure 5.11: Continuous experiments performed at 45°C and 80 ppm NEO-10 in the 250 mL separator at feed rates of 40 to 50 cm³/min. The symbols denote the experimental data points and solid lines correspond to the modeled profiles.

The initial coalescence rate constant from the corresponding decay experiment was used to predict the steady state emulsion layer height for all the three flow rates. The initial rate constant and the decay factor from the 45 cm³/min experiment were assumed to apply at the other flow rates. Figure 5.10 shows that the model predicted the steady state emulsion layer height (or final measured height) to within 0.3 cm (5%). Table 5.7 shows the model parameters used for all three flow rates.

Table 5.7: Model parameters used for continuous experiments performed in the 250 mL separator at 45°C and 80 ppm concentration of NEO-10 at feed rates of 40, 45, and 50 cm³/min.

Parameter	Flow Rate					
	40 cm³/min		**45 cm³/min**		**50 cm³/min**	
	Decay	*Continuous*	*Decay*	*Continuous*	*Decay*	*Continuous*
$\phi_o^{\ o}$	--	0.215	--	0.23	--	0.275
ϕ_o	0.70	0.70	0.64	0.64	0.52	0.52
k_o, min^{-1}	**0.23**	0.60	**0.23**	0.60	**0.23**	0.60
k_s, min^{-1}	0.02	**0.23**	0.02	**0.23**	0.02	**0.23**
c, min^{-1}	0.06	0.40	0.11	0.40	0.13	0.40

5.1.3.2 Effect of Separator Area

The separator area is also an input parameter that is independent of the coalescence rates and can be used to test the model. Continuous experiments were performed in a second separator with volume of 500 mL and cross sectional area of 14.4 cm^2. The experiments were performed at feed rates from 40 to 62 cm³/min, Figure 5.12. As before, the steady state emulsion layer height increased with flow rate and could be predicted to within 0.2 cm (4%) from the initial decay coalescence rate constant of 0.34 min^{-1}. Table 5.8 gives the model parameters for all four flow rates.

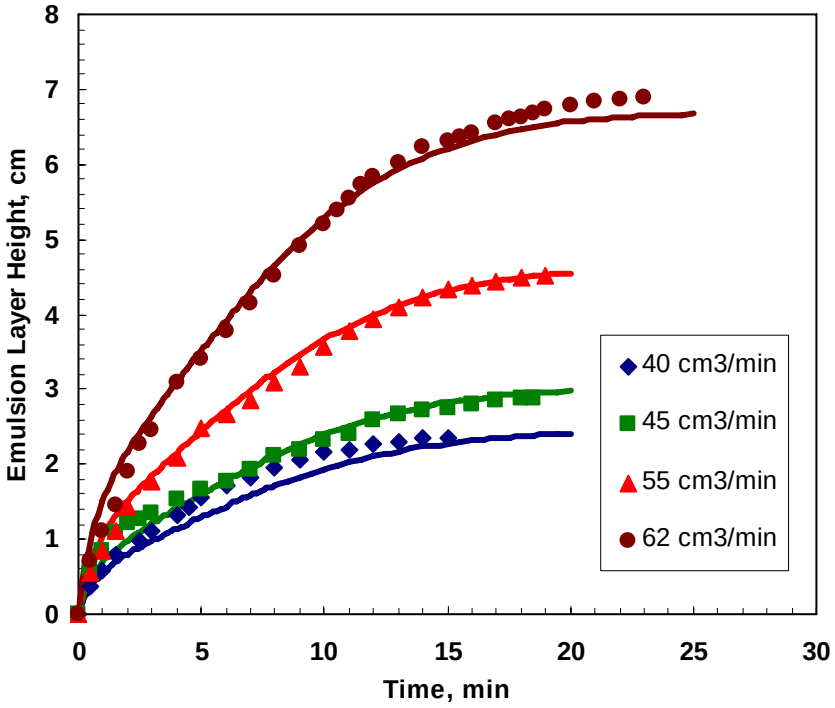

Figure 5.12: Continuous experiments performed with 80 ppm concentration of NEO-10 surfactant in the 500 mL separator at different feed flow rates. The symbols denote the experimental data points and solid lines correspond to the modeled profiles.

Table 5.8: Model parameters used for continuous experiments performed in the 500 ml separator with 80 ppm concentration of NEO-10 surfactant at various feed flow rates.

Parameter	Flow Rate							
	40 cm^3/min		**45 cm^3/min**		**55 cm^3/min**		**62 cm^3/min**	
	Decay	*Cont.*	*Decay*	*Cont.*	*Decay*	*Cont.*	*Decay*	*Cont.*
$\phi_o^{\,o}$	--	0.215	--	0.23	--	0.29	--	0.355
ϕ_o	0.73	0.73	0.695	0.695	0.70	0.70	0.67	0.67
k_o, min^{-1}	**0.34**	1.20	**0.34**	1.20	**0.34**	1.20	**0.34**	1.20
k_s, min^{-1}	0.025	**0.34**	0.037	**0.34**	0.031	**0.34**	0.044	**0.34**
c, min^{-1}	0.18	0.30	0.135	0.30	0.20	0.30	0.68	0.30

When the data from the large and small separator are compared, a discrepancy becomes apparent. The steady state coalescence rate constant for the large separator (k_s = 0.34 min^{-1}) was larger than the rate constant for the small separator (k_s = 0.23 min^{-1}). The emulsions prepared for these tests were identical; so why is the coalescence rate different? One difference is the surface area of the emulsion in contact with the separator walls. For a given feed flow rate, the emulsion layer height at any time was larger in the smaller separator than in the big separator. More emulsion was in contact with the walls of the smaller separator. If the walls reduced the coalescence rate in their vicinity, the average coalescence rate would be lower for the smaller separator.

5.1.3.3 Wall Effect

To investigate the wall effect, a series of batch experiments was performed where the surface area in contact with the emulsion was varied. Seven different experiments were performed with emulsion prepared at the same experimental conditions with a temperature of 45^{o}C, a mixer speed of 800 rpm, an organic phase of 50_heptol (50 vol%

n-heptane and 50 vol% toluene), a NEO-10 surfactant concentration of 70 ppm in RO-water, an aqueous phase volume fraction of 0.5. All the experiments were performed in the 2000 mL beaker and the emulsion was prepared as explained in Section 3.2.

The first batch experiment was performed as described in Section 3.3. In the remaining six experiments, immediately after the emulsion was prepared, a glass tube or combination of glass tubes was gently placed inside the beaker to create an extra contact surface for the emulsion. The emulsion and oil layer heights were measured for the emulsion which was confined between the glass tube and the inside periphery of the beaker. Then the coalescence rates were determined as before. Figure 5.13 shows seven different configurations used for the study the effect of wall on the emulsion stability.

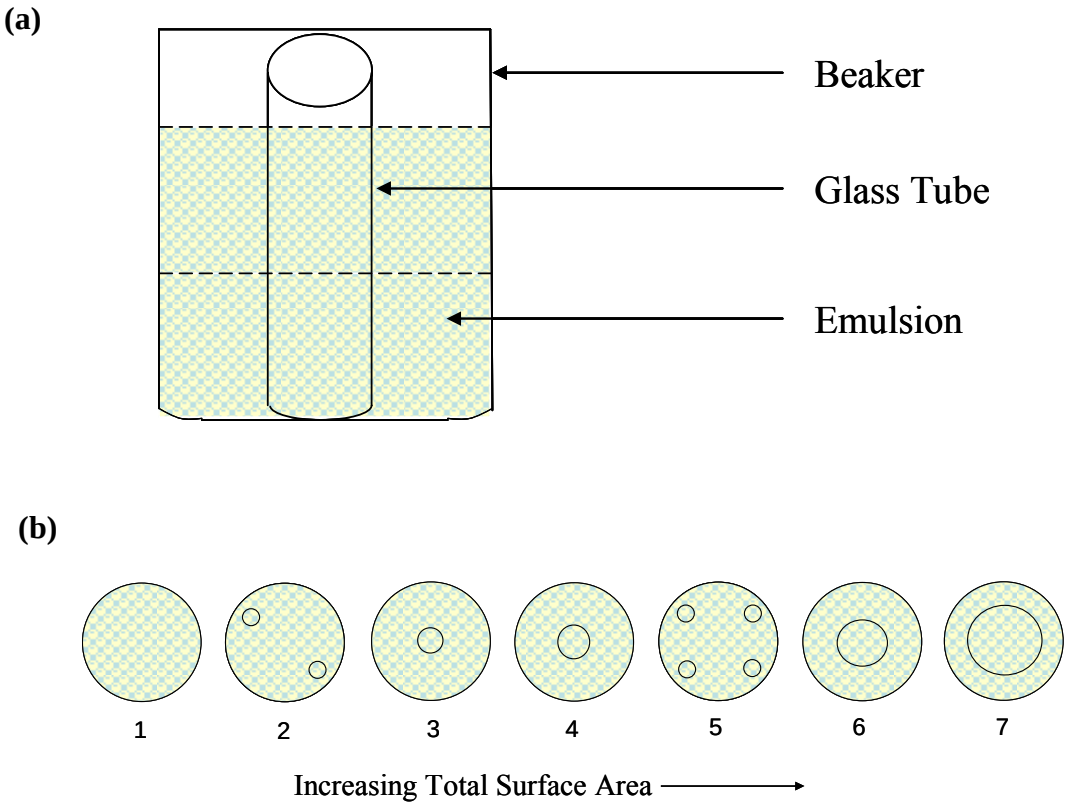

Figure 5.13: (a) Batch experiment with a glass tube inside the beaker; (b) Top views of all seven configurations with different glass tubes inside the beaker.

Table 5.9 shows the calculation for the ratio of surface area to volume (SA/V) and gives the coalescence rate constant values for each configuration. Figure 5.14 shows the plot between the coalescence rate constant and the ratio of the surface area to volume (SA/V) for each experiment. Figure 5.14 shows that, if all other experimental conditions are same, the coalescence rate constant decreases as SA/V increases. In other words, the more of the emulsion in contact with the walls, less is the coalescence.

Table 5.9: Dimensions for seven different configurations shown in Figure 5.13b.

Configuration Number	Radius of Beaker, cm	Radius of Glass Tube, cm	Number of Tubes	SA/V, cm^{-1}	k_s, min^{-1}
1	6.25	--	0	0.308	0.0125
2	6.25	1.20	2	0.452	0.013
3	6.25	2.25	1	0.471	0.013
4	6.25	3.25	1	0.615	0.011
5	6.25	1.20	4	0.619	0.011
6	6.25	4.25	1	0.889	0.009
7	6.25	5.25	1	1.600	0.005

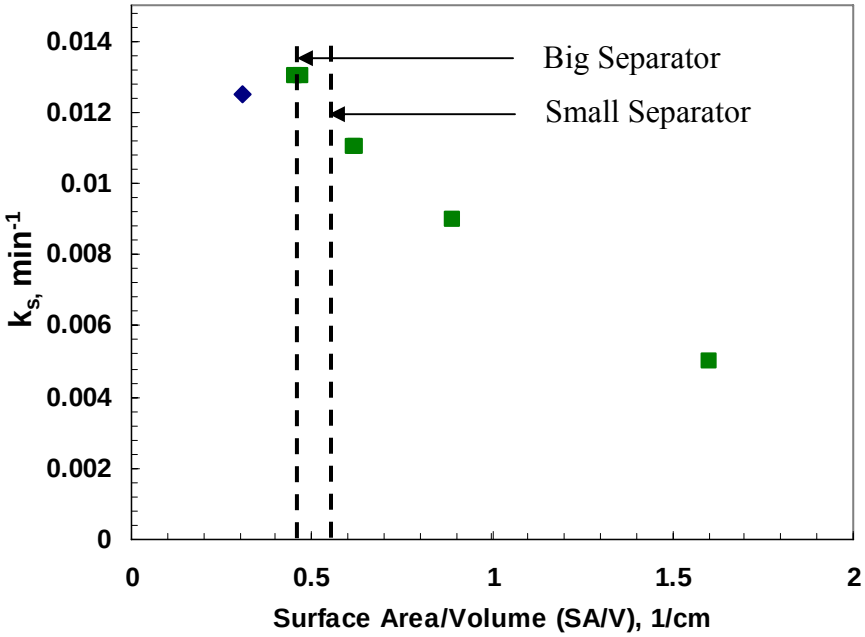

Figure 5.14: Effect of SA/V on the coalescence rate constant during the batch experiments performed at 70 ppm concentration of NEO-10.

The only exception in the Figure 5.14 is from Configuration 1 (indicated by a diamond), which corresponds to the beaker alone, to Configuration 2 (see Figure 5.13b). Although the SA/V increased, the coalescence rate constant increased. A possible explanation is that placing a tube in the beaker disturbed some of the emulsion and increased the local coalescence rate. Hence, there were two opposing effects: 1) increased SA/V which decreased coalescence and 2) disturbance of the emulsion which increased coalescence. In the other configurations, the emulsion was disturbed in all cases and the effect of increased SA/V dominated. Overall, the tests confirm the hypothesis that contact with the separator walls decreases coalescence.

Table 5.10 presents the dimensions for the small and big separator. The SA/V's of the two separators are illustrated with dashed lines on Figure 5.14. The coalescence rate

constant for the large separator is expected to be approximately 20% higher than that of the small separator. In fact, the steady state coalescence rate constant for the large separator was approximately 35% greater than that of the small separator (0.34 for the large separator versus 0.23 for the small separator). This quantitative difference was probably differences between the batch and continuous emulsion layers (discussed previously) as well as the more significant disturbance of the batch experiment emulsions during the experiment. Given these differences, the batch tests provide strong evidence that wall effects alter the average coalescence rates in the separators. The wall effect must be accounted for in future modeling to accurately predict the effect of separator area on emulsion layer growth.

Table 5.10: Dimensions for the small and big separator.

	Cross Sectional Area, cm^2	**Diameter, cm**	**SA/V, cm^{-1}**	**k_s, min^{-1}**
Small Separator	10.53	3.66	0.55	0.23
Big Separator	14.4	4.28	0.46	0.34

5.2 Emulsion Layers from Water-in-Oil Emulsions

5.2.1 Coalescence Rates from Batch Experiments

The batch experiments for asphaltene stabilized water-in-oil emulsions were performed as for the oil-in water emulsion described in Section 5.1.1. The only difference was that the aqueous phase was added from the top to create the emulsion, see Chapter 3. Figure 5.15 shows the dimensionless plot for the emulsion and free water layer heights over time during a batch experiment and Table 5.11 gives the corresponding parameters to model the batch experiment.

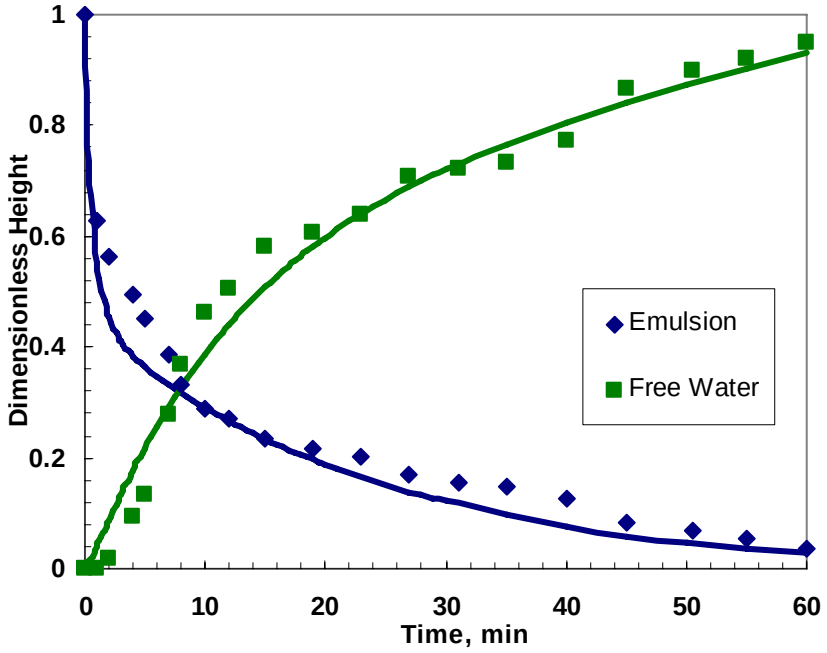

Figure 5.15: The emulsion and water layer heights over time for a batch experiment performed at 60°C, 1.5 g/l concentration of asphaltene with respect to oil phase and 50 ppm concentration of each AOT and Tween-80. The water volume fraction in the initial emulsion was 50%. The symbols correspond to the experimental data and solid lines indicate the modeled profiles.

Unlike the batch oil-in-water emulsion experiments, the coalescence rate was constant suggesting that surfactant/asphaltene accumulation did not occur in the water-in-oil emulsion layer. Figure 5.16 shows that the dispersed water phase volume fraction reached a maximum of 85% and then decreased to 70%. The reason for the decrease in water volume fraction is not known but it confirms that surfactant accumulation due to thinning films is unlikely to have occurred.

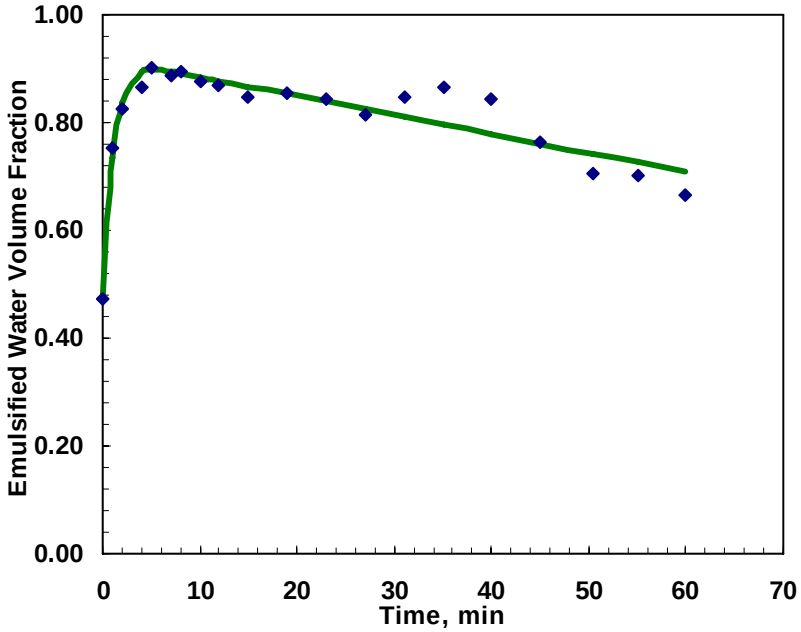

Figure 5.16: Emulsified water volume fraction in the emulsion layer during a batch experiment performed at 60°C, 1.5 g/l asphaltene concentration in the oil phase and 80 ppm concentration each of AOT and Tween-80. The initial emulsified water volume fraction was 50%. The symbols are experimental data and solid line is a curve fit.

Table 5.11: Model parameters used to model the batch experiments performed at 60°C, 1.5 g/l concentration of asphaltene with respect to organic phase and 50 ppm concentration of each AOT and Tween-80.

Model Parameter	
k_o, min^{-1}	0.047
k_s, min^{-1}	0.047
c, min^{-1}	0

5.2.2 Coalescence Rates from Decay Experiments

The decay experiments for asphaltene stabilized water-in-oil emulsions were also performed in the same manner as for the oil-in-water emulsions. The emulsion layer at the end of the continuous experiments was allowed to decrease over time into free oil and water layers with the cessation of the feed. Figure 5.17 shows the dimensionless emulsion and free water layer heights over time during a decay experiment and the Table 5.12 gives the corresponding model parameters used to model the decay experiment.

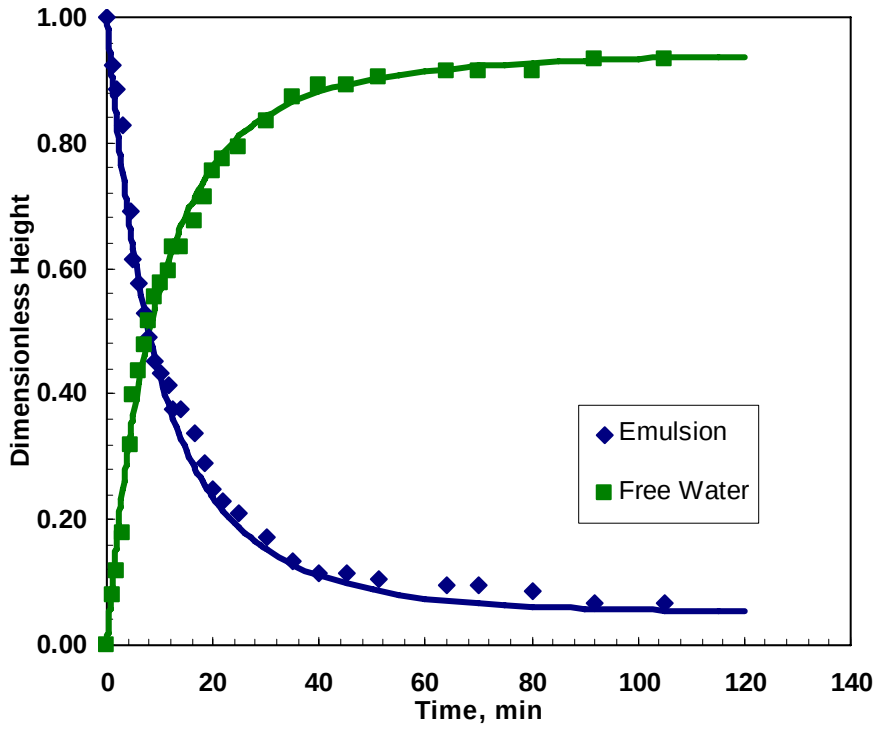

Figure 5.17: The emulsion and water layer heights over time for a decay experiment performed at 60°C, 1.5 g/l concentration of asphaltene with respect to oil phase and 50 ppm concentration of each AOT and Tween-80. The prior continuous experiment was performed at the feed flow rate of 30 cm^3/min. The symbols correspond to the experimental data and solid lines indicate the modeled profiles.

During the decay experiments it was observed that the coalescence rate constant was not constant and decreased with time. The dispersed water phase volume fraction was constant at 96%; that is, only 4% continuous oil phase. This initial high water volume fraction probably causes the higher initial coalescence rate constant value compared with the batch experiment performed at the same experimental conditions. In this case, surfactant/asphaltene trapping appears to have occurred in the thin films causing a decrease in the coalescence rate. Another factor may be aging of the asphaltene film at the interface which is known to increase emulsion stability (Sztukowski and Yarranton, 2005). The decay experiments take place for much longer duration for over almost 2 hours as opposed to 50 minutes for the batch experiments.

Table 5.12: Model parameters used to model the decay experiments performed at 60°C, 1.5 g/l concentration of asphaltene with respect to oil phase and 50 ppm concentration of each AOT and Tween-80. The continuous experiment was performed at the feed flow rate of 30 cm^3/min.

Model Parameter	
k_o, min^{-1}	0.1
k_s, min^{-1}	0.001
c, min^{-1}	0.037

5.2.3 Emulsion Layer Growth in Continuous Experiments

Figure 5.18 shows the emulsion layer growth during a continuous experiment and Table 5.13 shows the corresponding parameters used to model the emulsion layer. Note, $\phi_w°$ and ϕ_w are the emulsified water volume fraction in the feed and in the emulsion layer inside the separator, respectively. These values were measured for each experiment. The

dispersed water phase volume fraction was constant at 96%. Note the continuous phase films were much thinner than observed in the oil-in-water emulsion layers.

Figure 5.18 shows that, as observed for the oil-in-water emulsions, the decay coalescence rate constant could be used to predict the emulsion layer height present at the end of the continuous experiment but the batch coalescence rate constant was not able to predict the emulsion layer height.

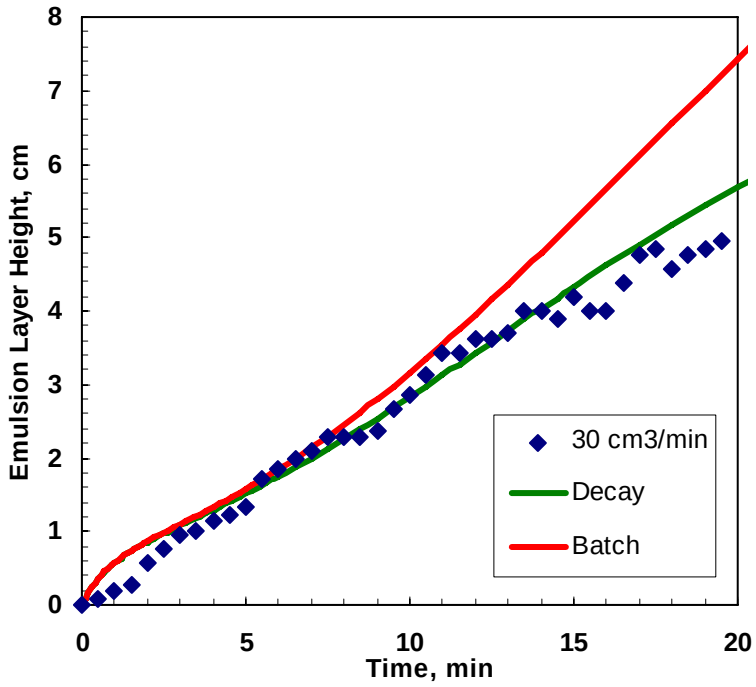

Figure 5.18: The emulsion layer growth during the continuous experiment performed at 60°C, 1.5 g/l concentration of asphaltene with respect to organic phase and 50 ppm concentration of each AOT and Tween-80 in the 250 mL separator at the feed flow rate of 30 cm^3/min. The symbols are experimental data points and solid lines correspond to the modeled profiles.

Table 5.13: Model parameters used for continuous experiment performed in the 250 mL separator at 60°C, 1.5 g/l of asphaltene concentration with respect to the organic phase and 50 ppm concentration of each AOT and Tween-80 at the feed flow rate of 30 cm³/min.

Parameters	Batch	Decay	Continuous
ϕ_w^o	--	--	0.29
ϕ_w	--	0.96	0.96
k_o, min^{-1}	**0.047**	**0.1**	1.1
k_s, min^{-1}	0.047	0.001	**0.1**
c, min^{-1}	0	0.037	0.23

The predictive capability of the model was tested on an experiment performed with the same emulsion but at a different flow rate. Figure 5.19 shows the emulsion layer growth at the original flow rate of 30 cm³/min and the new flow rate of 20 cm³/min. Table 5.14 presents the corresponding parameters to model the emulsion layer growth. As before, the final emulsion layer height could be predicted using the initial decay coalescence rate constant at the given flow rates. However, unlike the oil-in-water system, this initial coalescence rate increased as the flow rate increased. The increase may be caused by the decrease in film thickness (increase in dispersed phase volume fraction) with flow rate. During the continuous experiment and at the beginning of the decay experiment, there may not have been opportunity for the surfactant/asphaltenes to accumulate in the film and therefore thinner films give higher coalescence rates. In any case, the effect of flow rate cannot be predicted from a single decay experiment for the water-in-oil emulsion layers.

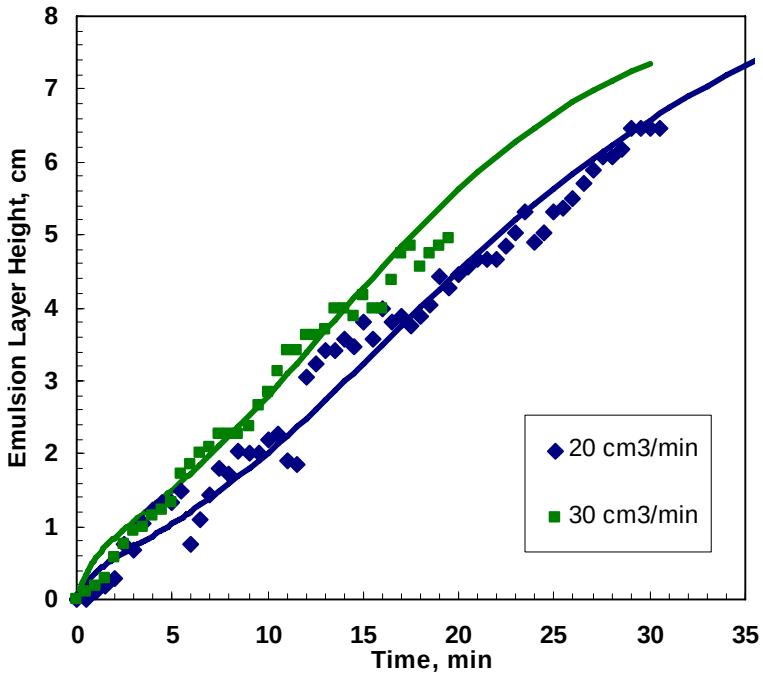

Figure 5.19: The emulsion layer growth during the continuous experiments performed at 60°C, 1.5 g/l concentration of asphaltene with respect to organic phase and 50 ppm concentration of each AOT and Tween-80 in the 250 mL separator at the feed flow rates of 20 and 30 cm^3/min. The symbols are experimental data points and solid lines correspond to the modeled profiles.

Table 5.14: Model parameters used for continuous experiments performed in the 250 mL separator at 60°C, 1.5 g/l of asphaltene concentration with respect to the organic phase and 50 ppm concentration of each AOT and Tween-80 at the feed flow rates of 20 and 30 cm^3/min.

Parameters	**Flow Rate**			
	20 cm^3/min		**30 cm^3/min**	
	Decay	*Continuous*	*Decay*	*Continuous*
$\phi_w^{\ o}$	--	0.26	--	0.29
ϕ_w	0.93	0.93	0.97	0.97
k_o, min^{-1}	**0.055**	1.1	**0.1**	1.1
k_s, min^{-1}	0.004	**0.055**	0.001	**0.1**
c, min^{-1}	0.032	0.23	0.037	0.23

All of the results discussed for asphaltene stabilized water-in-oil emulsions are preliminary. More experiments are required to identify aging and surfactant/asphaltenes accumulation effects for these emulsions and to adapt the model as appropriate.

CHAPTER 6
CONCLUSIONS AND RECOMMENDATIONS

The overall objective of this thesis was to study the relationship between coalescence and emulsion layer growth. Batch, continuous, and decay experiments were performed first on model oil-in-water emulsions and then on model water-in-oil emulsions. A batch experiment involved measuring the height of the water, oil, and emulsion layers over time for a settled emulsion. A continuous experiment involved the same measurements for an emulsion layer in a continuous separator. A decay experiment was a batch test performed on the emulsion layer formed in a continuous separator. Batch and decay experiments were modeled to determine the coalescence rates which were used to predict the emulsion layer height during a continuous experiment. The model was based on a material balance on the dispersed phase mass with the outlet mass flow rate determined solely by coalescence. The mass balance simplified to predictions of emulsion and free phase heights over time. The coalescence rate was adjusted to fit the measured heights.

6.1 Thesis Conclusions

6.1.1 Oil-in-Water Emulsions

The emulsions were polydisperse in size with droplets ranging from 5 to 350 microns in diameter. In batch experiments, the size distribution was invariant with time. In decay experiments, the distribution narrowed and shifted to smaller sizes over time.

The dispersed phase volume fraction in the emulsion layer increased over time from 50 to 85 vol% in the batch experiments but was invariant at approximately 64 vol% in the continuous and decay experiments.

The coalescence rate was found to decrease exponentially over time for both batch and continuous experiments. The decrease in coalescence rate was not caused by an increase in droplet sizes since the drop sizes either remained constant or decreased over time. In batch experiments, the decrease in coalescence rate correlated with a thinning of the film between droplets (an increase in dispersed phase volume fraction). This observation suggested that surfactant released from coalescing droplets may accumulate in sufficiently thin films, increasing emulsion stability and causing a decrease in coalescence rate over time. The hypothesis was tested by gently disturbing an emulsion layer to release trapped surfactant and a sustained increase in coalescence rate was indeed observed.

The coalescence rate constants for the decay experiments were found to be higher than the ones obtained for the batch experiments. The initial rates were higher due to the large dispersed phase fraction in the decay experiments. Large dispersed phase volumes provide closer contact between droplets and faster coalescence until surfactant accumulates. The final coalescence rates were also higher because the final dispersed phase volume fraction was lower than the batch experiments leading to less surfactant accumulation.

In continuous experiments, the emulsion layer height grew over time and reached a constant steady state height. In all cases, this steady state condition could be predicted from the coalescence rates determined from decay experiments on the same emulsion. The coalescence rates from the batch experiments could not be used probably because the batch experiments were performed with different initial dispersed phase volume fractions. A batch experiment was performed with high initial oil volume fraction to match that of a decay experiment and the coalescence rate constant was found to match that of the decay experiment. Hence, batch experiments can be used to predict steady state conditions in the continuous separation as long as the dispersed phase volume fractions are matched.

As expected, increasing the surfactant concentration increased the steady state emulsion layer height because the emulsions were more stable. Increasing the feed flow rate also increased the steady state height. The coalescence rate was independent of the flow rate and therefore the steady state heights could be predicted from a single decay experiment.

Two different separators were used to study the effect of the geometry. For a given flow rate or flux of the feed, the coalescence rate was smaller in the smaller separator leading to greater emulsion layer height. The difference in coalescence rate was attributed to a wall effect. A series of batch experiments was performed which proved that coalescence rates decreased near walls. The greater the surface area to volume ratio (SA/V), the slower was the coalescence. The small separator has a smaller SA/V than the large separator and hence slower coalescence.

6.1.2 Asphaltene Stabilized Water-in-Oil Emulsions

Preliminary experiments and modeling were performed on the asphaltene stabilized water-in-oil emulsions. Preliminary observations are given below.

In batch experiments the coalescence rate was invariant over time unlike the oil-in-water emulsions. The dispersed phase volume fraction in the batch experiments reached a maximum of 85 vol% and then decreased to 70%. It appears that the continuous phase films were thick enough to avoid surfactant accumulation. In decay experiments, the coalescence rate decreased exponentially with time similarly to the oil-in-water emulsions. The dispersed phase volume fraction was constant at 96 vol% and it appears that surfactant accumulation did occur. It is not clear why the batch and decay experiments follow different pathways.

The steady state emulsion layer height could be predicted using the initial decay coalescence rate constant from the decay experiment on the same emulsion. Unlike the oil-in-water emulsions, the coalescence rate was sensitive to flow rate. The effect of flow

rate on the steady state height could not be predicted from a single decay experiment but could be predicted at each flow rate from a decay experiment conducted on an emulsion layer prepared at that flow rate.

6.2 Recommendations

The developed methodology can be improved by including the effect of geometry. The SA/V needs to be correlated with coalescence rate constant in order to account for the effect of geometry in the existing model.

In this study, the emulsions were assumed to be mono-disperse, which is not the case as found by the droplet size distribution. The polydispersity can be accounted by relating the droplet size with the coalescence rate constant and this can bring the model close to the actual emulsion system.

More work on asphaltene stabilized water-in-oil emulsions can be performed and any required changes can be made to improve the predictive capabilities of the model. This can be accessed by examining the effect of aging on the interfacial film by making emulsions for different times.

The model emulsion system can be made more realistic by introducing precipitated asphaltenes, clays and solids into the model systems. This can provide insight into the role of solids in emulsion stability and rag layer growth and lead to a model more suited to oil sands separation processes.

REFERENCES

Andrade, J.L., Apparatus to Investigate Rag Layer Growth, *M.Sc. Thesis*, University of Calgary, 2009.

Barnea, E. and Mizrahi, J., Separation Mechanisms of Liquid-Liquid Dispersions in a Deep-Layer Gravity Settler: Part II- Flow Patterns of the Dispersed and Continuous Phases within the Dispersion Band, *Transactions of the Institution of Chemical Engineers*, 53 (2), 70-74, 1975b.

Barnea, E. and Mizrahi, J., Separation Mechanisms of Liquid-Liquid Dispersions in a Deep-Layer Gravity Settler: Part III-Hindered Settling and Drop-to-Drop Coalescence in the Dispersion Band, *Transactions of the Institution of Chemical Engineers*, 53 (2), 75-82, 1975c.

Barnea, E. and Mizrahi, J., Separation Mechanisms of Liquid-Liquid Dispersions in a Deep-Layer Gravity Settler: Part IV- Continuous Settler Characteristics, *Transactions of the Institution of Chemical Engineers*, 53 (2), 83-92, 1975d.

Barnes, G.T., and Gentle, I.R., Interfacial Science, an Introduction, Oxford University Press, 2005.

Basu, S., Nandakumar, K., and Masliyah, J.H., On bitumen liberation from Oil Sands, *Canadian Journal of Chemical Engineering*, 75 (2), 476-479, 1997.

Becher, P., Emulsions, Theory and Practice, 3rd Ed., American Chemical Society, Oxford University Press, 2001.

Binks, B., and Horozov, T., Colloidal Particles at Liquid Interfaces, Cambridge University Press, 2006.

Binks, B.P., Modern Aspects of Emulsion Science, The Royal Society of Chemistry, Cambridge, 1998.

Bourassin, R., Oil-Water Separation by High Speed Centrifuging, *New Technologies for the Exploration and Exploitation of Oil and Gas Resources Symposium, Luxembourg*, 630-636, 1985.

Canizares, P., Martinez, F., Lobato, J., and Rodrigo, M.A., Break-Up of Oil-in-Water Emulsions by Electrochemical Techniques, *Journal of Hazardous Materials*, 145 (1-2), 233-240, 2007.

Chen, F., Finch, J.A., Xu, Z., and Czarnecki, J., Wettability of Fine Solids Extracted from Bitumen Froth, *Journal of Adhesion Science and Technology*, 13 (10), 1209-1224, 1999.

Cooper, D.G., Zajic, J.E., Cannel, E.J., and Wood, J.W., The Relevance of "HLB" to De-Emulsification of a Mixture of Heavy Oil, Water and Clay, *The Canadian Journal of Chemical Engineering*, 58, 576-579, 1980.

Czarnecki, J., Moran, K., and Yang, X., On the "Rag Layer" and Diluted Bitumen Froth Dewatering, *Canadian Journal of Chemical Engineering*, 85 (5), 748-755, 2007.

Dalingaros, W., Jeelani, S.A.K., and Hartland, S., Prediction of Steady-state Dispersion Height in the Disengaging Section of an Extraction Column from Batch Settling Data, *Canadian Journal of Chemical Engineering*, 65 (2), 210-213, 1987.

Dickinson, E., Murray, B.S., and Stainsby, G., Coalescence Stability of Emulsion-sized Droplets at a Planer Oil-Water Interface and the Relationship to Protein Film Surface Rheology, *Journal of the Chemical Society Faraday Transactions I*, 84 (3), 871-883, 1988.

Farn R., Chemistry and Technology of Surfactants, Blackwell Publishing Ltd., 2006.

Fredrick, E., Walstra, P., and Dewettinck, K., Factors Governing Partial Coalescence in Oil-in-Water Emulsions, *Advances in Colloid and Interface Science*, 153 (1-2), 30-42, 2010.

Freer, E.M., and Radke, C.J., Relaxation of Asphaltenes at the Toluene/Water Interface: Diffusion Exchange and Surface Rearrangement, The Journal of Adhesion, 80 (6), 481-496, 2004.

Frising, T., Noik, C., and Dalmazzone, C., The Liquid/Liquid Sedimentation Process: From Droplet Coalescence to Technologically Enhanced Water/Oil Emulsion Gravity Separators: A Review, *Journal of Dispersion Science and Technology*, 27 (7), 1035-1057, 2006.

Gafonova, O., and Yarranton, H.W., The Stabilization of Water-in-Hydrocarbon Emulsions by Asphaltenes and Resins, *Journal of Colloid and Interface Science,* 241 (2), 469–478, 2001.

Golob, J., and Modic, R., Coalescence of Liquid/Liquid Dispersions in Gravity Settlers, *TransIChemE*, 55, 207-211, 1977.

Graham, D.E., Crude Oil Emulsions: Their Stability and Resolution, *In Chemicals in the Oil Industry, Odgen, P.H., Ed.; Royal Society of Chemistry, London*, 155-175, 1988.

Gu, G., Zhang, L., Xu, Z., and Masliyah, J.H., Novel Bitumen Froth Cleaning Device and Rag Layer Characterization, *Energy and Fuels*, 21 (6), 3462–3468, 2007.

Gu, G., Xu, Z., Nandakumar, K., and Masliyah, J.H., Influence of Water-Soluble and Water-Insoluble Natural Surface Active Components on the Stability of Water-in-Toluene-Diluted Bitumen Emulsions, *Fuel*, 81 (14), 1859-1869, 2002.

Hartland, S., Effect of Gravity on the Drainage of Thin Films in Two-Dimensional Dense-Packed Dispersions, *Chemical Engineering Science*, 34 (4), 485-491, 1979.

Hartland, S., and Vohra, D.K., Effect of Interdrop Forces on the Coalescence of Drops in Close-Packed Dispersions, *Journal of Colloid and Interface Science*, 77 (2), 295-316, 1980.

Hartland, S., and Jeelani, S.A.K., Relationship between Models for Predicting Steady-State Dispersion Height from Batch Settling Data, *Institution of Chemical Engineers Symposium*, 94, 21 l-223, 1985.

Hartland, S., and Jeelani, S.A.K., Choice of Model for Predicting the Dispersion Height in Liquid/Liquid Gravity Settlers from Batch Settling Data, *Chemical Engineering Science*, 42 (8), 1927-1938, 1987.

Hartland, S., and Jeelani, S.A.K., Prediction of Sedimentation and Coalescence Profiles in a Decaying Batch Dispersion, *Chemical Engineering Science*, 43 (9), 2421-2429, 1988.

Henschke, M., Schlieper, L.H., and Pfennig, A., Short Communication: Determination of a Coalescence Parameter from Batch-Settling Experiments, *Chemical Engineering Journal*, 85 (2-3), 369-378, 2002.

Hiemenz, P.C., and Rajagopalan, R., Principles of Colloid and Surface Chemistry, 3rd Ed., Marcel Dekker, Inc., 1997.

Jeelani, S.A.K., and Hartland, S., Prediction of Steady State Dispersion Height from Batch Settling Data, *American Institute of Chemical Engineers*, 31 (5), 71l-720, 1985.

Jeelani, S.A.K., and Hartland, S. Prediction of Dispersion Height in Liquid/Liquid Gravity Settlers from Batch Settling Data. *Chemical Engineering Research and Design*, 64 (6), 450-460, 1986a.

Jeelani, S.A.K., and Hartland, S., Scale-Up of Industrial Gravity Settlers from Batch Settling Data, *DECHEMA*, 3, 453-460, 1986b.

Jeelani, S.A.K., and Hartland, S., Variation of Drop-Size and Hold-Up in a Dense-Packed Dispersion, *Chemical Engineering and Processing*, 20 (5), 271-276, 1986c.

Jeelani, S.A.K., and Hartland, S., Dynamic Response of Gravity Settlers to Changes in Dispersion Throughput, *American Institute of Chemical Engineers*, 34 (2), 355-340, 1988.

Jeelani, S.A.K. and Hartland, S., The Continuous Separation of Liquid/Liquid Dispersions, *Chemical Engineering Science*, 48 (2), 239-254, 1993.

Jeelani, S.A.K. and Hartland, S., Effect of Dispersion Properties on the Separation of Batch Liquid-Liquid Dispersions, *Industrial and Engineering Chemistry Research*, 37 (2), 547-554, 1998.

Jeelani, S.A.K., Panoussopoulos, K., and Hartland, S., Effect of Turbulence on the Separation of Liquid-Liquid Dispersions in Batch Settlers of Different Geometries, *Industrial and Engineering Chemistry Research*, 38 (2), 493-501, 1999.

Jeelani, S.A.K., Hosig, R., and Windhab, E.J., Kinetics of Low Reynolds Number Creaming and Coalescence in Droplet Dispersions, *American Institute of Chemical Engineers*, 51 (1), 149-161, 2005.

Jiang, T., Hirasaki, G.J., Miller, C.A., and Moran, K., Using Silicate and pH Control for Removal of the Rag Layer Containing Clay Solids Formed during Demulsification, *Energy and Fuels*, 22, 4158-4164, 2008.

Kabalnov, A.S., and Shchukin, E.D., Ostwald Ripening Theory: Applications to Fluorocarbon Emulsion Stability, 38, 69-97, 1992.

Khadim, M.A., and Sarbar, M.A., Role of Asphaltene and Resin in Oil Field Emulsions, *Journal of Petroleum Science and Engineering*, 23 (3-4), 213-221, 1999.

Kim, Y.H., and Wasan, D.T., Effect of Demulsifier Partitioning on the Destabilization of Water-in-Oil Emulsions, *Industrial and Engineering Chemistry Research*, 35 (4), 1141-1149, 1996.

Kiran, S.K., Acosta, E.J., and Moran, K., Evaluating the Hydrophilic-Lipophilic Nature of Asphaltenic Oils and Naphthenic Amphiphiles Using Misroemulsion Models, *Journal of Colloid and Interface Science*, 336 (1), 304-313, 2009.

Liu, J., Xu, Z., and Masliyah, J., Role of Fine Clays in Bitumen Extraction From Oil Sands, *American Institute of Chemical Engineers*, 50 (8), 1917-1927, 2004.

Lobo, L., Ivanov, I., and Wasan, D., Dispersion Coalescence: Kinetic Stability of Creamed Dispersion, *American Institute of Chemical Engineers*, 39 (2), 322-334, 1993.

McLean, J.D., and Kilpatrick, P.K., Effects of Asphaltenes Solvency on Stability of Water-in-Crude-Oil Emulsions, *Journal of Colloid and Interface Science*, 189 (2), 242-253, 1997.

McLean, J.D., and Kilpatrick, P.K., Effects of Asphaltenes Aggregation in Model Heptane-Toluene Mixtures on Stability of Water-in-Oil Emulsions, *Journal of Colloid and Interface Science*, 196 (1), 23-34, 1997.

Moran, K., Yeung, A., and Masliyah, J.H., The Viscoplastic Properties of Crude Oil-Water Interfaces, *Chemical Engineering Science*, 61 (18), 6016-6028, 2006.

Myers, D., Surfactant Science and Technology, 2nd Ed., VCH Publishers, Inc., 1992.

Nadiv, C., and Semiat, R., Batch Settling of Liquid-Liquid Dispersion, *Industrial and Engineering Chemistry Research*, 34 (7), 2427-2435, 1995.

Ortiz, D., Effect of Surfactants on Asphaltene Interfacial Films and Stability of Water-in-Oil Emulsions, *M.Sc. Thesis*, University of Calgary, 2009.

Richardson, J.F., and Zaki, W.N., Sedimentation and Fluidization-I, *Institution of Chemical Engineers-Transactions*, 32 (1), 35-52, 1954.

Romanova, U.G., Yarranton, H.W., Schramm, L.L., and Shelfantook, W.E., Investigation of Oil Sands Froth Treatment, *Canadian Journal of Chemical Engineering*, 82 (4), 710-721, 2004.

Rosen, M., Surfactants and Interfacial Phenomena, 3rd Ed., John Wiley and Sons, Inc., 2004.

Saadatmand, M., Investigation of Rag Layers from Oil Sands Froth, *M.Sc. Thesis*, University of Calgary, Calgary, 2008.

Saadatmand, M., Yarranton, H.W., and Moran, K., Rag Layers in Oil Sand Froths, *Industrial and Engineering Chemistry Research*, 47 (22), 8828-8839, 2008.

Schramm, L., Emulsions: Fundamentals and Applications in the Petroleum Industry, *American Chemical Society*, 1992.

Singh, B.P., Chemical Resolution of Petroleum Emulsion, *Chemical Engineering World*, 29 (10), 203-209, 1994.

Singh, B.P., Laboratory Test Results on Ultrasound Treated Industrial Emulsions, *Acoustics Letters*, 19 (4), 1995.

Strassner, J.E., Effect of pH on Interfacial Films and Stability of Crude Oil-Water Emulsions, Journal of Petroleum Technology, 20 (3), 303-312, 1968.

Sztukowski, D.M., Jafari, M., Alboudwarej, H., and, Yarranton, H.W., Asphaltene Self Association and Water-in-Hydrocarbon Emulsions. *Journal of Colloid and Interface Science*, 265 (1), 179-186, 2003.

Sztukowski, D.M., and Yarranton, H.W., Oilfield Solids and Water-in-Oil Emulsion Stability, *Journal of Colloid and Interface Science,* 285 (2), 821-833, 2005.

Sztukowski, D.M., and Yarranton, H.W., Rheology of Asphaltene-Toluene/Water Interfaces, *Langmuir*, 21 (25), 11651-11658, 2005.

Tadros, T.F., Emulsion Science and Technology, Wiley-VCH Verlag GmbH & Co. KGaA, 2009.

Tambe, D., and Sharma, M., Factors Controlling the Stability of Colloids-Stabilized Emulsions: I. An Experimental Investigation, *Journal of Colloids and Interfaces Science*, 157 (1), 244-253, 1993.

Taylor, S.E., Investigations into the Electrical and Coalescence Behaviour of Water-in-Crude Oil Emulsions in High Voltage Gradients, *Colloids and Surfaces*, 29, 29-51, 1988.

Vieler, A.M.S., Glasser, D., and Bryson, A.W., The Relationship between Batch and Continuous Phase Disengagement, *Proc. Int. Sol. Extr. Conf., 1977, Canadian Inst. Mining Metal.* 1, 399-405, 1979.

Yan, N., Gray, M.R., and Masliyah, J.H., On Water-in-Oil Emulsions Stabilized by Fine Solids, *Colloids and Surfaces A: Physiochemical and Engineering Aspects*, 193 (1-3), 97-107, 2001.

Yarranton, H.W., Alboudwarej, H., and Jakher, R., Investigation of Asphaltene Association with Vapour Pressure Osmometry and Interfacial Tension Measurements, *Industrial and Engineering Chemistry Research*, 39 (8), 2916-2924, 2000.

Yarranton, H.W., Hussein, H., and Masliyah, J.H., Water-in-Hydrocarbon Emulsions Stabilized by Asphaltenes at Low Concentrations, *Journal of Colloid and Interface Science*, 228 (1), 52-63, 2000.

Yarranton, H.W., Sztukowski, D.M., and Urrutia, P., Effect of Interfacial Rheology on Model Emulsion Coalescence I. Interfacial Rheology, *Journal of Colloid and Interface Science*, 310 (1), 246-252, 2007.

Yeo, L.Y., Matar, O.K., Ortiz, E.S.P., and Hewitt, G.F., Film Drainage Between Two Surfactant-Coated Drops Colliding at Constant Approach Velocity, *Journal of Colloid and Interface Science*, 257 (1), 93-107, 2003.

Yu, G-Z., and Mao, Z-S., Sedimentation and Coalescence Profiles in Liquid-Liquid Batch Settling Experiments, *Chemical Engineering and Technology*, 27 (4), 407-413, 2004.

Zhang, L.Y., Breen, P., Xu, Z., and Masliyah, J.H., Asphaltenes Films at a Toluene/Water Interface, *Energy and Fuels*, 21 (1), 274-285, 2007.

APPENDIX A
EMULSIFIED OIL VOLUME FRACTION IN EMULSION LAYER

A.1 Oil Volume Fraction during Batch Experiment

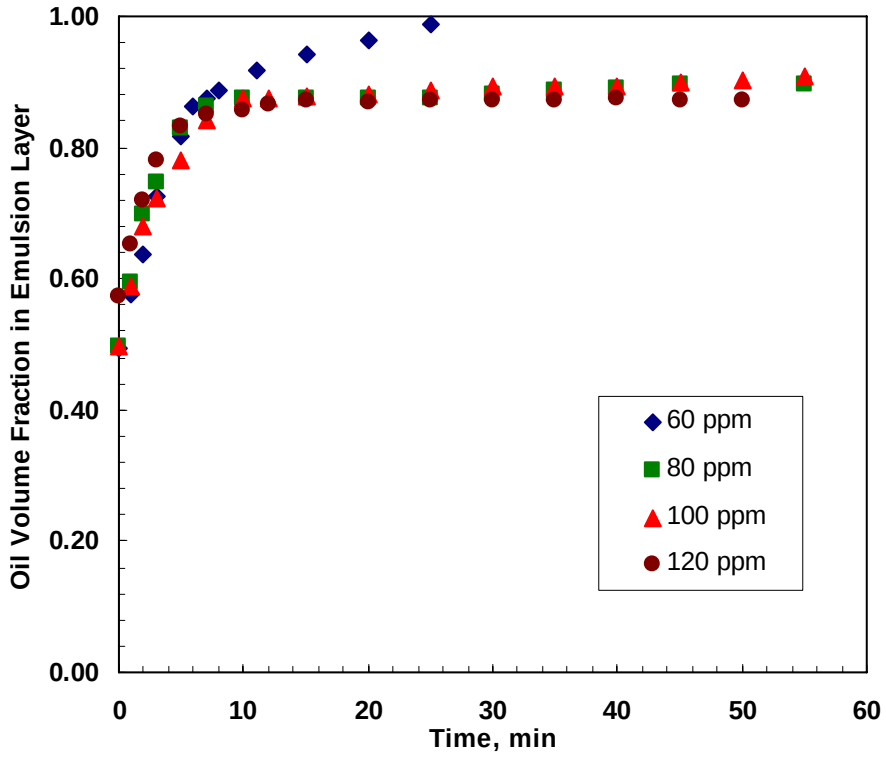

Figure A.1: The oil volume fraction in the emulsion layer during the batch experiment performed at various concentrations of NEO-10. Mixer speed was 800 rpm and the temperature was 45^{o}C.

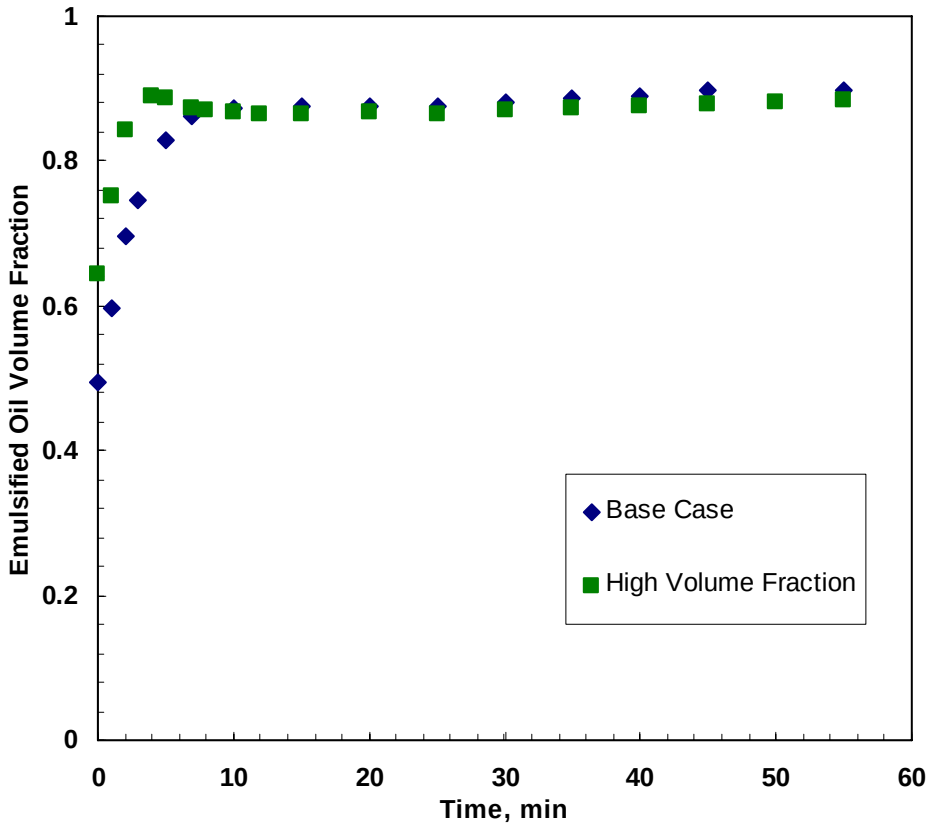

Figure A.2: The oil volume fraction in the emulsion layer during the batch experiment performed at 80 ppm concentrations of NEO-10. Mixer speed was 800 rpm and the temperature was 45^{o}C. The base case experiment started with 50 volume% of the oil phase and high volume fraction experiment started with 65 volume% of the oil phase.

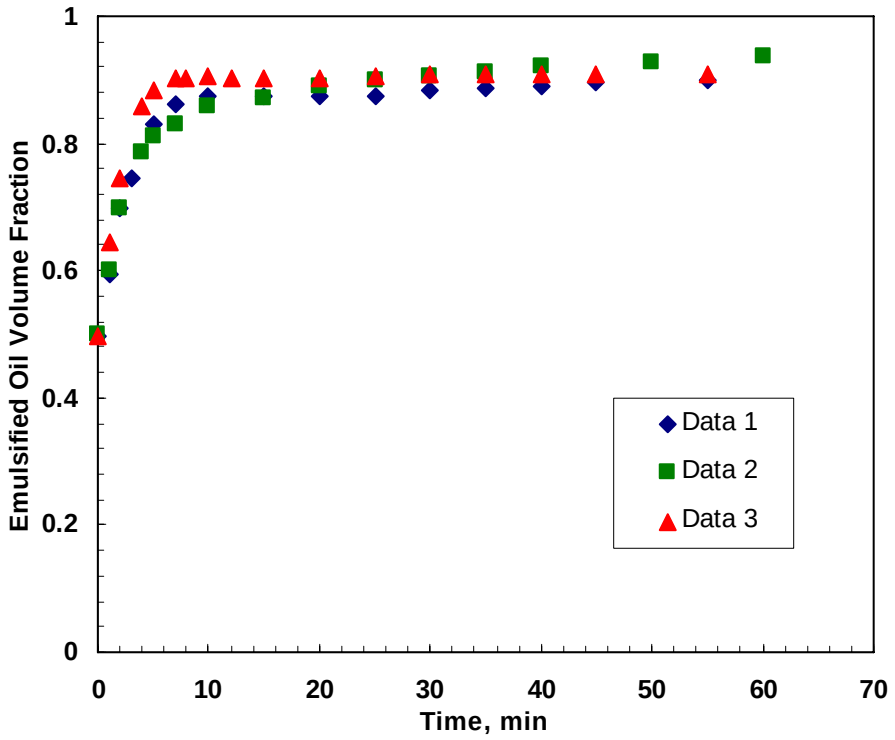

Figure A.3: The oil volume fraction in the emulsion layer during the batch experiment performed at 80 ppm concentrations of NEO-10. Mixer speed was 800 rpm and the temperature was 45^{o}C. Three different set of data are shown.

A.2 Oil Volume Fraction during Continuous Experiment

A.2.1 Oil Volume Fraction during Emulsion Layer Growth

Table A.1: Oil volume fraction in the emulsion layer during a continuous experiment performed at 80 ppm concentration of NEO-10 in the 250 mL separator at the feed flow rate of 45 cm^3/min. Mixer speed was 800 rpm and the temperature was 45°C.

NEO-10	Time, min	Oil volume fraction	
		Data 1	Data 2
80 ppm	3	0.62	0.66
45 cm^3/min	7	0.63	0.61
	10	0.66	0.64
	15	0.64	0.63
	Average	**0.64**	**0.63**

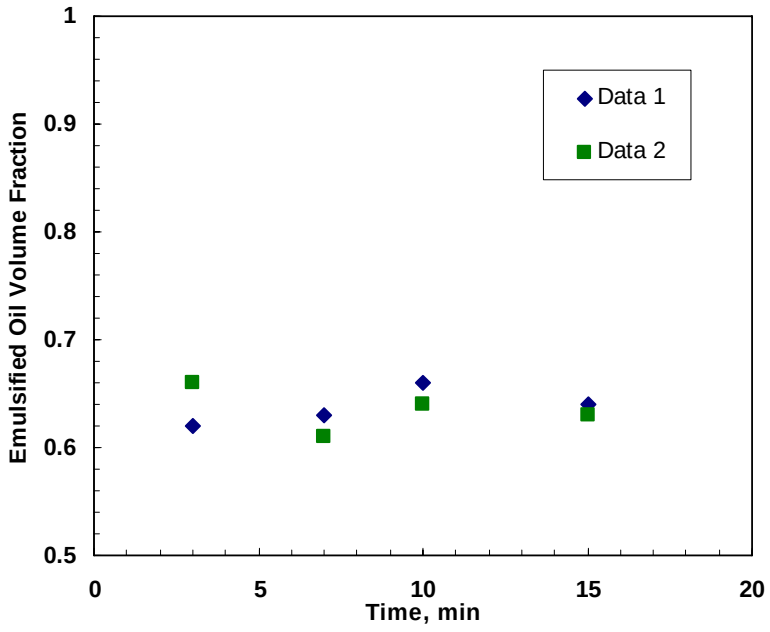

Figure A.4: The emulsified oil volume fraction in the emulsion layer during continuous experiment performed at 80 ppm concentration of NEO-10 in the 250 mL separator at the feed flow rate of 45 cm^3/min. Mixer speed was 800 rpm and the temperature was 45°C.

Table A.2: Oil volume fraction in the emulsion layer during a continuous experiment performed at 80 ppm concentration of NEO-10 in the 500 mL separator at the feed flow rate of 55 cm^3/min. Mixer speed was 800 rpm and the temperature was 45°C.

NEO-10	Time, min	Oil volume fraction	
		Data 1	Data 2
80 ppm	5	0.68	0.71
55 cm^3/min	10	0.71	0.68
	15	0.69	0.66
	19	0.70	0.69
	Average	**0.70**	**0.69**

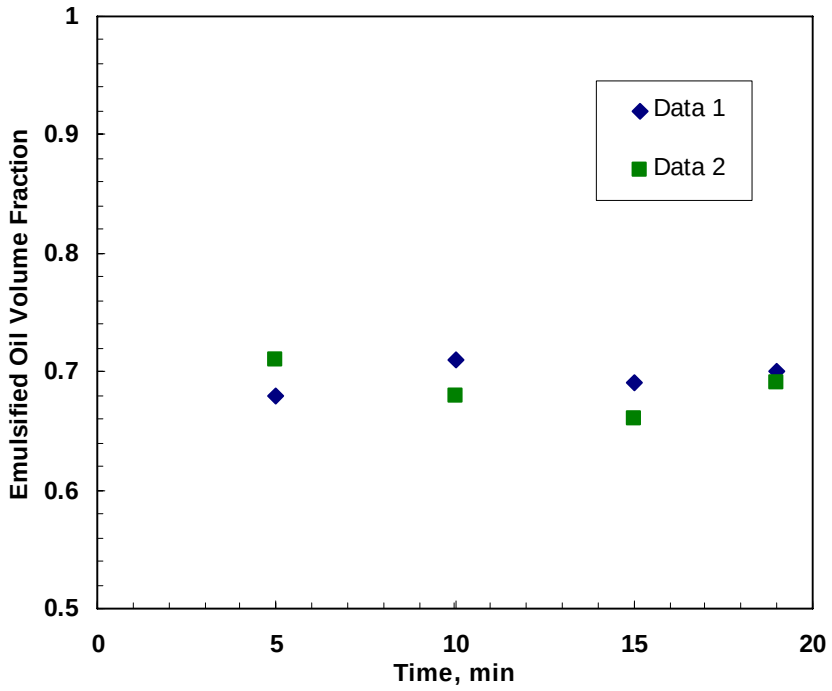

Figure A.5: The emulsified oil volume fraction in the emulsion layer during a continuous experiment performed at 80 ppm concentration of NEO-10 in the 500 mL separator at the feed flow rate of 55 cm^3/min. Mixer speed was 800 rpm and the temperature was 45°C.

A.2.2 Oil Volume Fraction in the Feed

Table A.3: The emulsified oil volume fraction in the feed during a continuous experiment performed at 80 ppm concentration of NEO-10 at the feed flow rate of 45 cm^3/min. Mixer speed was 800 rpm and the temperature was 45^oC. Test 1.

Time, sec.	Total free oil	Oil due to coalescence	Free oil from feed	Total oil from feed	Emulsified oil from feed	% of emulsified oil in feed
60	3.5	1.3	2.2	3.9	1.7	22.67
70	4	2	2	3.9	1.9	25.33
						24

Table A.4: The emulsified oil volume fraction in the feed during a continuous experiment performed at 80 ppm concentration of NEO-10 at the feed flow rate of 45 cm^3/min. Mixer speed was 800 rpm and the temperature was 45^oC. Test 2.

Time, sec.	Total free oil	Oil due to coalescence	Free oil from feed	Total oil from feed	Emulsified oil from feed	% of emulsified oil in feed
60	3.5	1.2	2.3	3.9	1.6	20
70	3.7	1.6	2.1	3.9	1.8	24
80	3.9	2	1.9	3.9	2	26.67
						23.55

Table A.5: The emulsified oil volume fraction in the feed during a continuous experiment performed at 80 ppm concentration of NEO-10 at the feed flow rate of 40 cm^3/min. Mixer speed was 800 rpm and the temperature was 45^oC. Test 1.

Time, sec.	Total free oil	Oil due to coalescence	Free oil from feed	Total oil from feed	Emulsified oil from feed	% of emulsified oil in feed
60	3.6	1.2	2.4	3.47	1.07	16
70	3.8	1.6	2.2	3.47	1.27	19
80	3.7	2	1.7	3.47	1.77	26.5
						20.5

Table A.6: The emulsified oil volume fraction in the feed during a continuous experiment performed at 80 ppm concentration of NEO-10 at the feed flow rate of 40 cm^3/min. Mixer speed was 800 rpm and the temperature was 45^oC. Test 2.

Time, sec.	Total free oil	Oil due to coalescence	Free oil from feed	Total oil from feed	Emulsified oil from feed	% of emulsified oil in feed
70	3.7	1.4	2.3	3.47	1.17	17.5
80	3.8	1.8	2.	3.47	1.47	22
90	4	2.1	1.9	3.47	1.57	23.5
						21

APPENDIX B
VARIABILITY ANALYSIS

The variability analysis of the data was performed by statistical *t*-distribution. The confidence interval was calculated using mean, standard deviation and 95% confidence level for the *t*-distribution. This section is divided into two major parts. In the first part, the variability analysis was done for oil volume fraction both during the batch and continuous experiments. In the second part, the variability analysis was performed for the emulsion layer heights during batch, decay and continuous experiments.

B.1 Oil Volume Fraction

For the given data set of oil volume fractions, the mean is calculated by following equation:

$$\bar{y}_j = \frac{\sum_{i=1}^{n_j} y_i}{n_j} \qquad \text{Equation } \mathbf{B.1}$$

where n_j is the number of measurements or repeats at any time, y_i is the measured value, $\bar{y}_j$ is the average value at any time.

It was assumed that the distribution of error was same for each set of repeats, so then the standard deviation was calculated using the following equation:

$$s = \sqrt{\frac{\sum_{i=1}^{n}\left(y_{ji} - \bar{y}_j\right)^2}{n-1}} \qquad \text{Equation } \mathbf{B.2}$$

where n is the total number of data.

The confidence interval for the measured value at each time was calculated as follows:

$$\bar{y}_j - t_{(\alpha/2,\nu)}\frac{s}{\sqrt{n_j}} \le \bar{y}_j \le \bar{y}_j + t_{(\alpha/2,\nu)}\frac{s}{\sqrt{n_j}} \qquad \text{Equation } \mathbf{B.3}$$

where α = 1-(%confidence level/100), ν = n-1, is the degrees of freedom. In this study, the confidence level is chosen as 95%, so the α is 0.05.

B.1.1 Oil Volume Fraction during Batch Experiment

The number of data used for each time is n_j = 3 and the total number of data points is n = 36 (Table B.1). So, ν in this case is 35 and the corresponding value of $t_{(0.025,\,35)}$ is 2.0301 (Dean, J.A., 1999). Since the number of repeats used at each time is same, the 95% confidence interval for oil volume fraction is same and equal to ±0.023.

Table B.1: Variability analysis for the oil volume fraction in the emulsion layer during a batch experiment performed at 80 ppm concentration of NEO-10. The mixer speed was 800 rpm and temperature was 45^{o}C.

Batch experiment	Time, min	Oil volume fraction				Standard deviation
		Data 1	Data 2	Data 3	Mean	
2000 mL	0	0.496	0.500	0.497	0.498	0.002
80 ppm	1	0.595	0.598	0.643	0.612	0.027
	2	0.697	0.699	0.744	0.713	0.027
	3	0.746	0.787	0.801	0.778	0.029
	5	0.829	0.812	0.884	0.842	0.037
	7	0.863	0.830	0.901	0.865	0.036
	10	0.874	0.859	0.905	0.879	0.024
	15	0.875	0.871	0.902	0.883	0.017
	20	0.875	0.889	0.903	0.889	0.014
	30	0.882	0.906	0.910	0.889	0.015
	40	0.890	0.917	0.910	0.906	0.014
	55	0.898	0.929	0.910	0.912	0.016

B.1.2 Oil Volume Fraction during Continuous Experiment

The number of data used for each time is $n_j = 2$ and the total number of data points is $n = 16$ (Table B.2 and B.3). So, ν in this case is 15, so the corresponding value of $t_{(0.025,\ 15)}$ is 2.1315. Since the number of repeats used at each time is same, the 95% confidence interval for oil volume fraction is same and equal to ±0.026.

Table B.2: Variability analysis for the oil volume fraction in the emulsion layer during a continuous experiment performed at 80 ppm concentration of NEO-10 in the 250 mL separator with feed flow rate of 45 cm^3/min. The mixer speed was 800 rpm and temperature was 45^oC.

Continuous experiment	Time, min	Oil volume fraction			Standard deviation
		Data 1	Data 2	Mean	
45 cm^3/min	3	0.62	0.66	0.64	0.028
80 ppm	7	0.63	0.61	0.62	0.014
	10	0.66	0.64	0.65	0.014
	15	0.64	0.63	0.64	0.007

Table B.3: Variability analysis for the oil volume fraction in the emulsion layer during a continuous experiment performed at 80 ppm concentration of NEO-10 in the 500 mL separator with feed flow rate of 55 cm^3/min. The mixer speed was 800 rpm and temperature was 45^oC.

Continuous experiment	Time, min	Oil volume fraction			Standard Deviation
		Data 1	Data 2	Mean	
55 cm^3/min	5	0.68	0.71	0.70	0.021
80 ppm	10	0.71	0.68	0.70	0.021
	15	0.69	0.66	0.68	0.021
	19	0.70	0.69	0.70	0.007

B.2 Emulsion Layer Height

During the emulsion layer height experiment it was observed that the change in the relative error was random. So, the relative standard deviation of the distribution of relative deviations was calculated by the following equation:

$$s = \sqrt{\frac{\sum_{i=1}^{n}\left(y_{ji} - \bar{y}_j \big/ \bar{y}_j\right)^2}{n-1}} \qquad \text{Equation } \mathbf{B.4}$$

The confidence interval for each set of repeats was determined as follows:

$$\bar{y}_j\left(1 - t_{(\alpha/2,\nu)}\frac{s}{\sqrt{n_j}}\right) \le \bar{y}_j \le \bar{y}_j\left(1 + t_{(\alpha/2,\nu)}\frac{s}{\sqrt{n_j}}\right) \qquad \text{Equation } \mathbf{B.5}$$

The term $\pm t_{(\alpha/2,\nu)}\frac{s}{\sqrt{n_j}}$ is the 95% confidence interval for the relative deviation.

B.2.1 Emulsion Layer Height during Batch Experiment

The number of repeats used at each time is 3 for the batch experiment performed in the 2000 mL beaker (Table B.4) and the number of repeats used at each time is 2 for the batch experiment performed in the 4000 mL beaker (Table B.5). The total number of data considered is 42. So, ν is 41 and 95% confidence interval for the relative deviation is 8.72%.

Table B.4: Variability analysis for the emulsion layer height during a batch experiment performed at 80 ppm concentration of NEO-10. The mixer speed was 800 rpm and temperature was 45^{o}C and emulsion was created in the 2000 mL beaker.

Batch experiment	Time, min	Emulsion layer height, cm				Standard deviation, cm
		Data 1	Data 2	Data 3	Mean	
2000 mL	1	10.28	10.38	9.56	10.073	0.447
80 ppm	2	8.21	8.38	7.23	7.940	0.621
	3	7.05	6.30	5.77	6.373	0.643
	5	4.69	5.00	3.78	4.490	0.634
	7	3.80	4.17	3.14	3.703	0.522
	10	3.10	3.33	2.64	3.023	0.351
	15	2.56	2.71	2.15	2.473	0.290
	20	2.24	2.34	1.95	2.177	0.203
	30	1.87	1.94	1.72	1.842	0.115
	40	1.64	1.75	1.51	1.632	0.123
	55	1.37	1.58	1.39	1.445	0.117

Table B.5: Variability analysis for the emulsion layer height during a batch experiment performed at 80 ppm concentration of NEO-10. The mixer speed was 800 rpm and temperature was 45^{o}C and emulsion created in the 4000 mL beaker.

Batch experiment	Time, min	Emulsion layer height, cm			Standard deviation, cm
		Data 1	Data 2	Mean	
4000 mL	1	9.2	9.05	9.125	0.106
80 ppm	3	6.93	6.79	6.860	0.099
	5	6.22	6.03	6.125	0.134
	7	5.38	5.14	5.260	0.170
	10	4.41	4.22	4.315	0.134
	15	3.13	2.83	2.980	0.212
	20	2.65	2.47	2.560	0.127
	30	2.2	2.08	2.140	0.025
	50	1.69	1.54	1.615	0.106
	70	1.34	1.26	1.300	0.057

B.2.2 Emulsion Layer Height during Decay Experiment

The number of repeats used at each time is 2 (Table B.6 and B.7). The total number of data considered is 42. So, ν is 41 and 95% confidence interval for the relative deviation is 12.6%.

Table B.6: Variability analysis for the emulsion layer height during a decay experiment performed at 80 ppm concentration of NEO-10. The continuous experiment was performed in the 250 mL separator at the feed flow rate of 45 cm^3/min. The mixer speed was 800 rpm and temperature was 45^oC.

Decay experiment	Time, min	Emulsion layer height, cm			Standard deviation, cm
		Data 1	Data 2	Mean	
250 mL	0.5	7.17	7.03	7.101	0.101
45 cm^3/min	1.5	5.92	6.03	5.976	0.081
80 ppm	3	4.71	4.67	4.693	0.027
	5	3.18	3.42	3.301	0.168
	7	2.47	2.46	2.465	0.007
	10	1.83	1.79	1.810	0.034
	15	1.28	1.21	1.245	0.054
	20	1.01	0.90	0.955	0.074
	30	0.72	0.56	0.641	0.114
	40	0.58	0.42	0.499	0.114

Table B.7: Variability analysis for the emulsion layer height during a decay experiment performed at 80 ppm concentration of NEO-10. The continuous experiment was performed in the 500 mL separator at the feed flow rate of 55 cm^3/min. The mixer speed was 800 rpm and temperature was 45^oC.

Decay experiment	Time, min	Emulsion layer height, cm			Standard deviation, cm
		Data 1	Data 2	Mean	
500 mL	0.5	3.81	3.91	3.861	0.069
55 cm^3/min	1.5	2.95	3.03	2.993	0.059
80 ppm	3	2.19	2.13	2.160	0.039
	5	1.54	1.47	1.503	0.054
	7	1.24	1.13	1.181	0.079
	10	0.94	0.85	0.892	0.064
	15	0.68	0.60	0.639	0.059
	20	0.53	0.41	0.472	0.088
	30	0.38	0.28	0.330	0.074
	40	0.32	0.20	0.260	0.083

B.2.3 Emulsion Layer Height during Continuous Experiment

Continuous experiments performed at different experimental conditions are considered for the variability analysis. The number of repeats used at each time is 2 (Table B.8 to B.11). The total number of data considered is 52. So, ν is 51 and 95% confidence interval for the relative deviation is found as 7.2%.

Table B.8: Variability analysis for the emulsion layer height during a continuous experiment performed at 80 ppm concentration of NEO-10 in the 250 mL separator at the feed flow rate of 45 cm^3/min. The mixer speed was 800 rpm and temperature was 45^oC.

Continuous experiment	Time, min	Emulsion layer height, cm			Standard deviation, cm
		Data 1	Data 2	Mean	
250 mL	1	1.43	1.25	1.340	0.121
45 cm^3/min	3	2.64	2.23	2.437	0.289
80 ppm	5	3.47	3.59	3.529	0.087
	7	4.39	4.53	4.460	0.101
	10	5.44	5.56	5.501	0.081
	12	6.16	6.25	6.204	0.067
	15	6.43	6.47	6.451	0.027

Table B.9: Variability analysis for the emulsion layer height during a continuous experiment performed at 80 ppm concentration of NEO-10 in the 250 mL separator at the feed flow rate of 40 cm^3/min. The mixer speed was 800 rpm and temperature was 45^oC.

Continuous experiment	Time, min	Emulsion layer height, cm			Standard deviation, cm
		Data 1	Data 2	Mean	
250 mL	1	1.06	0.92	0.993	0.101
40 cm^3/min	3	2.07	1.92	1.995	0.107
80 ppm	5	2.73	2.58	2.655	0.101
	7	3.54	3.34	3.444	0.141
	10	4.42	4.28	4.346	0.101
	13	4.71	4.69	4.703	0.013

Table B.10: Variability analysis for the emulsion layer height during a continuous experiment performed at 80 ppm concentration of NEO-10 in the 500 mL separator at the feed flow rate of 55 cm^3/min. The mixer speed was 800 rpm and temperature was 45^oC.

Continuous experiment	Time, min	Emulsion layer height, cm			Standard deviation, cm
		Data 1	Data 2	Mean	
500 mL	1	0.85	0.97	0.913	0.083
55 cm^3/min	3	1.76	1.94	1.854	0.128
80 ppm	5	2.48	2.59	2.535	0.079
	7	2.86	3.76	3.313	0.638
	10	3.57	3.64	3.604	0.049
	12	3.94	4.12	4.028	0.128
	15	4.31	4.42	4.366	0.081
	19	4.52	4.58	4.550	0.037

Table B.11: Variability analysis for the emulsion layer height during a continuous experiment performed at 40 ppm concentration of NEO-10 in the 250 mL separator at the feed flow rate of 45 cm^3/min. The mixer speed was 800 rpm and temperature was 45^oC.

Continuous experiment	Time, min	Emulsion layer height, cm			Standard deviation, cm
		Data 1	Data 2	Mean	
250 mL	1	0.87	0.68	0.779	0.134
45 cm^3/min	3	1.38	1.27	1.325	0.074
40 ppm	5	1.62	1.50	1.558	0.081
	7	1.67	1.59	1.629	0.060
	9	1.69	1.62	1.653	0.054